CHARACTERIZATION OF ENVIRONMENTALVARIABILITY IN IDENTIFIED DYNAMIC PROPERTIES OF A SOIL-FOUNDATION-STRUCTURE SYSTEM

by

Ali Asghari

A Dissertation Presented to the

FACULTY OF THE VITERBI SCHOOL OF ENGINEERING

UNIVERSITY OF SOUTHERN CALIFORNIA

In Partial Fulfillment of the

Requirements for the Degree

DOCTOR OF PHILOSOPHY

(CIVIL ENGINEERING)

October 2009

Signature Page

Dedication

I dedicate this dissertation to all the parents who sacrifice their lives for their kids and raise them responsibly so that they can constantly contribute to their societies; those who educate their kids so wisely that they could be fully motivated in obtaining broader vision in life and also provide them with peaceful environment so that they could pursue their dreams enthusiastically.

Acknowledgements

Had it not been for a collaborative teamwork, I would not have been able to accomplish this research and dissertation. I would like to thank all those who helped in this effort. On top of my list, I would like to appreciate my advisor, Professor Erik A. Johnson, for providing inspiration and support to make this work possible.

I do not have enough words to say how grateful I am to have worked under the supervision of my co-advisor, Professor Robert Nigbor; not only for his academic guidance, but also for his fabulous personality that has always been a great source for motivation and encouragement since I initiated my research career at USC.

I would also like to appreciate my Ph.D. committee members Prof. Sami Masri, Prof. Roger Ghanem and Prof. Carter Wellford for their time and encouragement.

My valued friends Dr. A. Doostan, Dr. A. Sadjadpour, Dr. R.D. Nayeri, Dr. F. Banaei, Dr. N. Nastar, Dr. M. Jahangiri, my dear cousin, Gita, my uncle and his wife, Shohreh, have each also provided support in different aspects of my Ph.D. journey.

Most importantly, I would like to give my deepest gratitude to my very dear parents, my loving wife, Setareh, and my in-laws whom without their constant encouragement and understanding my degree might never have been accomplished. I would also like to thank my dear grandma who has been a key supporter of my education from early on. I further appreciate my brother, Iman, for his kind support to our parents which allowed me to pursue my doctorate degree so conveniently whilst being far from my home and family.

Last but not least, I would like to appreciate the National Science Foundation and the George E. Brown, Jr. Network for Earthquake Engineering Simulation (NEES) for creating such unique facilities for advancement of earthquake engineering research, in particular NEES@UCSB for operating and maintaining the SFSI Test Structure site.

Table of Contents

List of Tables

List of Figures

Abstract

For more than thirty years, researchers have attempted to establish effective local and global methods for monitoring civil, aerospace and mechanical structures. The unpredictable nature of soil and the nonlinear behavior of civil structures, however, make monitoring rather complex. In fact, the combined soil-structure system can be influenced by environmental factors on daily to annual time scales. Identification of structural damage using vibration-based methodologies in the presence of such influences requires some data normalization to reduce uncertainties and variations introduced by environmental factors.

To better understand the correlation between environmental variations and the dynamics of soil-structure interaction, semi-continuous monitoring of a large-scale field test structure has been conducted. The analysis uses data from sensors placed at several locations on the NEES Soil Foundation Structure Interaction (SFSI) Test Structure, which is located on very well-characterized soil in southern California, as well as sensor arrays monitoring the soil response under the foundation. A network of sensors was designed and positioned to record temperature at various locations on the structure; some pertinent soil properties are also monitored.

The observations of measured environmental data and the identified structural system parameters demonstrated strong correlation between variations in the environmental

features and in the dynamic properties of the structure; for example daily shifts in the structure's fundamental frequencies are as much as10% due to temperature change or seasonal shifts due to ground water table variation under the foundation. An example is given, based on novelty detection, of how "unusual" dynamic behavior can be indicated for the SFSI test structure in the presence of environmental variations.

To explain the effect of the soil saturation on the rocking frequency of SFSI systems, a predictive model based on Wolf's Cone Model approach was developed. The results from parametric study validated the observations from both the SFSI test structure and the scaled model of decreased natural frequency for dry soil. Further, the study shows that the opposite effect — that is, higher natural frequency with soil saturation — occurs for structures with different characteristics relative to the soil.

A 1/14 scale model of the SFSI test structure was constructed to validate the observed effect of the water level under the foundation on the rocking frequency of SFSI systems in a controlled laboratory environment. These experiments showed a similar correlation between the identified rocking frequency of the scaled prototype and the rise and fall of the water level under the foundation.

This work shows that understanding the environmental variability of an identified model is critical to developing methodologies for cleansing data and reducing uncertainty to allow more robust health monitoring in real civil structures.

1 Introduction

The dynamic behavior of civil structures is affected by environmental conditions, such as temperature, humidity, soil moisture and precipitation. Temperature, with both ambient and localized variations due to sunlight, rain or wind, causes thermal expansion that can tighten or loosen bracing and joints or change the effective stiffness of some materials, thereby changing the dynamic behavior. Rain may have mass and seepage pressure effects, but also causes changes in the soil behavior, thus changing the dynamics of the soil-foundation-structure system. Seasonal variation of soil moisture and water table will also affect system dynamic behavior. Clearly, observed variations in structural behavior of real structures outside the laboratory are due not only to changes in the structure alone, but are also due to the induced changes in the soil and foundation.

Several different methodologies for the identification of structural damage have received significant consideration in the civil engineering community over the past few decades. In particular, vibration-based damage detection, as a nondestructive evaluation (NDE) technique, has been widely studied in the research community and has begun to be put into practice. In global vibration-based damage detection methodologies, the dynamic behavior of a structural system is monitored continuously or at intervals tracking damage-sensitive parameters. Chapter 2 provides background on this subject. In civil structures (*e.g.*, buildings and bridges) in particular, the combined soil-foundation-structure system

can be heavily influenced by environmental factors on daily to annual time scales. The presence of such influences requires more meticulous considerations in both monitoring and analysis, necessitating better understanding of the physics of the interaction between the soil-foundation-structure system and the environment.

This dissertation describes an investigation of environmental effects on the dynamics of the Soil-Foundation-Structure-Interaction (SFSI) Field Test Structure (Asghari *et al*., (2006) that is part of the George E. Brown Jr. Network for Earthquake Engineering Research (NEES). The SFSI Test Structure, located in Garner Valley, CA, is a simple (4m in length, width and height) open steel frame, with large reinforced concrete base and top slabs, that is instrumented for both dynamic and static response experiments. It has continuous and triggered monitoring and an internet-controlled shaker allowing unattended forced vibration testing. Chapter 3 details the design, construction, and operation of this test structure.

Monitoring data of the NEES SFSI Test Structure and its environment were collected over a 2-year period. Chapter 4 describes this data collection and the processing and analysis of the various types of data, including ambient, earthquake and forced vibration. Observations show day-to-day shifts in the structure's fundamental frequencies on the order of 10% for the braced structure and 3% for the unbraced configuration. In addition to longer seasonal trends that are related to temperature (*e.g*., summer vs. winter temperatures), some variations are clearly related to precipitation. Specifically, the SFSI

structure data demonstrates a correlation between the fundamental frequency and the level of the water table in the soil surrounding the test structure, with frequency decreasing with higher water level (*i.e.*, water-table closer to the surface of the ground).

Chapter 5 attempts to explain these observed behaviors through analytical modeling. For better understanding of the physics of the effect of saturated versus dry soil under a soil-structure system, and to explain the observed environmental effects, past research on the dynamic behavior of rigid surface footings on poroelastic half-space is reviewed, specifically the works of Halpern and Christiano (1986), Philippacopoulos (1989), Kassir *et al*. (1989) and Todorovska and Al Rjoub (2006). Wolf (1985) provides a good basis for an explanation of the observed phenomena. An equivalent linear model of the soil-structure system is derived and used to explain the observed environmental dependencies in the measured SFSI test structure's dynamic response. It is shown that the apparent rocking frequency of a SFSI system is a function of saturation level and might increase or decrease, relative to the dry soil, depending on the relative characteristics of the structure with respect to the soil under its foundation.

To understand these environmental dependencies at small strain linear levels of vibration, small-scale controlled modeling of the SFSI test structure is described in Chapter 6. A simple 1/14 scale physical model of the SFSI Test Structure was built and tested to validate the observations from the SFSI Test Structure in more environmentally-controlled conditions. The main focus of this experiment was to validate the observed

effect of water table variation upon the system's modal properties. Indeed, the decreased frequency of the SFSI structure with shallower (*i.e.*, higher) water table is consistent with the SFSI test structure but contrary to results reported by others (*e.g.*, Bradford *et al.*, 2005) of frequency increases after heavy rain.

Pattern recognition tools can be applied to vibration-based structural health monitoring for extraction of parameters of interest from noisy data. This approach is studied and applied to the SFSI test structure data in an attempt to find a methodology for tracking the structural response within the environmental "noise" found in this real field structure. Chapter 7 gives background on pattern recognition and details these efforts in conjunction with some regression analyses to cleanse the SFSI data set.

Based on the result of the current research and observations made on the SFSI test structure, it is concluded that to establish more robust health monitoring in real civil structures, it is crucial to study the environmental variability of identified modal properties. Thus, it is necessary to develop methodologies for cleansing data and reducing uncertainties caused by environmental variation on each site — further investigation on this task is left to future research.

2 Background

2.1 Structural Health Monitoring and Damage Detection

Structural Health Monitoring (SHM) and vibration-based damage detection have been popular research topics for almost three decades. The oil industry expended considerable effort in the 1970s and early 1980s for monitoring offshore platforms (Vandiver, 1977). The civil engineering community has been investigating structural health monitoring for bridges since the early 1980s (Doebling *et al*., 1996), though it has its roots in much earlier studies to identify dynamic characteristics of structures.

Numerous industries and research communities have attempted to develop algorithms for structural monitoring purposes. The essential premise of vibration-based damage detection, as presented by Sohn *et al*. (2001), is that the dynamic response characteristics of the structure would change due to the physical properties alteration of the structures (*e.g*., reductions in stiffness resulting from the onset of cracks or the loosening of a connection). Such variations (*e.g*., the resonance frequency) can be detected by utilizing system identification methods and by monitoring the changes in the structure on a global basis. Doebling *et al*. (1996), and a recent update by Sohn *et al*. (2004), present an extensive survey of global vibration-based structural monitoring methods.

In addition to effects from damage, there are also measurable changes in resonance frequencies of structures due to other factors (Cornwell *et al*., 1999). For instance, weather conditions, rain/wind events, and soil nonlinear behavior are two important factors which are a recent focus of attention in the research community.

Pioneers have conducted several long-term monitoring projects of buildings and bridges to observe the environmental effects on natural frequencies and attempt to develop different techniques (*e.g*., pattern recognition) to more accurately identify damaged structures. It is commonly concluded that, in order to attain more accurate and reliable vibration-based damage detection methodologies, the influence of environmental effects should be recognized and eliminated. Several researchers (Farrar *et al*., 2000; Sohn *et al*., 2002; Kullaa, 2002–2004) have emphasized the importance of removing environmental or/and operational variations, and have proposed some data cleansing procedures for SHM. Further, Kulla (2008) validated his proposed method (*i.e*., factor analysis) for eliminating the influence of environmental effects by using both numerical models and experimental data.

The effects of environmental variation on the SFSI test structure (identified frequencies) and a mechanism for extracting them are discussed further in Chapter 4 and Chapter 7, respectively.

2.2 Environmental Effects

The fact that environment can have an impact on structural dynamics has been known for some time. As explained by Sohn and Law (2000), an experimental study in the UK (Wood, 1992) showed that some concrete bridges absorbed moisture during periods of damp weather, resulting in an increase in the bridge mass; clearly, this would tend to decrease the natural frequencies of the structure (assuming, of course, that all other properties remain fixed). Friswell and Penny (1997) discuss the difficulties of the damage detection due to the environmental effects on dynamic properties, especially on highway bridges. Sohn *et al*. (1999) showed that temperature changes caused 5% daily variations in the natural frequencies of the Alamosa Canyon Bridge; these variations were several times the expected damage-induced changes in natural frequencies, masking the effects of damage. Sohn *et al*. (1999–2004) have also examined the changes of modal parameters due to structural damage versus those caused by temperature changes.

Similarly, Porter *et al*. (2004) believe that, the variations in modal data due to changing environmental conditions, creates uncertainty in deciding whether actual damage in the structure have occurred. In the bridge health monitoring community, Peeters and De Roeck (2001) focused on the impact of changes in environmental parameters on the dynamics of structures. They contemplated that temperature may have an impact on the material properties and the boundary conditions. Peeters *et al*. (2001) also discussed the effect of temperature on measured eigenfrequencies as an inevitable issue for vibration-

based damage detection applications. Similarly, short-term and long-term monitoring and study of the environmental effects on the Singapore–Malaysia Second Link bridge by Omenzetter and Brownjohn (2006) revealed that it is possible that some of the observed model changes may, in fact, have been caused by abnormal temperature variations and were not associated with structural changes. In their research on monitoring of bridges, Liu and DeWolf (2007) could also observe 4–5% changes in the natural frequencies during the spring and winter. A recent study by Nayeri *et al*. (2008) presents the results of time-domain modal identification of a full-scale 17-story building, based on ambient vibration measurements. It is shown in their result that there is a strong correlation between the modal frequency variations and the temperature variations in a 24-hour period.

A structure that has, perhaps, received the most research attention over the years for its dynamic properties is the Robert A. Millikan Library, located on the campus of the California Institute of Technology (Caltech). Since its construction in the mid-1960s, the dynamics of the Millikan Library have been studied through ambient and forced vibration tests as well as through its response to small and moderate ground motions during various earthquakes in southern California. Clinton *et al*. (2006) provides a good background of some of the history of these studies. A test bed has been installed at Caltech for on-line monitoring of the Millikan Library and one other Caltech building; implemented in the *Caltech Online Monitoring and Evaluations Testbed* (COMET) website (Lam *et al*.,

2004), this computer-based system is designed to receive, analyze, and disseminate near-real-time accelerometer data-streams from instruments in (currently) two facilities (Porter *et al*., 2004).

Clinton *et al*. (2006) also reports the results of recent experiments showing the impact of environment on vibration-based frequency analysis of the Millikan Library. The observations showed that, in a particularly intense windstorm without rain, the natural frequencies of the structure show consistent decreases of several percent for the duration of the most intense winds, both for the rocking and the torsional modes of vibration. In contrast, during a two-day, 4 in. rainfall, both translational and torsional natural frequencies increased by about 3%, returning to the nominal values in 1–2 weeks. Furthermore, a direct correlation between increasing temperatures and higher frequencies were detected, probably from thermal expansion of the concrete (Bradford *et al*., 2005). Clinton *et al*. (2006) conclude that the rain-induced increases in natural frequencies were due to an increase in soil-structure stiffness caused by soil saturation and, perhaps, soil swelling; they state that their hypothesis could be tested using pore-water pressure measurements near the structure.

To investigate all of these environmental parameters, a fully instrumented test structure would be of great value to be able to thoroughly study the various effects, incorporating the soil-foundation-structure interaction phenomenon.

2.3 Soil-Foundation-Structure Modeling; Cone Models

In recent years, a number of studies have been conducted in the area of soil–structure interaction modeling in various sophisticated ways. As a matter of fact, soil has very complex characteristics and many researchers and engineers have attempted to develop accurate, yet pragmatic approaches to model such systems. There are several reviews and publications about this specific topic. For instance, Dutta and Roy (2002) have reviewed quite a few idealization methodologies. They believe that, the use of a rigorous model representing the real system will not necessarily lead to better results, because the determination of the input parameters often involves quite significant uncertainties. They also suggest two main avenues for modeling dynamic soil-structure interaction: a) modeling the soil as an elastic half-space, b) modeling the soil with a lumped mass or lumped parameter method. The advantages and limitations of these approaches have been discussed by Seed and Lysmer (1975) and Hall *et al*. (1976).

One of the popular methods, known as Winkler's idealization, represents the soil medium as a system of identical but mutually independent and linearly elastic springs (Dutta and Roy, 2002). Though this method introduces a good level of simplicity, the commonly known problem with the use of this model is the intricacy of determining accurate input parameters (*e.g*., the stiffness of springs). On the contrary, methods based on the elastic continuum model have the advantage of less vagueness in the input parameters (*e.g*., modulus of elasticity) but they often lead to very complex mathematical formulations.

Also, the uncertainty in modeling boundary condition and contact surfaces still need to be carefully quantified.

To address the disadvantages of the modeling approaches mentioned above, there are also some suggested modified methods in the literature. For instance, Horvath (1993) presents a modified formulation for the classical problem of beams on an elastic foundation. His formulation shows how the continuity among the individual Winkler springs can be achieved.

The scope of numerical methods is significantly wider than that of analytical methods; thus, the use of the general-purpose finite element method has attracted a lot of attention for studying the complex interactive behavior of soil-foundation systems. Furthermore, some studies recommend that the infinite soil should be modeled by using the boundary element method and the finite structure with the finite element method. Dobry and Gazetas (1986) believe that these two different means of idealizations may be suitably matched at the interface through equilibrium and compatibility conditions.

Some improvements also on the coupling of the finite element approaches have been suggested. As a very good example, the analysis of a soil-structure interaction system using a coupling model of finite elements, boundary elements, infinite elements and infinite boundary elements has been presented in Zhang *et al*. (1999).

In the dynamic analysis of soil-structure systems, the presence of water in the soil, either by causing soil saturation or by fluctuation of the water-table under the foundation, could extensively add to the complexity of the soil modeling. The real deformation characteristics of soil media, particularly in fine-grained-types of soil, are always time-dependent, to some extent depending on the permeability of the soil media. An increase in pressure in the pore water of soil and the contribution of the added mass both significantly change the dynamic characteristics of the soil-structure interaction.

Several modeling approaches and studies of the dynamic stiffness and vibrations of rigid surface footings on poroelastic half-space been presented. For instance, the two-phase models which are based on the theory of wave propagation in fluid saturated poroelastic soil, has been exploited by Todorovska and Al Rjoub (2006) to conduct a chain of studies of a circular foundation embedded in a water-saturated poroelastic half-space. Their theoretical model is mainly to explain the observed increase of the apparent frequencies of the Millikan library in Pasadena, CA. The hypothesis in their work is that the observed increases in frequency are due to the water saturation of the soil and increased soil-foundation stiffness.

Another series of studies by Halpern and Christino (1986) investigated the compliance matrices of a square rigid plate on a water saturated poroelastic half-space. Their conclusion implies that the saturated soil shows more stiffness — for both rocking and vertical motion. Philippacopoulos (1989) provided evidence that the effect due to

saturation on the impedance function is generally very significant for high dimensionless frequency (*i.e.*, between 3 and 6). In the discussion of his results, contrary to the others, he states ‘‘the effect of the pore fluid is to generally reduce the stiffness and increase the damping compared to the dry case.”. Kassir *et al*. (1996) also studied the impedances for a drained surface circular footing for rocking and horizontal motions. They concluded “for rocking motion, the presence of pore fluid significantly affects the impedance of the dynamic system.”.

With a strength of material approach, Wolf (1994) has shown that a simple spring-dashpot-mass model with frequency-dependent coefficients can represent soil-structure systems. Wolf's approach is mainly by using conical bars and beams, called Cones. The modeling technique used herein will be based on the Cone Modeling approach, which is discussed further in Chapter 5.

2.4 Statistical Pattern Recognition

Various earthquake engineers and researchers have recognized that structural health monitoring and damage detection are effectively applications of pattern recognition. Structural health monitoring — as a systematic non-destructive procedure — is performed to be able to classify a damaged structure. The main objective of classifying a damaged structure is to ascertain, based on measured dynamic characteristics, if damage

is present or not. Often, after defining the sensitive features and training the system based on a given existing data set, the equation of the classifier must be mathematically determined.

It is important to note that the classifying process is usually prone to false identification due to potential uncertainty in sensing/measurement/calculation of the selected feature(s). Hence, defining the right features is a very crucial step for obtaining a precise, yet high performance pattern recognition mechanism; therefore, it requires profound application specific knowledge and experience.

When it comes to selecting damage sensitive features, it is imperative to understand that structures are subject to changing environmental and operational conditions which affect the measured signals; as a result, the process of classifying the structure (*i.e.*, damaged vs. undamaged) could be easily mislead. One solution would be that enough samples are available and appropriate *features* (properties of interest) are included to train the mathematical system. This process is described in Sohn *et al*. (2001) and Farrar *et al*. (2000). It includes several systematic steps; data acquisition and cleansing followed by data normalization are preprocesses before using the classification algorithm. Then, feature extraction and information condensation is the delicate step to virtually build the pattern recognition techniques for the SHM application.

Features essentially are types of data to be acquired for the pattern recognition problem (*e.g.*, frequency variation, environmental parameters, temperature, etc.). For damage detection, the features are typically application specific. Each feature, in fact, would add a new dimension to the pattern recognition problem, which may improve the accuracy of the classification; however, an efficient low dimensional feature vector is practically more affordable. To identify and quantify sources of feature variability for each classification problem, intensive research with sufficient samples is required.

Pattern recognition problems are divided into two main categories: supervised versus unsupervised. Most health monitoring problems though, will fit into the latter category as data from the damaged structure is generally not available to mathematically train the pattern recognition system. If supervised learning is required, there will be serious demands associated with it: data from every conceivable damage situation should be available. The two possible sources of such data would be either via computation or modeling and experiment. Rather, in unsupervised learning, a threshold with a specific margin is defined; the variation of certain features beyond that threshold would represent a damaged status. Sohn *et al*. (2001) states that "the philosophy is simple: during the normal operation of a system or structure, measurements are recorded and features are extracted from data, which characterize the normal conditions. After training the diagnostic procedure in question, subsequent data can be examined to see if the features deviate significantly from the norm."

That is said, herein a methodology for damage detection based on the concept of *novelty detection* (Worden, 1997) is discussed, which is also founded in multivariate statistics. In a typical novelty detection process, in contrast with a classification problem, classifier act as a detector rather than as a classifier; that is, to detect whether the new test data belongs to the cluster of the trained data or not. If not, it can be concluded that an abnormality has occurred. This technique can be useful for damage detection purposes where the data from the damaged case might not be available. Nevertheless, it is an important qualifier that the novelty detectors should flag only certain deviations from normal operating condition. It is important to remember that real systems are subject to measurement noise and usually operate in a changing environment; therefore, the novelty detector must be able to distinguish between a statistical fluctuation in the data and a real deviation from normality (Worden *et al*., 2002). Fan *et al.* (2004) suggest a methodology to create a margin around the trained data (by artificial novelties). Recent work by Worden and Manson (2003) has also established a skeleton based on the novelty detection. Yet another simple statistical technique was exploited by Ruotolo and Surace (1997) in which, hypothesis testing for novelty detection is based on determining whether the test sample(s) come from the same distribution as training data or not. Their test was performed at 0.05 and 0.01 significance levels and showed promising results. In another approach, Roberts (2000) discussed Extreme Value Theory (EVT) approach; that concerns, low or high values in the tails of data distributions. Tax and Duin (2000)

suggest a method that is useful for quickly-decaying-probabilities distribution. Their modeling is for normally distributed data and is based on the Mahalanobis distance. As a statistical measure, the Mahalanobis distance was introduced by Mahalanobis (1936) more than seventy years ago. In certain aspects, it is different from Euclidean distance; the Euclidean distance is commonly used in mathematics and is dependent on the scale measurement, and its main disadvantage is being blind to correlated variables. The Mahalanobis distance by definition can take into account the covariance among the variables in calculating distances by normalizing the distance with respect to the covariance matrix. With this measure, the problems of scale and correlation inherent in the Euclidean distance are addressed.

The Mahalanobis distance mainly relies on the covariance matrix computation, which is a matrix of covariance between elements of a vector. In fact, it is a generalization of the variance of a scalar-valued random variable to higher dimensions. Let $\mathbf{x}$ be an $n\times1$ vector

$$\mathbf{x} = \begin{bmatrix} X_1 \\ \vdots \\ X_n \end{bmatrix} \tag{1}$$

of random variables X_i denote a point in n-dimensional space. Then the sample mean of the whole population can be written as a vector consisting of the mean corresponding to each variable

$$\boldsymbol{\mu} = \begin{bmatrix} \mu_1 \\ \vdots \\ \mu_n \end{bmatrix} \tag{2}$$

For each of these variables there is a finite variance. Since, in general, there are possible correlations among the variables, the covariance matrix $\sum$ can be defined as a matrix whose (*i, j*) entry is the covariance of *i*th and *j*th variable; $\sum_{ij} = \mathrm{E}[(X_i - \mu_i)(X_j - \mu_j)]$.

In the matrix form, the covariance matrix then can be written

$$\sum = \begin{bmatrix} \sum_{11} & \sum_{12} & \cdots & \sum_{1n} \\ \sum_{21} & \sum_{22} & \cdots & \sum_{2n} \\ \vdots & \vdots & \ddots & \vdots \\ \sum_{n1} & \sum_{n2} & \cdots & \sum_{nn} \end{bmatrix} \tag{3}$$

The diagonal terms in the covariance matrix are variances of the random variables

$$\sum_{ii} = \sigma_i^2 = \mathrm{var}(X_i) = \mathrm{E}[(X_i - \mu_i)^2] \tag{4}$$

Knowing all these terms, the Mahalanobis distance $D_{\mathrm{M}}(\mathbf{x})$ for the vector of random variables is

$$D_{\mathrm{M}}(\mathbf{x}) = \sqrt{(\mathbf{x} - \boldsymbol{\mu})^T \sum^{-1} (\mathbf{x} - \boldsymbol{\mu})} \tag{5}$$

Suppose there is a potential outlier $\mathbf{x}_\xi = [x_1 \; x_2 \cdots x_n]^T$, that needs to be tested against a normal system, where $x_1, x_2, \cdots x_n$ are selected variables (*e.g.*, identified structure's natural frequency, mode shapes, operational temperature, etc.). Based on the Mahalanobis definition, the distance between this point in *n*-dimensional space and the

training data (representing the normal condition) can be obtained by the following formulation: $D_{\mathrm{M}}(\mathbf{x}_\xi) = \sqrt{(\mathbf{x}_\xi - \boldsymbol{\mu})^T \sum^{-1} (\mathbf{x}_\xi - \boldsymbol{\mu})}$, where $\boldsymbol{\mu}$ and $\sum$ are the mean vector and covariance matrix of the data respectively.

There are several different methods that are utilized in the novelty detection approach. For instance, methods based on simple distance measures, statistical approaches and artificial neural networks are commonly used approaches. While previous work by Worden (1997) has been focused on the neural network and statistical procedures, the suggested statistical approaches for the novelty detection purposes are mostly to estimate, based on statistical modeling, whether a test samples comes from the same distribution or not (Odin and Addison, 2000). The distance of the sample from a class mean (considering certain number of standard deviations away) could be another indicator for detection novelties as suggested by Manson *et al.* (2001).

Again, novelty detection has become very popular, as stated by King *et al*. (2002), since it can offer solutions for the cases that the data from the damaged condition is not available. It also has the capability to be utilized for other applications that are more complicated and quite often not with enough samples. It is clear that the success or failure of a novelty detection approach is dependent upon the description of the normal condition and the accuracy of corresponding data. Hence, the data needs to be collected from the full range of structural/environmental conditions which may be encountered in any

testing situation. The disadvantage with this option is that much of the detector sensitivity to damage may be lost within this broad definition of so-called “normal condition”.

To restore sensitivity, an alternative approach can be introduced, by dividing the normal condition data into many sub-sets, each describing an environmental condition in which a novelty detector is constructed, similar to what Cempel (1985) proposed. Thus, the subsequent data would be tested against that sub-set alone. This approach is conceptually similar to the statistical *latent class analysis* discussed by Clogg (1979, 1981), McCutcheon (1987), Arminger *et al*. (1994) and Hagenaars and McCutcheon (2002). This approach — similar to the *finite mixture models* — decompose a density function into component density functions. The latent class analysis (LCA) for analyzing categorical variables, widely applied in social and behavioral research, is a methodology for finding subtypes in a set of multivariate categorical data. It is also well suited to many health applications (Uebersax, 1990). Other common areas of LCA application include psychology, education and marketing research. In another context, Wolfe (1970) and Everitt (1996) consider finite mixture models whose underlying class probability densities have been approximated by finite-length discrete signals and use finite mixture densities to partition data from populations into subpopulations.

3 NEES SFSI Test Structure Facility

The National Science Foundation (NSF) created the George E. Brown, Jr. Network for Earthquake Engineering Simulation (NEES) to give researchers the tools to learn how earthquakes impact the buildings, bridges, utility systems and other critical components of today's society. NEES is a network of 15 large-scale, experimental sites that feature such advanced tools as shake tables and centrifuges, as well as a Soil-Foundation-Structure-Interaction (SFSI) facility, that simulate and study earthquake effects. The NEES SFSI facility provides a unique opportunity to study variations in structural behavior due to changes in temperature, moisture and water table under the foundation (Asghari *et al*. 2006). The SFSI facility, currently maintained by NEES@UCSB, is located in southern California, close to two major active faults (see Figure 1, left), at the Garner Valley Downhole Seismic Array (GVDSA).

The general objective of the SFSI test structure at GVDSA is to provide a well-characterized, well-instrumented, simple structure for the study of soil-structure interaction at large scale. The structure has a reconfigurable steel-frame founded on a rigid, massive concrete slab on grade (see Figure 1, right). Dimensions are 4 × 4 × 4m, approximately. The superstructure is of a size appropriate for testing on one of the NEES shake tables or for the installation of one of the NEES eccentric mass shakers. Provisions were made for mounting such shakers on the roof for active experiments to complement

passive earthquake monitoring (Nigbor and Asghari, 2003). Further a web-portal to analyze the SFSI remotely was developed, the details of which can be found in Nigbor *et al*. (2004a).

The sections below provide details of the SFSI test structure pertinent to the research described in this dissertation. More details can be found at http://nees.ucsb.edu/facilities/gvda.

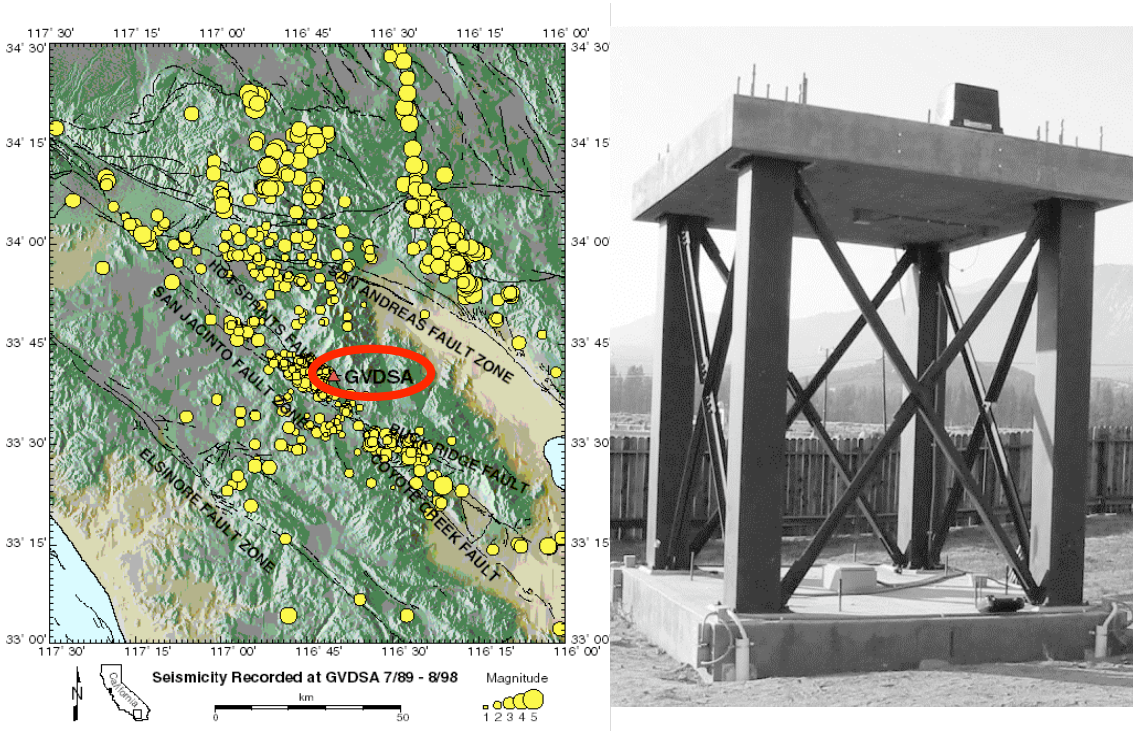

Figure 1: The location of the NEES facility and the seismicity records at the site (left) and photo of the Test Structure (right).

3.1 Site Geotechnical Characteristics

The Garner Valley site was constructed by researchers at UCSB in the 1990's as a test bed for site response studies. site is very close to the active San Jacinto fault, and there are many small earthquakes under or near the site every year.

There are many previous investigations of the site, using various geophysical and geotechnical techniques, that very thoroughly characterize the subsurface soil and rock properties (Steidl *et al*., 2000).

For this research project, additional geotechnical and geophysical measurements were done at the GVDSA site (Youd *et al*., 2004). Combined with the previous studies, these show that the upper 18–25 meters consists of soil rich in organics and alluvium. Soil types present are silty sand, sand, clayey sand and silty gravel. There is a gradual transition from alluvium to decomposed granite from 18–25 meters. Decomposed granite, mechanically similar to gravely sand, exists between 25 and 88 meters. At 88 meters, the contact with hard competent granitic bedrock is reached. The water table fluctuates at the GVDSA site depending on the season and rainfall totals. In the wetter years, the water table is at, or just below, the surface in the winter and spring months. In the summer and fall months, or the entire year when dry, the water table drops to 1–4 meters below the surface.

To characterize the soil, extensive geotechnical experiments have been performed at the site. Youd *et al*. (2004) and Steidl and Nigbor (2004) have carried out extensive research for soil characterization at this site; as a result, most of the necessary static and dynamic soil parameters of the soil for the soil-structure-interaction modeling have been characterized. Figure 2 illustrates some of the properties of the soil at different depths.

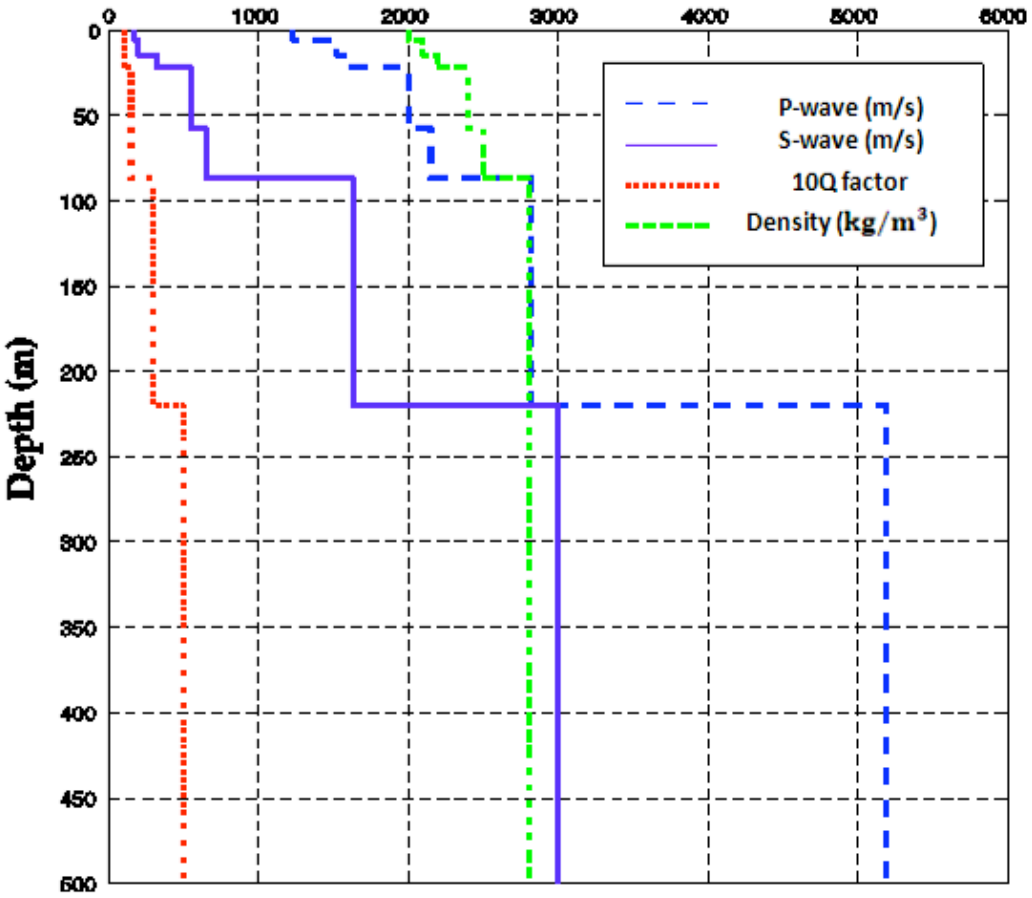

Figure 2: Soil characteristic of the GVDA site at different depths; P-wave velocity, S-wave velocity, 10Q factor (soil pressure resistance) and the density of the soil are illustrated.

3.2 SFSI Test Structure Analysis and Design

Since the 1960s, soil-structure interaction has been recognized as an important factor that significantly affects dynamic building response, the motion of its base, and the motion of the surrounding soil; this interaction often experienced during analysis and real experiments. That is, lower of strains and forces in the building at resonant frequency due to the inclusion of the soil. It may cause significant rotation of the base and changes the natural frequencies of the structure as well. Furthermore, the foundation input motion relative to the free-field motion is significantly impacted by the kinematic interaction between the soil and foundation; at higher frequencies, the translation of the foundation is reduced, but its rotation increases.

Various researchers (*e.g.*, Bielak, 1971) observe that, by considering the soil-structure system, the fundamental natural frequency always decreases, but the effective damping can increase or decrease relative to the damping in fixed base models. When it comes to SFSI research, an important and dynamically meaningful parameter is the relative stiffness between the soil and the structure. The most fundamental challenge would be to identify the stiffness of the soil, because it requires extensive laboratory and ad hoc testing over each site. Since the NEES site's soil parameters were determined by several experiments in the course of a decade (Steidl *et al*., 2000), the soil of the site could be considered as "well-characterized"; therefore, designing and building a test structure for the soil-foundation-structure interaction research seemed very promising at this site.

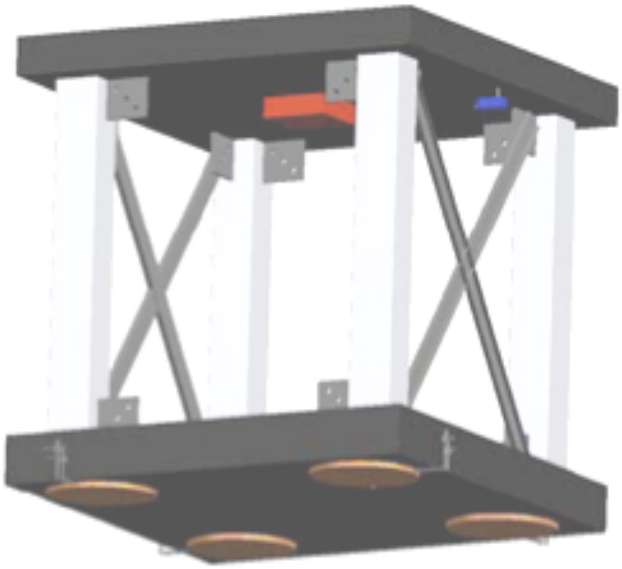

Figure 3: 3D rendering of the initial SFSI Test Structure design showing the positions of the pressure sensors underneath the foundation, and a shaker and a camera under the ceiling.

The main intent for building this test structure is to facilitate studies of the physics of soil-foundation-structure interaction in a controlled field setting. Thus, the SFSI test structure is designed as an open frame with a large reinforced concrete (RC) base slab on grade, four steel columns, a top steel frame, and a top RC slab to provide mass and in-plane stiffness. Connections top and bottom are rigid, bolted moment connections. Provisions were built-in for the addition of mass to the top or bottom slabs and for the modification of stiffness through the removable braces.

The SFSI test structure, therefore, provides a medium-scale reconfigurable steel-frame super structure, which would be of appropriate size for testing on one of the NEES shake

tables and for the field installation of large NEES eccentric mass shakers on the upper slab. Certain provisions for mounting shakers on the roof for forced vibration experiments to complement passive earthquake monitoring (Figure 3). General design requirements for the GVDA SFSI Test Structure were as follows:

- Simple, spread footing at grade
- 700–1000 psf footing load to insure high soil stresses
- Superstructure size appropriate for NEES shake tables (4m in length and width, 50 ton maximum)
- Steel moment frame to allow flexibility
- Configurable bracing system to allow stiffness/damping modification
- Strong RC rigid roof slab to allow mass addition and shaker mounting
- 7–10 Hz fixed-base natural frequency of superstructure (can be adjusted from ~5–15Hz with stiffness & mass)
- Cladding with flexible connections.

The procedures for designing the test structure was:

1. Idealization and modeling of the SFSI system
2. Analysis of response
3. Full-scale experimental verification of assumed model

First, a simple analytical model (stick model) was developed. Considering the design criteria and first frequency to be ~10 Hz, and by performing some frequency analyses, the preliminary size of the columns, and the mass and dimensions for the top and the bottom slabs were obtained. In order to satisfy the dimension requirements, a square foundation (4m in length) was proposed for the bottom slab, based on which the height of the structure (4m) was decided. To perform frequency analysis on the structure and for preliminary investigation on the effects of the soil-foundation interaction, a few finite element models (three-dimensional model) were developed. Some time-history analyses of these models assisted in assuring that the structure would meet the requirements for possible future forced vibration experiments, shaker location and so forth.

The main 3D finite element model of the structure, which is shown in Figure 4, consisted of four steel columns with rectangular hollow sections, two cross bracings on each side and two shell elements to model the top and bottom concrete slabs. This model was developed using SAP 2000 software. Various static and dynamic linear analyses were performed on the following models for braced and un-braced configurations were performed:

1. Fixed-based foundation model (soil-structure interaction excluded)
2. Soil-structure interaction model by introducing zero-mass spring elements under the foundation.

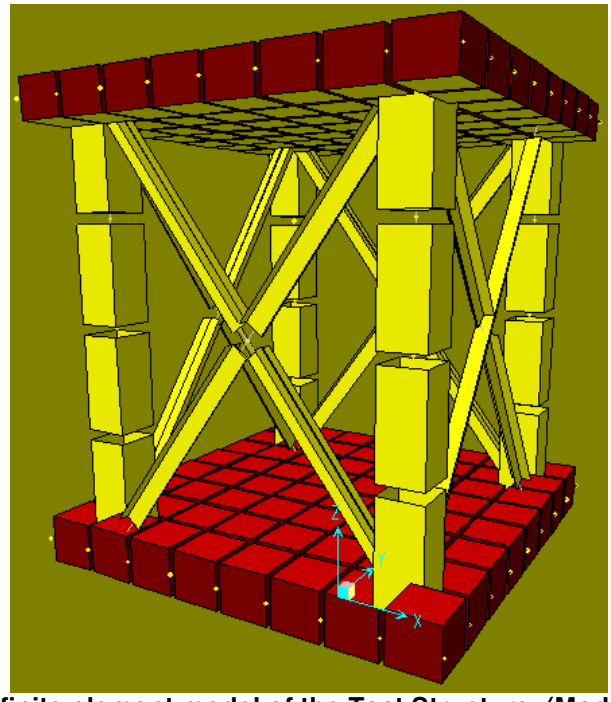

Figure 4: Primary finite element model of the Test Structure. (Modeled by SAP 2000)

In Figure 6 (right) the locations of the introduced massless spring elements are depicted. Inspired by Wolf's cone model (Wolf, 1985), the spring coefficients were defined to represent the soil under the foundation.

As is common in many structural dynamic analyses, the first dominant modes of vibration for the SFSI test structure were analyzed. To obtain the desired frequency range, different columns' size and shape (*i.e.*, Tube/H section) were used for the preliminary frequency analysis. The comparison between using Tube sections (TS14×14×5/8) versus H sections (W12×106) is summarized in Table 1. Since the H section column causes asymmetrical mode shapes, the square tube section seemed to be a

good candidate. Later, however, due to welding limitations, a thinner section, yet bigger in size (*i.e.*, TS16X16X1″) was used, which provides comparable bending resistance.

Table 1: Result of the frequency analysis of the FEM with two different section shapes.

	3-D Model Frequency Analysis				
	Fixed base		SFSI analysis		Mode
	Tube	H	Tube	H	Shape
1st freq. [Hz]	10.17	6.54	7.16	5.55	(Rocking)
2nd freq. [Hz]	10.17	9.94	7.16	7.09	(Rocking)
3rd freq. [Hz]	17.24	12.47	13.86	11.49	(Rotation)
4th freq. [Hz]	49.02	45.87	16.42	16.42	(Vertical)

While the soil effect is taken into account, the first two modes for this symmetric structure are combinations of rocking motion of the foundation along with the bending of the structure. The higher modes of vibration, such as torsional motion about the z-axis in Figure 5, vertical motion and so forth are of less interest in the current research.

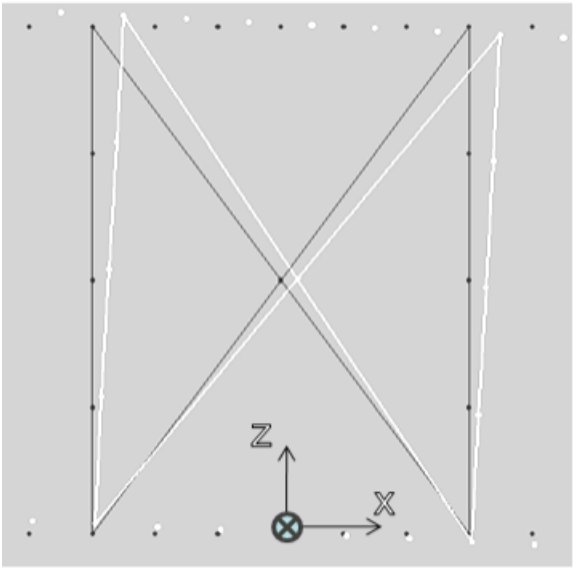

Figure 5: Two dimensional diagram of the first rocking mode of the SFSI Test Structure, which shows the original status (in black) compared with the deformed status (in white).

The RC foundation and the top slab were designed after a performing series of stress analyses on the SFSI test structure. For instance, as is shown in Figure 6, the Von-Mises stress, due to a static loading identifies the concentration of stress in the proximity of the 4 columns. After applying various combination of static and dynamic loading, the thicknesses for the bottom and the top slabs, concerning the allowable stress criterion and the desired mass on top and bottom, were designed at 50cm and 40cm, respectively.

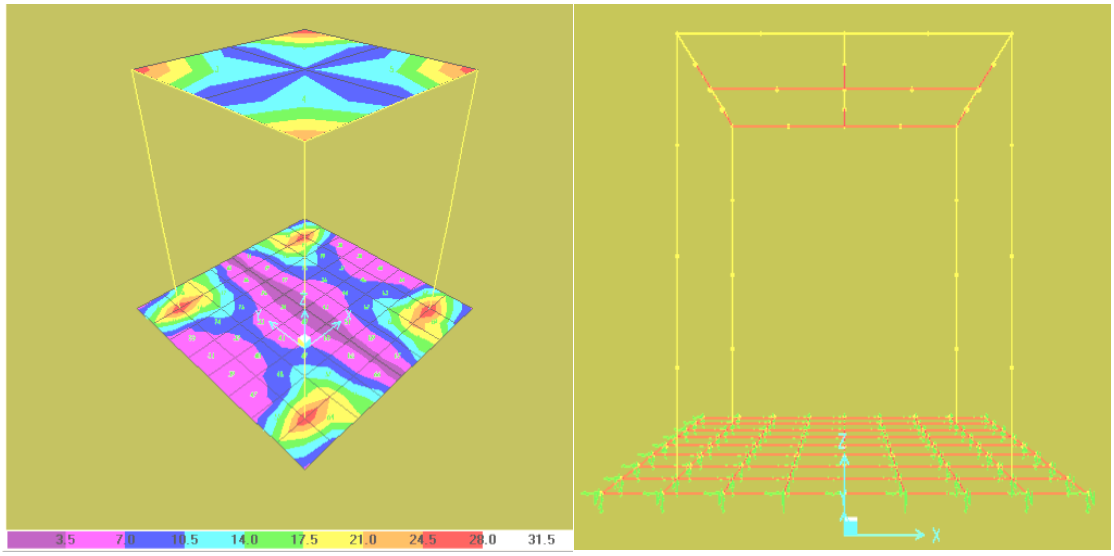

Figure 6: The Von-Mises stress analysis of the top and bottom slabs of the SFSI test structure(left), and the foundation spring nodes(right).

To ensure enough structural rigidity for the top and bottom slabs during the experiments (e.g., forced vibration experiments), a few time-history response of the structure due to sinusoidal harmonic loading — at various locations and with different frequencies — were analyzed. To simulate a forced vibration experiment on the SFSI structure, a harmonic force is applied at the center of the roof, which is the possible location of the shaker. Since shakers are capable of generating forces with various frequency contents, and knowing that the worst case scenario (i.e., highest displacement and stress) would occur close to the natural frequency of the SFSI system, the response of the top slab due to a sinusoidal input with frequency of 10 Hz was simulated. In Figure 7, the result of the analysis is illustrated; clearly because of the resonance phenomenon, the response of the

top slab is amplified (relative to the input function) due to the fact that the applied force's frequency matches the structure's first frequency.

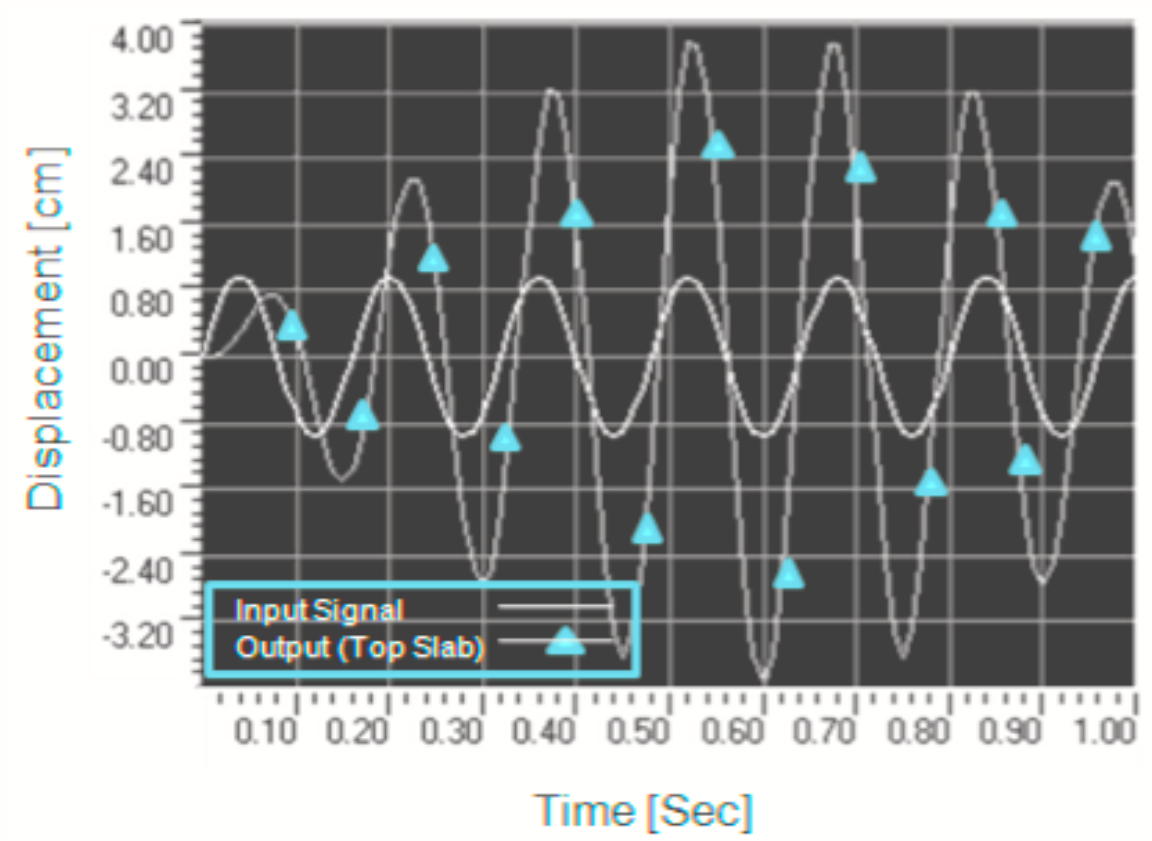

Figure 7: The FEM simulation of the top slab displacement due to a sinusoidal harmonic input (at the resonance frequency of 10 Hz), applied at the center of the top slab.

After performing several static and dynamic analyses on the SFSI test structure and considering all the design requirements, the final design of the structure and the foundation with all the construction detailing was proposed (Figure 8); for more details, the interested reader is directed to the design report by Nigbor and Asghari (2003).

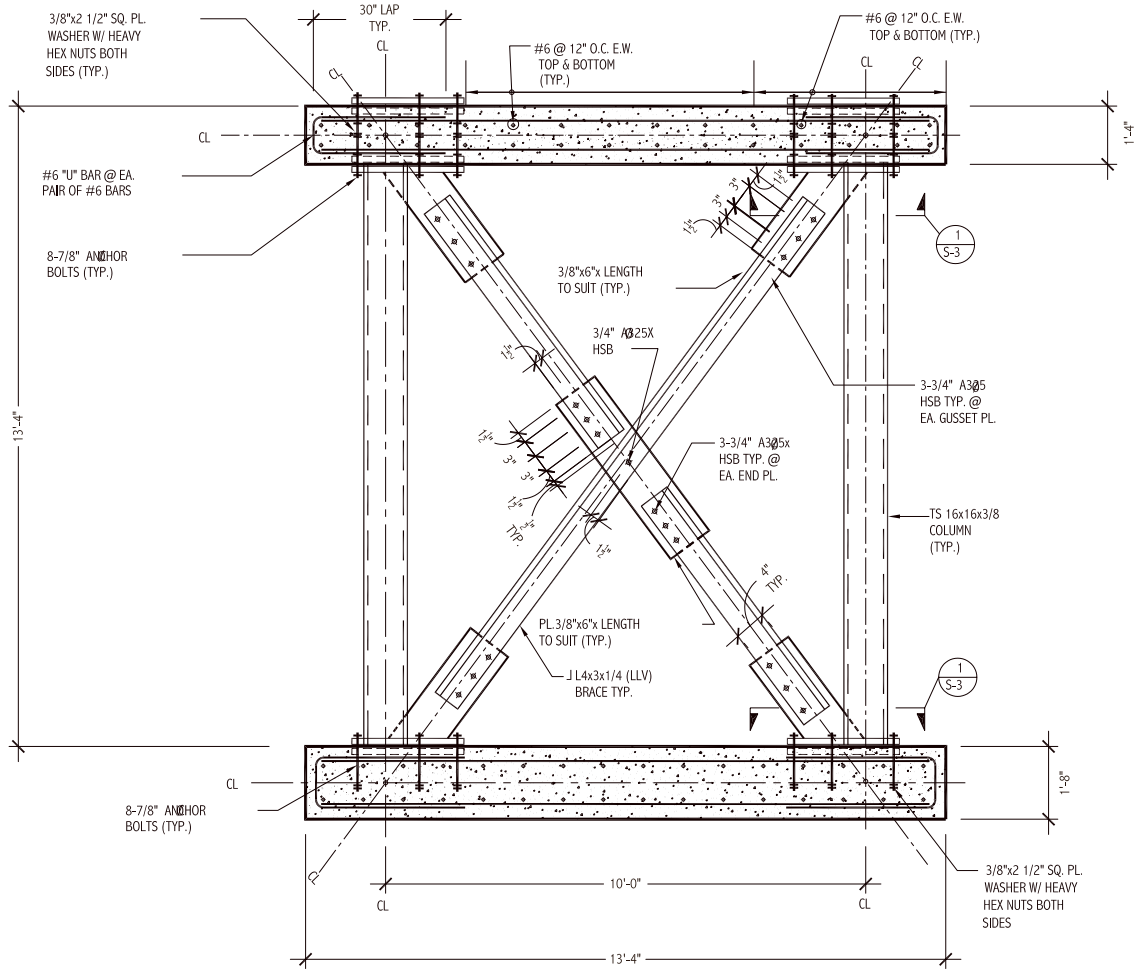

Figure 8: 2D drawing of the final design and construction details of the SFSI Test Structure.

3.3 Sensor Layouts and Descriptions

To perform accurate and comprehensive experimental research, many sensors are required to monitor a structural system. Questions for researchers monitoring a system would be: What to measure? How to measure? How frequently to measure? Where are the important locations to measure? Typical sensors for structural monitoring are comprised of vibration sensors (accelerometers), strain gauges, pressure sensors and so forth. There exist several different types of sensors pertinent to soil dynamics (*e.g.*, pore pressure sensors) as well.

The NEES facility at GVDA has a dense geotechnical array of accelerometers and pore pressure sensors, with both horizontal and vertical arrays of sensors. The accelerometers and pore pressure sensors throughout the site are installed for earthquake engineering and seismology research. Thus, this facility is a unique opportunity for a soil-structure interaction research because of the excellent site characterization and dense free-field ground motion monitoring. Figure 9 shows a schematic of the geotechnical array. For more details of the locations and types of available sensors at the site, see the report by Steidl and Nigbor (2004).

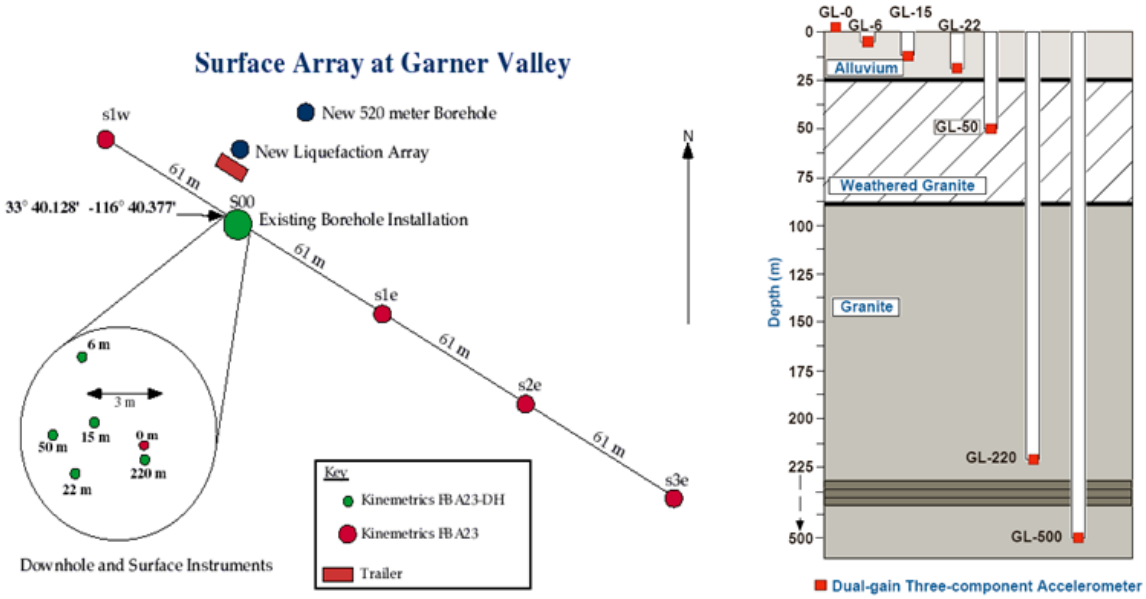

Figure 9: The distribution of the sensors, horizontally and vertically, throughout the GVDSA site for recording the ground motion.

Similarly, to measure and monitor the structure's response, the SFSI Test Structure has also been fully instrumented as shown in Figure 10. This sensor system was designed by a team that included the author of this dissertation, and was installed by a small team Consisting of Ali Asghari, Navid Nastar, and Robert Nigbor.

Sensors used on the SFSI structure include: accelerometers, soil pressure sensors, pore pressure sensors, displacement sensors, and a rotational sensor. The accelerometers are Applied MEMS SF1500S sensors, based on micro-electro-mechanical (MEMS) technology. They have a full-scale range of +/-3*g* and a resolution of abut 1 micro *g*. Their frequency response is flat from 0 to 1000 Hz. One tri-axial accelerometer package

is installed at the bottom of a 5 meter cased borehole directly underneath the middle of the bottom slab. The others are bolter to different locations on the top and bottom slabs.

Four pressure cells were also installed, one at each corner of the foundation, after precise dynamic calibration and careful installation during construction. Figure 10 includes a photo of the sensor, which consists of an 18-inch diameter, 1 inch high closed stainless steel bellows with rigid stainless steel pressure lines connected by welding. The actual sensing mechanism is a strain gage-based pressure transducer at the free end of the stainless steel tubing. These sensors were placed on graded and leveled native soil below the bottom slab, and were tied to the reinforcing steel cage prior to pouring concrete. Pressure lines were purged after slab curing to set a new baseline "zero" pressure at the full weight of the structure. Note that these are dynamic pressure sensors capable of measuring frequencies from about 0–20 Hz, covering the earthquake frequency range.

Four string pot displacement sensors were installed at the bottom corners of the bottom slab to measure uplift. The potentiometer bodies are attached to the concrete slab, and the tensioned cable is attached to a 2 m-long metal rod driven into the soil directly below the slab corner.

All structural sensors were housed in weatherproof enclosures and their cables are routed through watertight conduit back to the recording system.

In addition to the structural sensors, several sensors for measuring the environmental parameters (*e.g.*, ambient temperature) and ground water level were installed. A complete list of structural sensors is tabulated in Table 2. The exact location of each sensor and the channel number to which it is connected to the data acquisition system is also depicted in Figure 10.

After the original construction of the SFSI site, to collect the preliminary data described in the next section, the structure was equipped with two additional sets of sensors to log the ambient temperature and water table level under the structure on an hourly basis. Self-contained temperature loggers (Onset Instruments "Hobotemp") were placed in the soil under the bottom slab and underneath the top slab to measure soil and air temperatures, respectively.

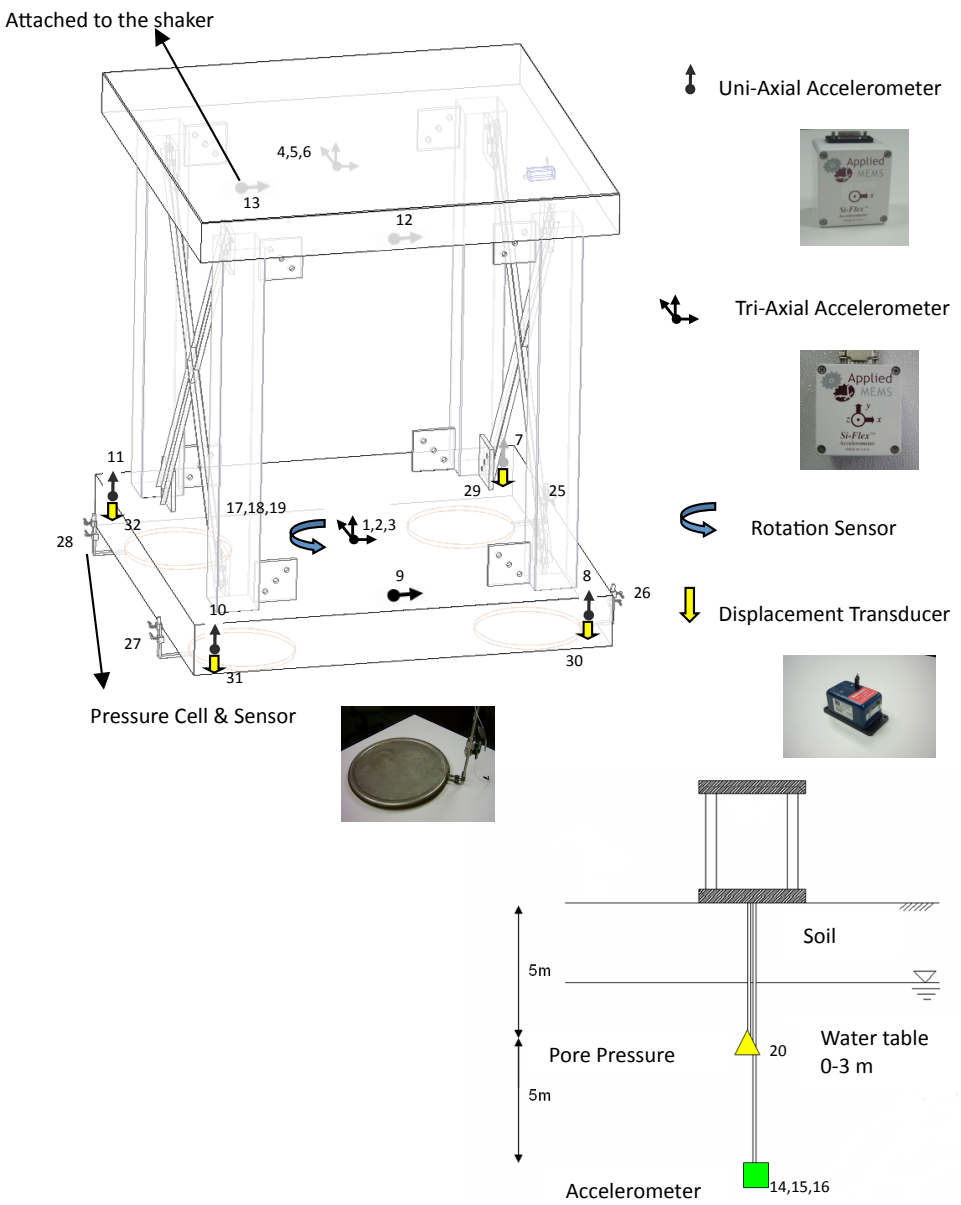

Figure 10: Sensor descriptions and locations on/under the SFSI Test Structure.

Table 2: SFSI test structure sensor locations, types and channel numbers.

Channel No.	Type of Instrument	Location
1	Tri-axial Accel. (*x*)	Bottom Slab
2	Tri-axial Accel. (*y*)	Bottom Slab
3	Tri-axial Accel. (*z*)	Bottom Slab
4	Tri-axial Accel. (*x*)	Top Slab
5	Tri-axial Accel. (*y*)	Top Slab
6	Tri-axial Accel. (*z*)	Top Slab
7	Uni-axial Accel. (*z*)	Bottom Slab
8	Uni-axial Accel. (*z*)	Bottom Slab
9	Uni-axial Accel. (*x*)	Bottom Slab
10	Uni-axial Accel. (*z*)	Bottom Slab
11	Uni-axial Accel. (*z*)	Bottom Slab
12	Uni-axial Accel. (*x*)	Top Slab
13	Uni-axial Accel. (*x*)	Shaker
14	Tri-axial Downhole Accel. (*x*)	Under the Soil
15	Tri-axial Downhole Accel. (*y*)	Under the Soil
16	Tri-axial Downhole Accel. (*z*)	Under the Soil
17	Rotation Sensor (x-x)	Bottom Slab
18	Rotation Sensor (y-y)	Bottom Slab
19	Rotation Sensor (z-z)	Bottom Slab
20	Pore Pressure	Under the Soil
21	Spare	n/a
22	Spare	n/a
23	Spare	n/a
24	Spare	n/a
25	Soil Pressure Sensor	Bottom Slab
26	Soil Pressure Sensor	Bottom Slab
27	Soil Pressure Sensor	Bottom Slab
28	Soil Pressure Sensor	Bottom Slab
29	Displacement Transducer	Bottom Slab
30	Displacement Transducer	Bottom Slab
31	Displacement Transducer	Bottom Slab
32	Displacement Transducer	Bottom Slab

After the original construction of the SFSI site, to collect the preliminary data described in the next section, the structure was equipped with two additional sets of sensors to log the ambient temperature and water table level under the structure on an hourly basis.

A small electromagnetic shaker has been installed under the roof slab to allow active, low-strain modal testing and experimentation. The shaker's specifications provided by the manufacture, APS Dynamic Electro-Seis, are as follows: Long Stroke Shaker Model 400, 100 lb (400 N) force, 30 inch/s velocity, 6.25 in peak-to-peak stroke. To monitor the input force applied to the system by the shaker, a uni-axial accelerometer was also attached on top of the shaker.

3.4 Data Acquisition (DAQ) System

The data acquisition (DAQ) system specification must be defined in accordance with certain criteria including the number of sensors, the precision and bandwidth required for transmitting data, etc. Since the location of the NEES site is fairly remote, a DAQ system with real-time remote data transmission capability was one of the main requirements. The high performance system that was customized for this project is a 32-channel real-time data acquisition and analysis system, with manual and event driven triggering (on any 10 channels). The system has a sampling rate of up to 500 samples per second per channel with 24-bit digital resolution. For most of the data collection described herein, a sampling

rate of 200 samples per second was utilized. The system also offers an extensive set of remote tools for real-time monitoring, broadcasting streaming data (Internet, TCP, and FTP), remote tele-control, and event driven notification. This DAQ system has been customized by the Digitexx Company (http://www.digitexx.com) in desired ways to provide remote sensing functionalities for the project (Figure 11). The real-time features integrated with the DAQ system are: real-time response spectrum, real-time FFT, real-time transfer function, a remote event-driven triggering mechanism and on-demand and scheduled remote recording for statistical analysis studies.

Figure 11: The data acquisition (DAQ) system used for the SFSI test structure monitoring.

Digitexx's DAQ system has several useful features such as high performance scalable data acquisition software with multiple filtering and data recording and broadcasting options. The interface of the program (Figure 12) provides a user-friendly control panel to select, edit and mange the recording options (*i.e.*, sampling rate, buffer size, averaging option, multiple filtering, etc.).

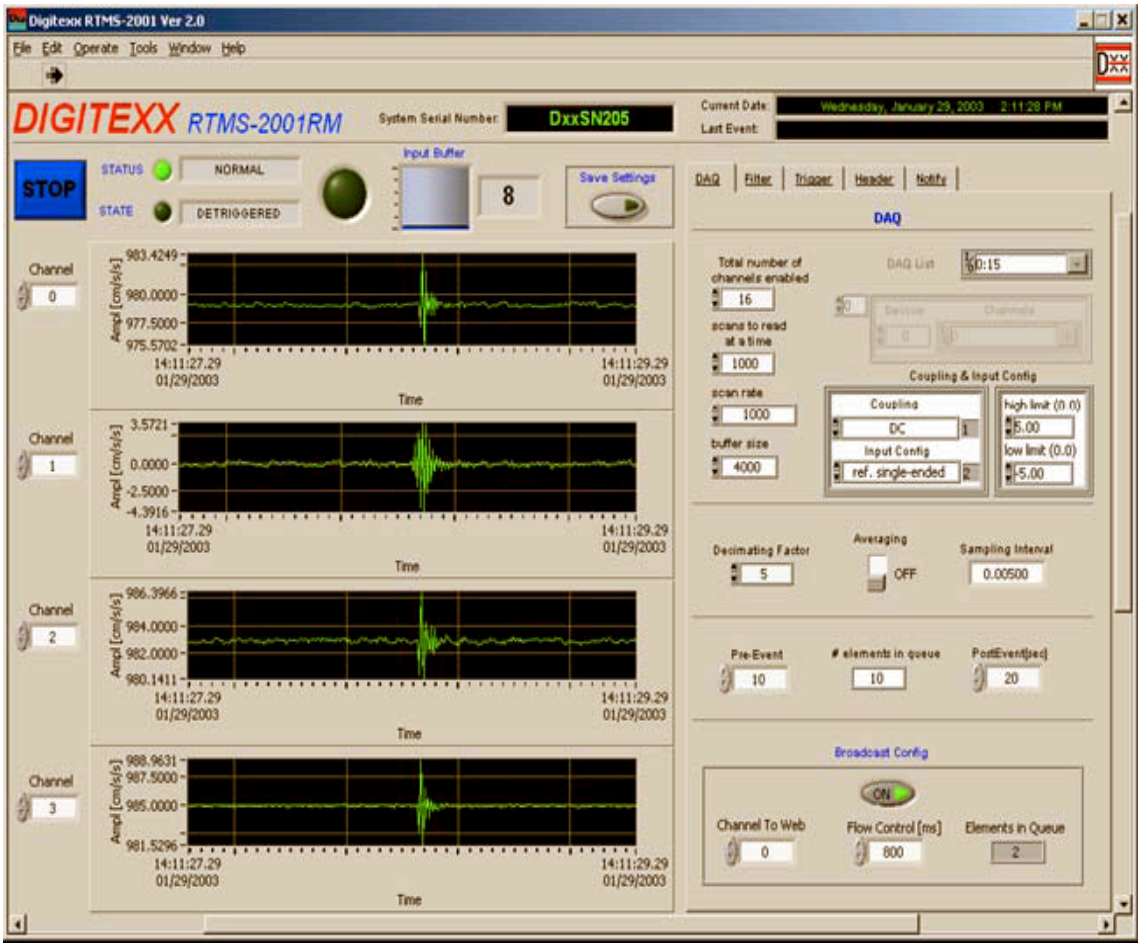

Figure 12: Snapshot of the user interface of the DAQ system.

As illustrated in Figure 13, the end-user features of the system assist in performing some preliminary real time analyses, such as real-time monitoring of all channels, real time FFT, on-demand and scheduled recording, etc.

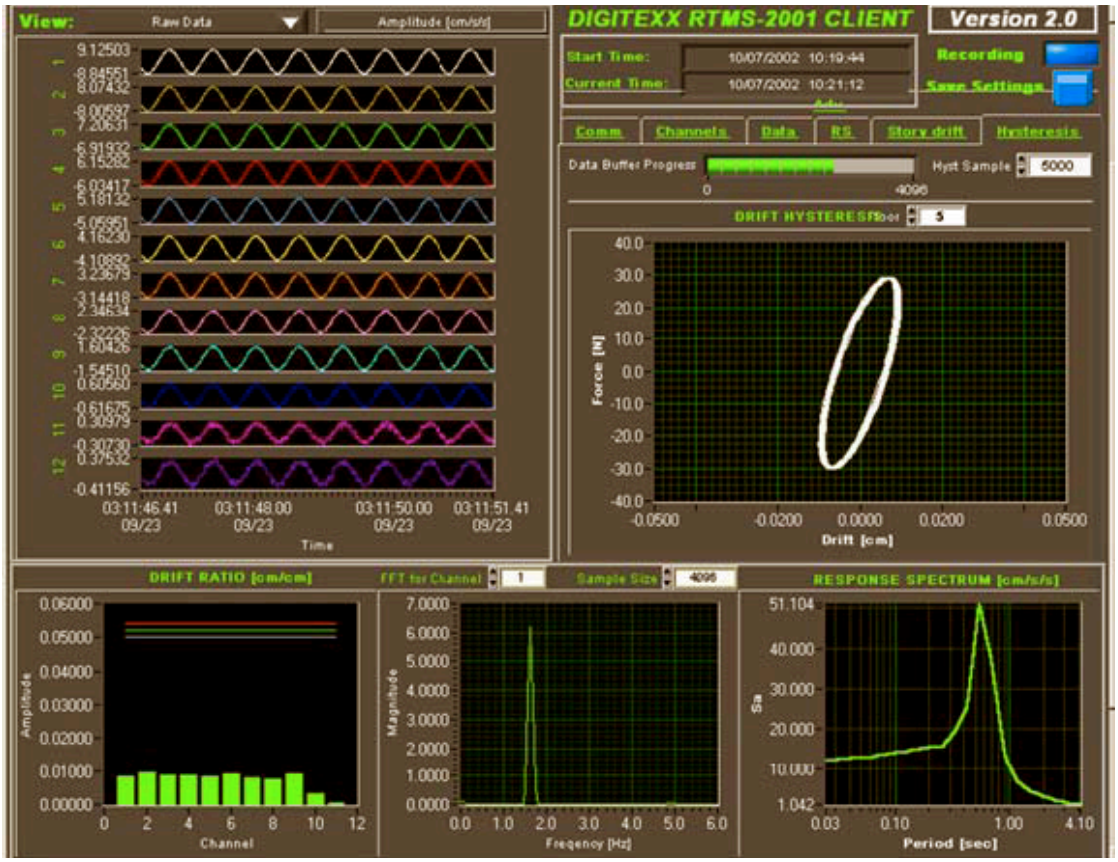

Figure 13: Real-time features integrated with the DAQ system.

4 Modal Properties Identification and Environmental Effects

4.1 Introduction

System identification for structural health monitoring purposes is often performed via modal parameter estimation. It is commonly known that the Experimental Modal Analysis (EMA) underwent a radical change with the implementation of the Fast Fourier Transform (FFT) in early 1970s. A set of modal characteristics (*e.g.*, modal frequency, modal damping value and mode shape) can be used to represent the modal behavior of a linear structure.

Depending on the source of excitation, vibration-based EMA methods are categorized as either forced vibration induced by an actuator, or ambient vibration relying on natural excitation. Forced vibration is typically used when both the input(s) and the output(s) of a system are easily producible and measurable. Nevertheless, the application of ambient category (output-only EMA) methods is growing fast, not only in civil engineering, but also in mechanical and aerospace engineering (*e.g.*, to obtain the modal parameters of a building or a car in road testing). There are numerous algorithms available that can be used for each category to assist the system identification process. In this current work, the combination of two widely-used methodologies (*i.e.*, the Natural Excitation Technique and the Eigensystem Realization Algorithm) along with impulse response analysis are used.

The development of the Natural Excitation Technique (NExT) by James *et al*. (1992, 1993, and 1996), Farrar and James (1997) and Beck *et al*. (1994a, b, 1998) was a step forward in identification of structures using response data only. Using NExT, assuming stationarity of the input, one can convert the forced stochastic response to a deterministic free vibration response. The cross-correlation function between the response vector and the response of a selected reference degree-of-freedom (DOF) satisfies the homogeneous equation of motion, provided the excitation is a stationary random noise. If the response vector happens to coincide with a particular degree of freedom to be studied, the auto-correlation function would be used accordingly. The Eigensystem Realization Algorithm (ERA) (Juang and Pappa, 1985) can then be used to identify the modal parameters of the system from the auto/cross correlation record.

4.2 Methodologies

To assure that the data collection/analysis or system identification is performed with minimum uncertainty, there are many guidelines to be considered. To identify a particular mode of a structure, the output data (location of the sensors) and the input (source of excitation) should be carefully defined. They can be controlled to minimize distortion or nonlinear response of the structure.

Furthermore, since there is always a well-known resolution trade-off between time-domain and frequency-domain approaches, a systematic trial and error approach is required to choose the right components for data processing that compromise on window size, overlap of the windows, etc. For instance, in EMA it is commonly known that, for averaging given time domain data, the window size must be large enough to include at least 20 cycles of the first fundamental mode of the system. On the other hand, if the window size is very large compared to the record length, it will result in less averaging and more noisy correlation time histories.

That said, an accurate experimental modal analysis, in fact, requires a great deal of experience when it comes to deciding the right testing approach and the data processing. Despite the presence of uncertainties, utilizing different methodologies that converge to a consistent set of results increases the level of confidence in the system identification process; therefore, for the SFSI test structure, various methodologies with different sources of excitations were utilized.

4.3 Sources of Excitation

The NEES site facility, as discussed in detail in the previous chapter, has been designed and equipped to be capable of undergoing various forced vibration tests. As shown in

Figure 14, several possible real and artificial sources of excitation can be used at the NEES facility.

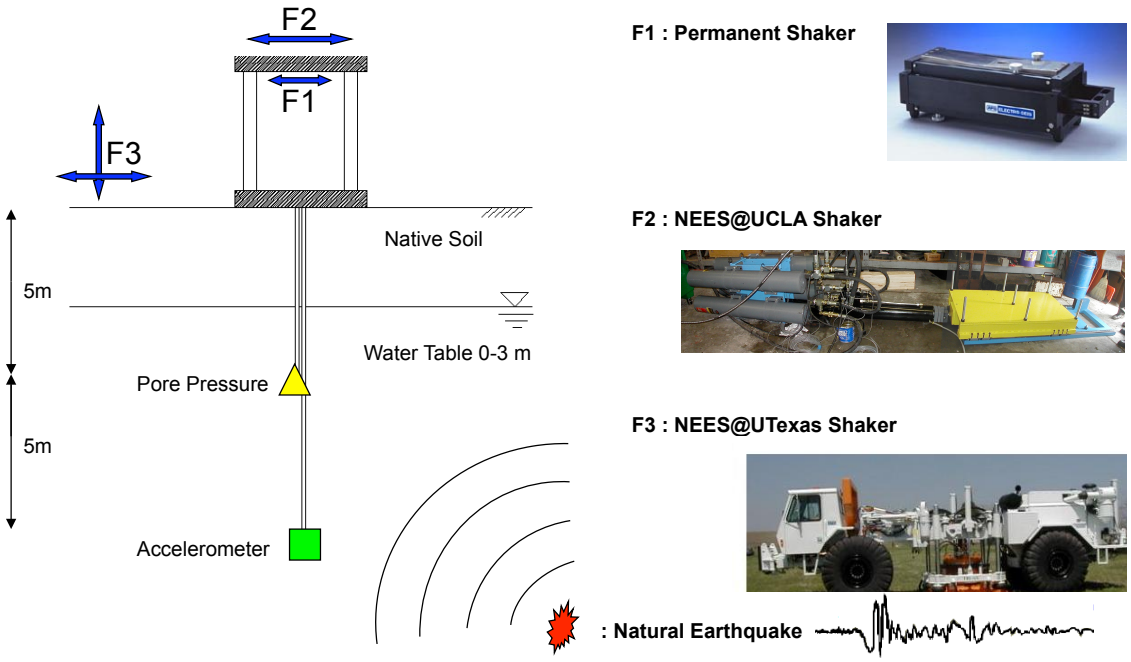

Figure 14: Different possible sources of excitation at the NEES facility site include: F1: Permanent Shaker, F2: NEES@UCLA Linear Shaker, F3: NEES@UTexas Mobile Shaker and natural earthquakes at the site.

Note that some of the equipment are permanently installed at the site and have the capability to be controlled remotely over the internet. There are also other mobile sources of the excitation that could be borrowed from other NEES facilities such as the NEES@UTexas mobile shaker and NEES@UCLA's linear shaker.

To identify the first (rocking) mode frequency of the SFSI test structure, as a first estimate, a sinusoidal sweep signal with various frequency content (*e.g.*, 5 to 25 Hz) is introduced by the shaker on top slab. It is expected that the response of the top slab is larger at certain frequencies of excitation than at others due to the resonance phenomenon. However, modal parameter estimation relying on the excitation induced by the shaker on top of the structure has limitations, because (1) the signals are subject to shaker-structure interaction; (2) the shaker bandwidth may be restricted. Thus, to verify the natural frequencies, the NEES@UTexas mobile shaker, which has the capability of producing waves from shaking the ground both horizontally and vertically, was also used. Figure 15 shows the responses of the top slab (dashed line) and bottom slab (solid line) due to the sweep sine waves induced by NEES@UTexas shaker. Clearly, the input/output signals are of high signal to noise ratio and the fundamental resonance frequency of the system, at which the response amplitude is maximized, can be identified to be 9 Hz. It is also important to remember when relying on both input (excitation) and output (response) signals, the data from all channels should be very well synchronized.

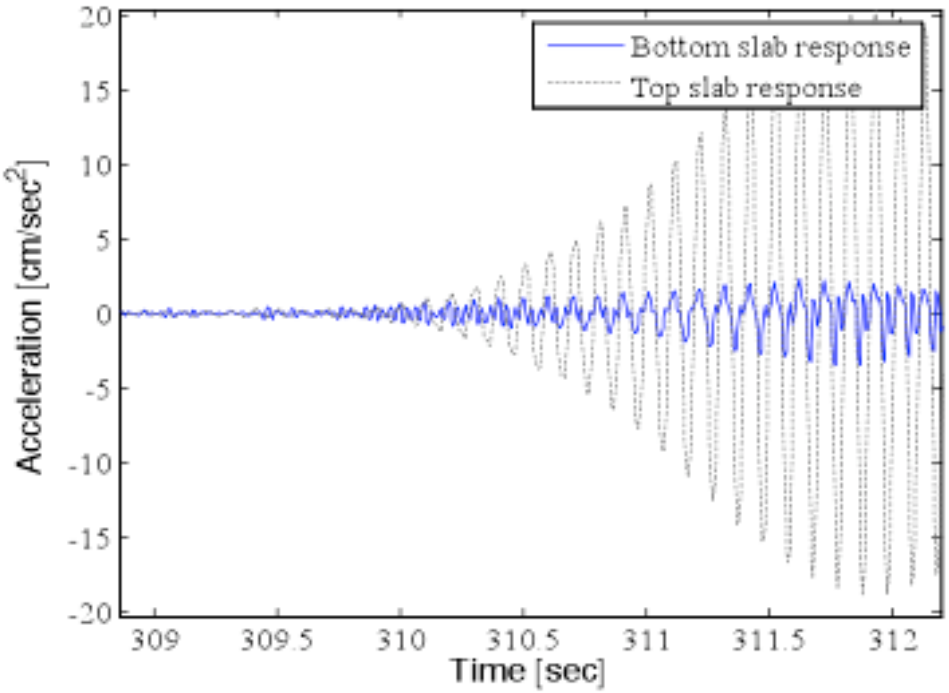

Figure 15: The response of the top Slab (dashed line) versus the bottom slab's response (solid line) induced by the UTexas shaker.

4.4 Impulse Response Measurement

The hammer test is another very common test to analyze the impulse response of the structure for modal parameter estimation. Even though a hammer is a very simple source of excitation, the result can be very informative and reproducible. However, as stated by Brown *et al*. (1977), it is recognized that there are certain limitations associated with the hammer test (*e.g*., relative less control over the frequency content of the excitation).

Not only is it used for the frequency identification of the SFSI test structure, but also for the damping coefficient estimation of the few first modes of vibration (including the

torsional mode). For modal frequency estimation, the time-domain response can be transformed (*e.g.*, by FFT, PSD, etc.) to the frequency domain. In order to accumulate sufficient energy in the output signal—which will result in better frequency-domain analysis—several time-domain impulse responses of the top slab are joined together (each response will be added to the end of the other) and then are utilized for frequency-domain transformation. As far as the windowing for FFT analysis is concerned, the interval of the impulse responses (in time-domain) are preferred to be evenly distributed over time beforehand. For building structures, 10 impacts typically are required (Reynolds and Pavic, 2000).

4.5 Curve Fitting Approach

For estimating modal properties from measured data, numerous algorithms have been developed and implemented in different formats. One of the common methodologies is based on the least squares (*i.e.*, curve fitting) tools. Excellent overviews of most of the previously proposed algorithms and a mathematically consistent reformulation of those have been presented by Allemang and Brown (1998).

In this current work, by utilizing MATLAB's system identification toolbox, and by exploiting the curve fitting approach, the modal parameters of the SFSI Test Structure were analyzed and identified. The drawback of using the curve fitting tool in MATLAB

is that the initial guess should be in the vicinity of the answer otherwise some misleading results might be obtained.

For a (single degree of freedom) mass-spring-dashpot model, shown in Figure 16, the equation of motion can be written as:

$$\ddot{x} + 2\zeta\omega_n\dot{x} + \omega_n^2 x = \frac{F}{K}\omega_n^2 = \frac{F}{m} \tag{6}$$

where ζ is the damping ratio ($c/c_{critical}$), ω_n is the natural frequency, m is the mass, K is the stiffness, F is the excitation force and $c_{critical} = 2m\omega_n$.

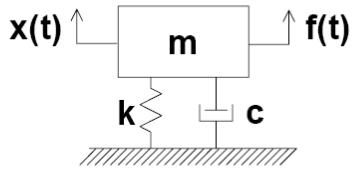

Figure 16: Single Degree Of Freedom (SDOF) mass-spring-dashpot model.

Prior to the curve fitting process in the frequency domain, the frequency response function (FRF) of the system is required. The FRF is simply a complex transfer function, formed from either measured data or analytical functions, with real and imaginary components. It represents the structural response (displacement, velocity, or acceleration) to an applied force as a function of frequency.

The transfer function from force to displacement (representing the inverse of dynamic stiffness), is called the receptance (or compliance) function and can be written as:

$$TF_{\mathrm{d}}(\omega) = (1/K)\frac{\omega_{\mathrm{n}}^2}{(\omega_{\mathrm{n}}^2 - \omega^2 + 2i\zeta\omega_{\mathrm{n}}\omega)} \tag{7}$$

where $i = \sqrt{-1}$. The accelerance function (acceleration response over the force), similarly would be written

$$TF_{\mathrm{a}}(\omega) = (1/K)\frac{-\omega^2\omega_{\mathrm{n}}^2}{(\omega_{\mathrm{n}}^2 - \omega^2 + 2i\zeta\omega_{\mathrm{n}}\omega)} \tag{8}$$

The accelerance magnitude is:

$$\left|TF_{\mathrm{a}}(\omega)\right| = (1/K)\frac{-\omega^2\omega_{\mathrm{n}}^2}{\sqrt{(\omega_{\mathrm{n}}^2 - \omega^2)^2 + (2\zeta\omega_{\mathrm{n}}\omega)^2}} \tag{9}$$

or

$$\left|TF_{\mathrm{a}}(\omega)\right| = (1/m)\frac{-\omega^2}{\sqrt{(\omega_{\mathrm{n}}^2 - \omega^2)^2 + (2\zeta\omega_{\mathrm{n}}\omega)^2}} \tag{10}$$

For preliminary modal parameter identification, the SFSI test structure is assumed to be a linear SDOF system. The results of the experimental data (from forced vibration testing) can be fit to the analytical FRF of the assumed SDOF system; two scenarios are considered:

1. Sinusoidal sweep signals as excitation, which are induced by the shaker on the top slab (mainly used for the rocking frequency identification).

2. By suddenly turning off the shaker at the resonance frequency, a free vibration is created, which is used for estimating the damping coefficient.

Given the input signals and by measuring the output response, the frequency response function of the structure is computed. Knowing the weight of the shaker and the acceleration of the shaker (one accelerometer is attached on the shaker), the input force is known. Thus, by measuring the output (acceleration) of the structure response on the top slab, the accelerance function magnitude can be plotted as depicted in Figure 17 (dotted line). Clearly, two additional modes are present. Therefore, a linear transfer function (TF) from the superposition of three SDOF accelerance function is fit to the data. The mathematical equation of the curve is obtained by summation of each function as follows:

$$|TF_{\mathrm{a}}(\omega)| = \sum_{\varphi=1}^{3} (1/_{m_{\varphi}}) \frac{-\omega^2}{\sqrt{(\omega_{\mathrm{n}_{\varphi}}^2 - \omega^2)^2 + (2\zeta_{\varphi}\omega_{\mathrm{n}_{\varphi}}\omega)^2}} \tag{11}$$

The best fit 3DOF transfer function (solid line) in Figure 17, computed by the curve fitting tool of MATLAB, is used to estimate the modal properties. The two additional peaks in the frequency domain are speculated to represent the bracings' vibration modes. The estimated frequencies and damping ratios corresponding to the SFSI test structure rocking mode and two additional modes are tabulated in Table 3.

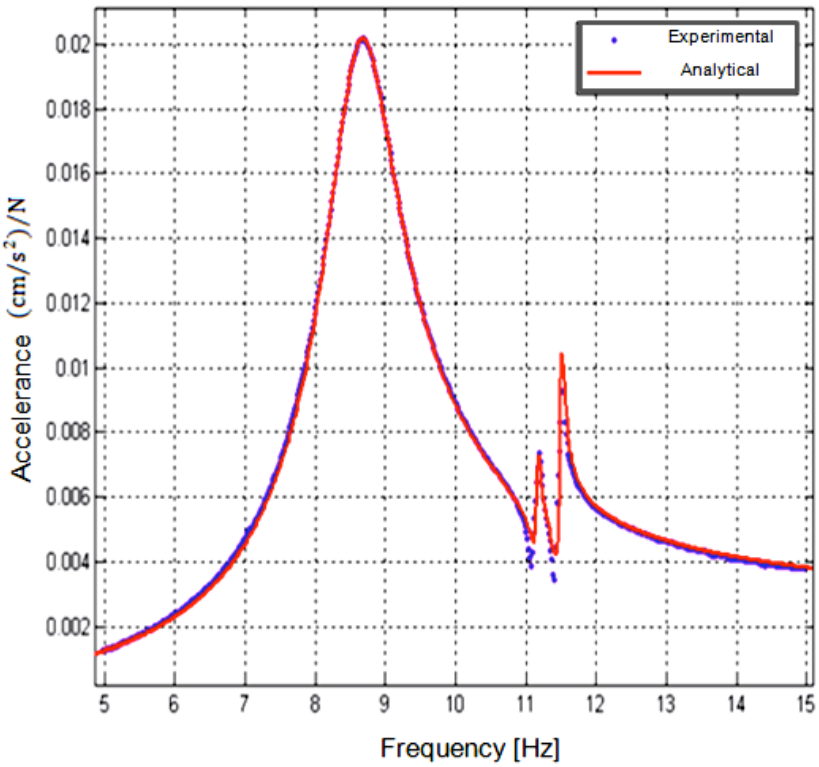

Figure 17: 3DOF transfer function curve fit to the SFSI frequency response.

Table 3: Identified model properties utilizing the curve fitting technique.

Mode	Frequency [Hz]	Damping ratio
Rocking	8.65	0.0612
Bracing?	11.16	0.0029
Bracing?	11.50	0.0035

To better understand the cause for the two additional peaks in the experimental FRF of the SFSI test structure, the effect of out-of-plane vibration of the bracings is studied. To do so, the response of the bracings in a forced vibration experiment must be analyzed. Therefore, an accelerometer is attached on the bracing intersection — sensing the *y*-*y* direction in Figure 18 — while the response of the structure perpendicular to the bracings plane (*i.e.*, the *y*-*y* direction under the top slab) is measured.

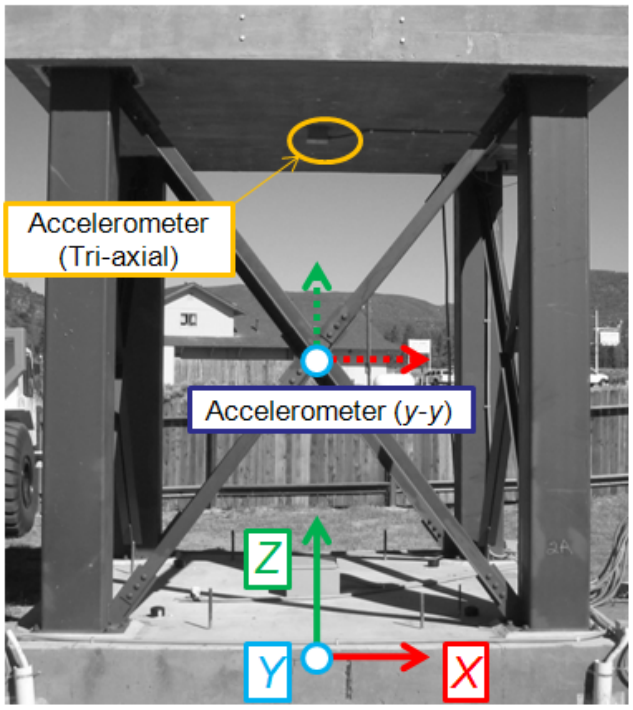

Figure 18: The location of the accelerometer measuring acceleration on *y*-*y* direction.

The accelerance function of the bracings, along with that of the top slab of the SFSI test structure, is plotted in Figure 19. The peaks of the FRF confirm the hypothesis that the

two extra peaks occurred due to the bracing modes in perpendicular direction of the rocking vibration. In the figure, the dotted line shows the transfer function of the bracings, whereas the blue solid line shows the accelerance of the top slab of the SFSI test structure. In fact, Figure 19 clearly shows that the bracing has a mode (black circle) that exactly coincides with one of the peaks observed in the top slab transfer function (solid line). Thus, the hypothesis of the effect of the bracings on the top slab accelerance is validated.

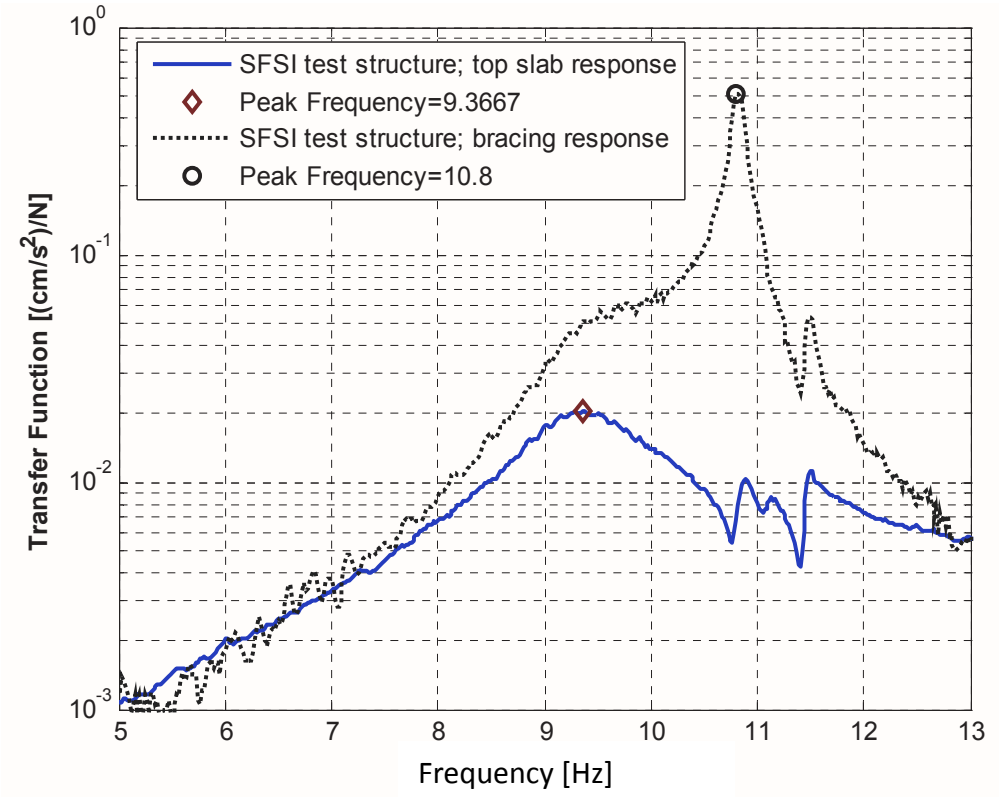

Figure 19: The accelerance function of the SFSI test structure; bracing response (green line) and the top slab response (solid line).

It is important to note that the identified frequency from this experiment (~9.37 Hz) is slightly different from the result of the curve fitting approach reported in Table 3. Since these two experiments were not performed at the same time, could environmental effects justify this? In Section 4.7, which discusses the correlation of frequency variations with temperature effects, it is seen that removing the bracings significantly reduces the variations in the identified frequency.

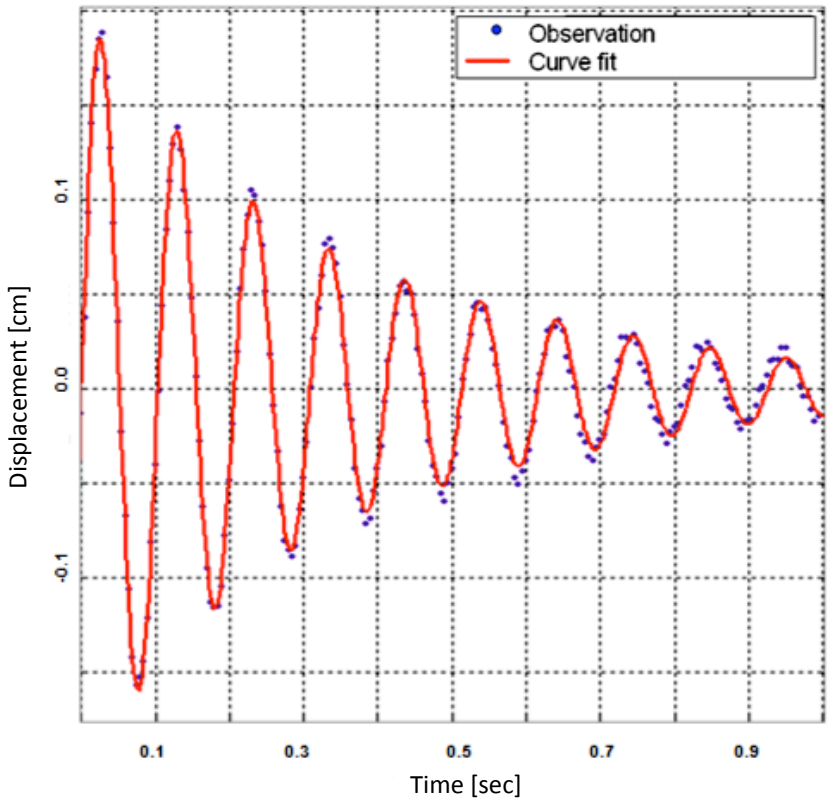

Figure 20: Time-domain curve fit to the measured displacement from a pressure cell underneath the structure induced by a free vibration.

The SFSI system parameter identification is also performed in the time domain. By suddenly turning off the shaker after exciting at the resonance frequency, a free vibration is created which can be used to estimate modal parameters. For instance, the signals from the pressure cells underneath the structure (sensing the displacement of the corners of the foundation) can be utilized for rocking mode parameter estimation. In Figure 20, the displacement of the SDOF system — formulated in (12) — is plotted as solid red line chose to fit the measured response (plotted as dotted blue line). The graph shows how the rocking motion of the foundation is very similar to a damped SDOF system, the displacement of which (for free vibration) can be formulated as:

$$x(t) = e^{-\zeta\omega_n t}\left\{x(0)\cos(\omega_d t) + \left[\frac{\dot{x}(0) + (\zeta\omega_n)x(0)}{\omega_d}\right]\sin(\omega_d t)\right\} \tag{12}$$

where $\omega_d = \omega_n\sqrt{1-\zeta^2}$ is the damped natural frequency.

4.6 Identified Parameters, Observations and Environmental Effects

It is well-known that there are many sources other than damage that can cause variations in identified dynamic properties of a structure. These sources of variation can be divided into three main categories: (1) environmental conditions, such as temperature variation and soil condition, (2) operational conditions, such as traffic conditions and excitation

sources, and (3) measurement and processing errors, including non-stationarity, measurement noise and errors associated with digital signal processing. In this current research, two major environmental effects on the identified modal properties are studied: first the correlation of the identified rocking frequency with the ambient air temperature and, secondly, its correlation with the water-level under the foundation.

In order to monitor the system over a long period, acceleration response data, from both ambient and forced vibration tests, were taken periodically at the site over 18 months during 2005 and 2006. Air and soil temperatures, soil pore pressure and water table level were also monitored on an hourly basis to study short-term and long-term environmental effects on the apparent frequency of the structure. Utilizing different system identification techniques discussed previously, the modal properties of the SFSI Test Structure were identified and their correlations with environmental effects were studied.

4.7 Temperature Dependency

To analyze the effect of the temperature and its correlation with the identified frequency, a systematic procedure was implemented to collect the ambient vibration data while the ambient temperature was measured under the top slab by a temperature sensor. As illustrated in Figure 21, the typical variation of the identified fundamental natural frequency (first mode) of the structure over a period of a couple days shows 10%

fluctuation of the identified frequency in a daily basis, with an increase in the rocking frequency during the day time that starts to decrease in the afternoon. As illustrated in Figure 22, the correlation between the collected temperatures and the identified frequency over a two-day period is evident.

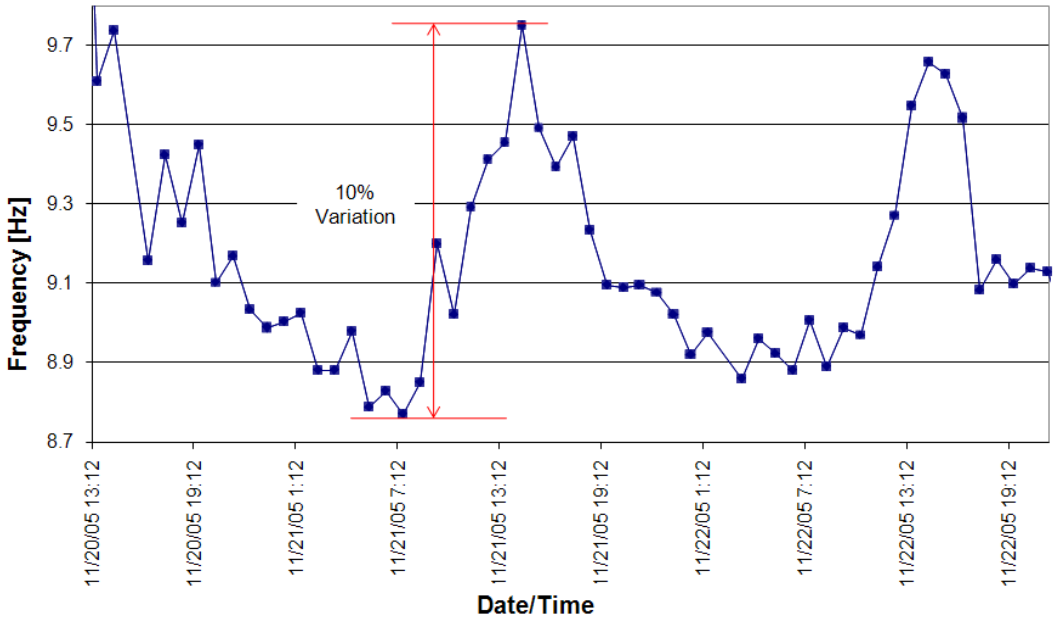

Figure 21: Typical daily variation in the identified rocking frequency of the SFSI Test Structure from 11/20/05 to 11/23/05.

In Figure 23, the scatter plot of 520 identified frequencies during 18 months and their corresponding ambient temperatures is shown; the positive correlation can again be observed.

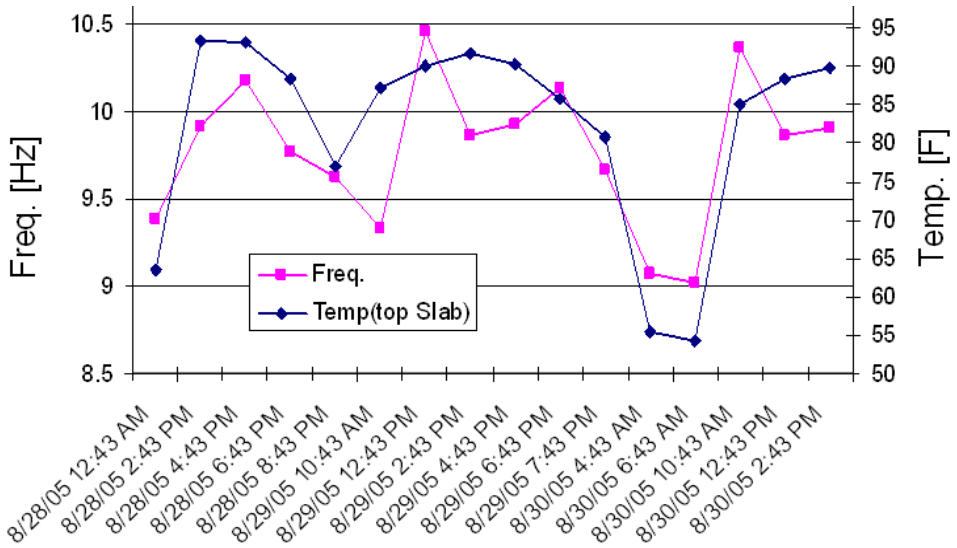

Figure 22: First mode (rocking) frequency in East-West direction of the SFSI Test Structure (pink squares) and ambient temperature recorded from 8/28/2005-8/30/2005 (blue diamonds).

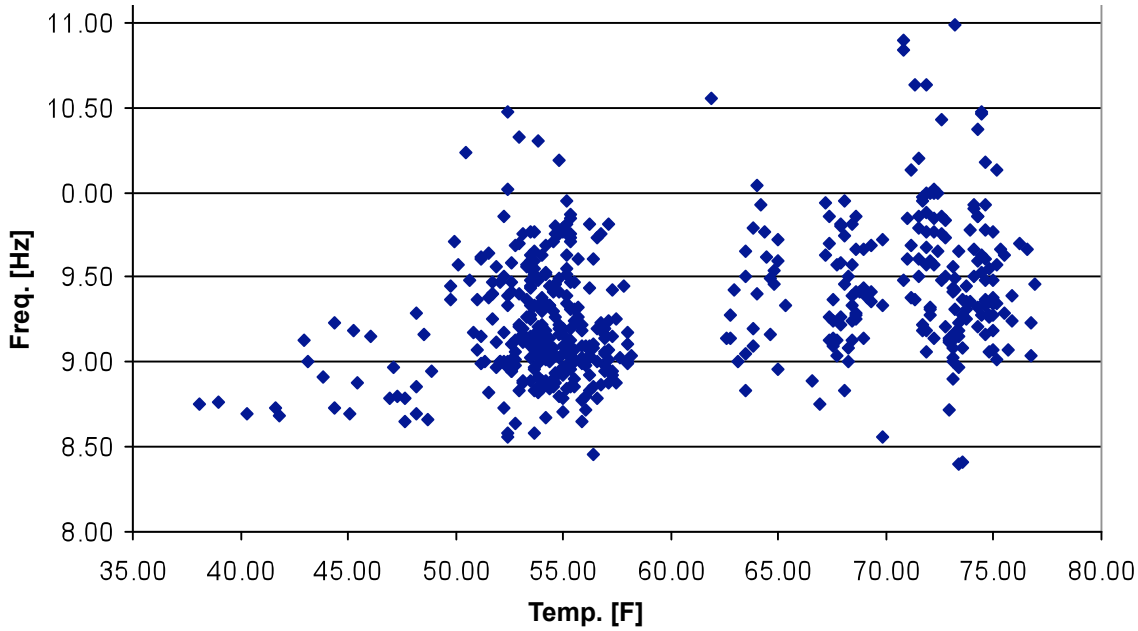

Figure 23: Identified rocking frequency versus the ambient temperature during the 18 months in 2005-2006.

Since the SFSI test structure is an open frame structure, it was speculated that the bracings contributed significantly to the variation of the identified modal frequencies as temperature changed. To verify this speculation, the bracings were removed from all faces of the structure and data were again collected with a similar procedure.

Figure 24: Picture of the SFSI Test Structure after the bracings were removed.

Obviously, the rocking frequency decreased (from about 9Hz to about 6Hz) but, interestingly, the daily variation of the identified frequency reduced significantly as well. As illustrated in Figure 25, the rocking frequency of the system, as well as its variation with respect to temperature, has been significantly reduced (from 10% daily variation down to 3%) relative to the braced cases.

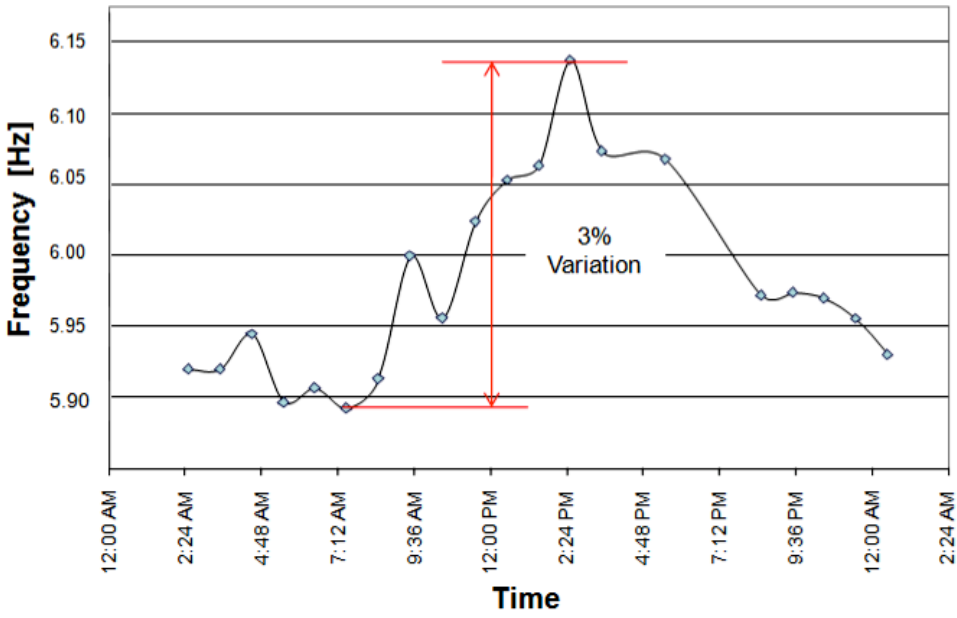

Figure 25: Typical daily variation of the identified rocking frequency of the SFSI Test Structure (recorded on 2 Jan. 2008) after the bracings were removed.

To see the variation in identified frequencies, the histogram of 520 identified frequencies for the braced configuration between 6/15/05 and 3/15/06 is plotted in Figure 26. The mean and standard deviation of the rocking frequencies are computed for both braced ad unbraced configurations. As shown in Figure 27, the estimated mean and standard deviation for the braced configuration are $\mu = 9.35\text{Hz}$ and $\sigma = 0.47\text{Hz}$. Fewer samples were available from the unbraced configuration; the estimated mean and standard deviations are $\mu = 6.02\text{Hz}$ and $\sigma = 0.07\text{Hz}$ respectively. The estimated coefficient of variation (CoV) for the braced and unbraced configurations are 5% and 1.1%, respectively.

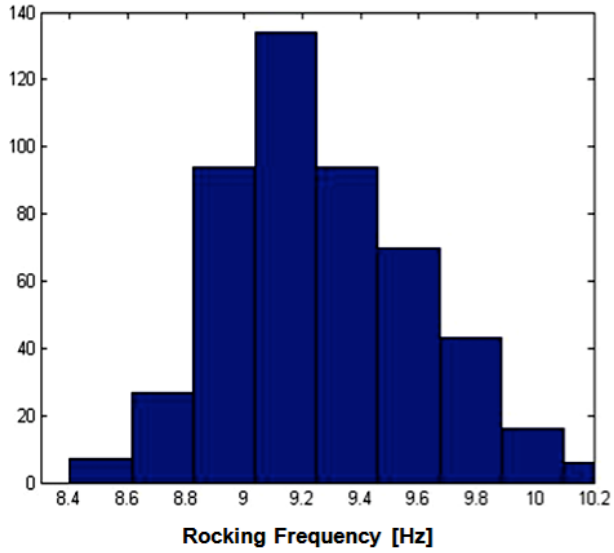

Figure 26: Histogram of 520 identified frequencies of the SFSI Test Structure between 6/15/05 and 3/15/06 in the braced configuration.

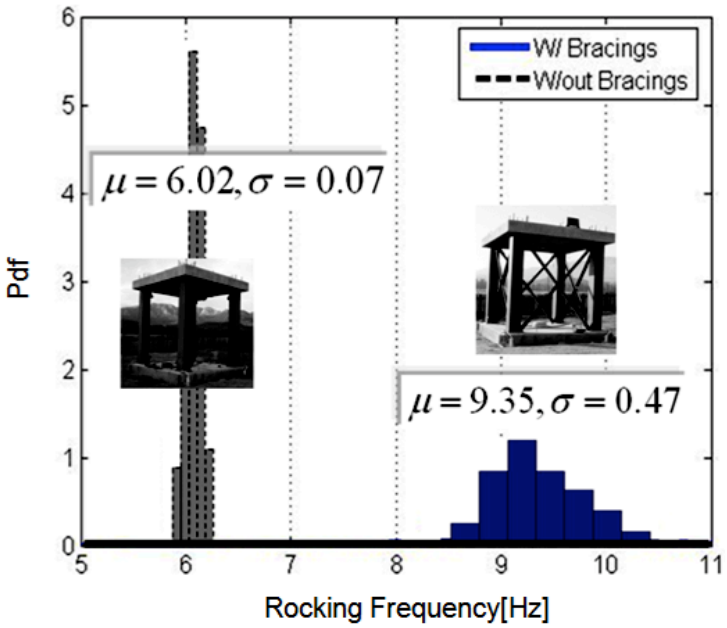

Figure 27: Probability density function (PDF) of identified frequencies; the blue solid line and black dash line demonstrate the distributions for the braced and un-braced configuration, respectively.

Because of the significant shifts in dynamic parameters from temperature effects, shifts due to damage may be masked by these environmental effects. Hence, damage detection would be more difficult in such cases. Consequently, understanding and detecting (quantifying), subtracting or/and cleansing the effect of temperature conditions on the estimated local and global structural parameters appears to be necessary. The regression analysis and a methodology to normalize the data in Chapter 7 for achieving more robust damage detection are developed to do this cleansing.

4.8 Ground Water-level and Soil Saturation Dependency

Rain may not only have mass and seepage pressure effects, but it also causes changes in the soil behavior. A study of the correlation between the identified frequency and rainfall was recently reported by Clinton *et al*. (2006). Their research focused on analyzing the impact of environment on vibration-based frequency identification of the Millikan Library, located on the campus of the California Institute of Technology (Caltech). In particular, they observed that during a two-day, 4 in. rainfall, natural frequencies increased by about 3%, returning to the nominal values in 1–2 weeks. They concluded that the rain induced increases in natural frequencies through an increase in soil-structure stiffness caused by soil saturation and, perhaps, soil swelling.

To investigate this phenomenon on the fully instrumented SFSI test structure at the NEES facility, the water level under the foundation (as opposed to rainfall) is measured and used herein. Even so the measurement of the ground water-level under foundations is practically more difficult than rainfall quantity but, the NEES facility provided fully instrumented structures including the water table sensors.

During the preliminary monitoring of the SFSI test structure between 6/17/2005 to 7/17/2005, an increasing trend in the identified rocking frequencies of the structure was noticed (Figure 28). Thus, besides the daily temperature effect, the question arose as to whether any other environmental variation (*e.g.*, ground water table) could have impact on the natural frequency of the structure.

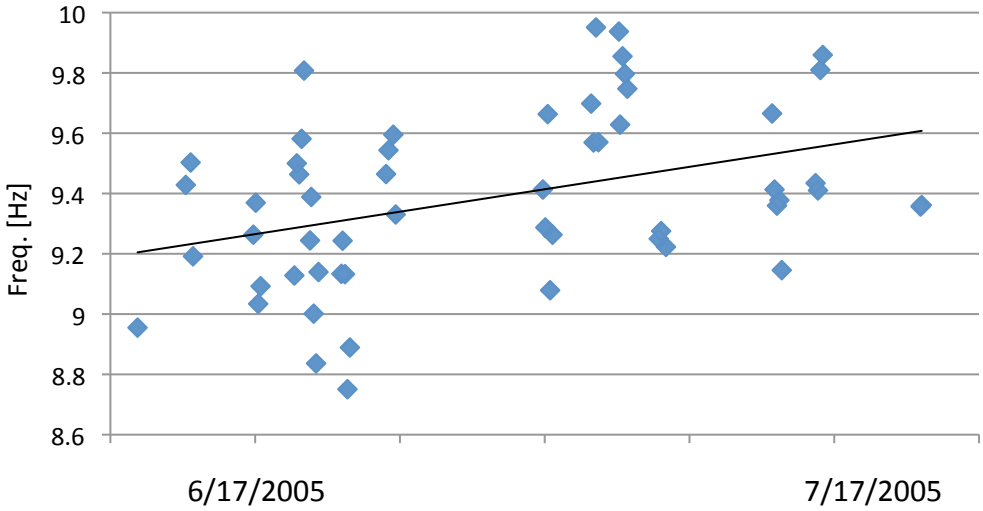

Figure 28: Observed trend of increases in the identified rocking frequencies of the SFSI test structure over one month (6/17/2005–7/17/2005).

As part of the sensor network at the site, the water-level sensors allowed the ground water table under the foundation to be monitored. Thus, changes in the dynamics of the soil-foundation-structure system in conjunction with the water-level fluctuations could be investigated. The water table level for the same monitoring period, 6/17/2005–7/17/2005, was logged. As shown in Figure 29, the water table under the foundation dropped during that time, albeit not very significantly. Thus, a longer monitoring period, particularly to investigate the effect of more significant variation of water table on the identified frequency, was planned.

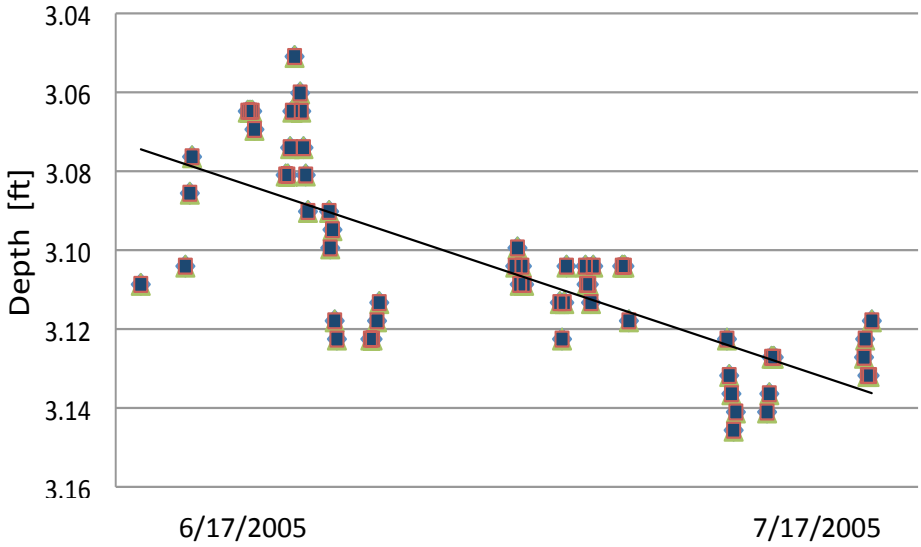

Figure 29: Measured ground water table under the SFSI test structure's foundation over one month (6/17/2005–7/17/2005).

The ground water table fluctuation under the SFSI test structure was monitored for a longer period, from Jun. 2005 to Sep. 2005 as illustrated in

Figure 30. The data collected from the site showed some correlation between the ground water-level and the identified rocking frequency of the structure. As illustrated in Figure 32, the identified frequency and water table as functions of time at the site between 6/17/05 through 9/4/05 for the braced configuration is graphed.

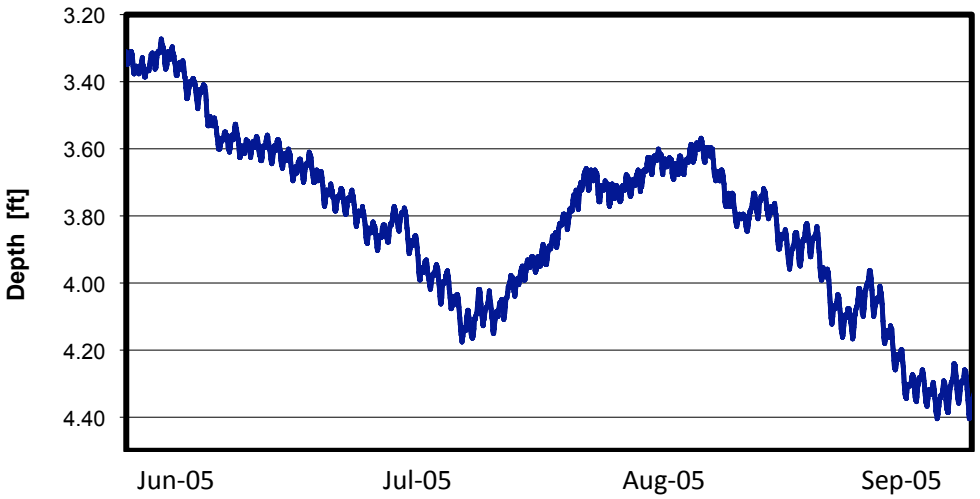

Figure 30: Fluctuation of the ground water table fluctuation under the SFS test structure

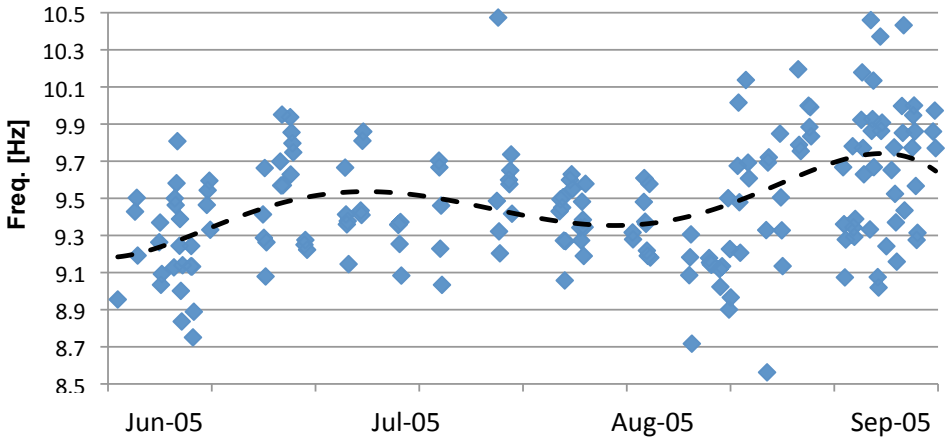

Figure 31: Variation in identified rocking frequencies of the SFSI test structure, and a polynomial trend line (dashed line)

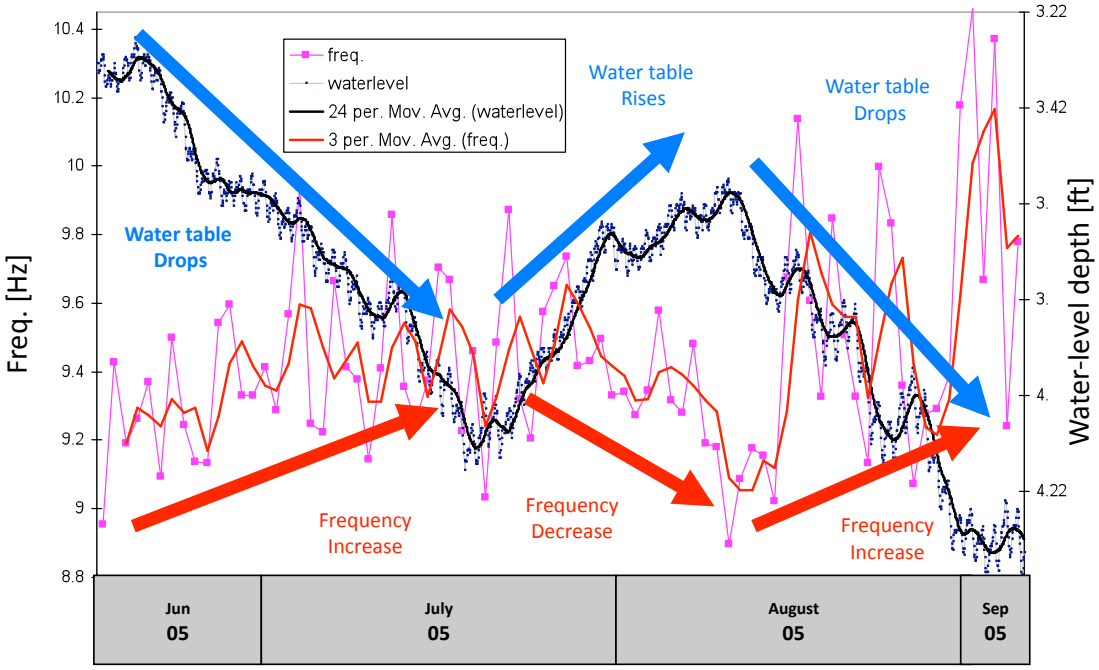

Figure 32: Observation on the Water-level and the identified frequency at the site from 6/17/05 thru 9/4/05. Note: The water-level axis has been plotted reversely.

Admittedly, the daily fluctuations due to temperature make it difficult to see the long-term effects of the more slowly changing water table level. However, using a moving average to smooth out the shorter-term trends, and looking at the data over a long period, as is in Figure 32, the water table level shows some correlation with variation in identified natural frequency. Higher water table level has, likely, a dual effect on the soil-structure interaction: decreasing the stiffness of the soil (at least at the small motion levels used here), and increasing the mass of the moving structure-foundation-soil-water system. It is also likely that the water table affects the damping of the system as well.

5 Modeling of SFSI Test Structure Behavior

5.1 Introduction

For decades, numerous studies have been conducted in the area of soil-structure interaction modeling. Since soil-structure systems have very complex characteristics, many researchers and engineers have attempted to develop accurate, yet pragmatic approaches to model such systems. More detailed background can be found in section 2.3.

To explain the observations made on the variation of the rocking frequencies of the two SFSI systems (*i.e.*, the SFSI test structure in Chapter 4 and the small-scale prototype introduced in Chapter 6), a model is developed in this chapter based on the cone modeling approach. The main intent of the modeling is to characterize the effect of soil saturation on a single-degree-of-freedom structure on a foundation sitting on a sandy soil. For both SFSI systems, pragmatic idealizations of the soil-media, which could assist studying the physics of the soil-structure interaction were investigated; eventually a strength-of-material modeling technique inspired by the Cone Modeling (Wolf, 1997) approach is proposed.

By introducing the empirical concept of the trapped mass under the foundation that moves in-phase with the foundation, the rocking frequency of SFSI systems as a function of soil saturation is parametrically studied. It is shown that the shift (increase or decrease)

of the rocking frequency of the SFSI system is strongly dependent on the characteristics of structure relative to the soil under its foundation.

5.2 Cone Modeling

Since the intent of this study is for low-strain vibration-based structural monitoring, it is important to remember that the modeling implicitly assumes that the soil remains linearly elastic with linear-hysteretic material damping. Linearity is justified since the displacement of the foundation is just fractions of millimeter in the test described in the previous chapters. In addition, it is assumed that the structure is on rigid foundation resting on the surface of a homogeneous soil half-space.

Even though several rigorous mathematical approaches for soil modeling based on three-dimensional elasto-dynamics are available, Wolf (1997) suggests that these methods — due to their considerable mathematical complexity — obscure the physical insight of the problem; as a result, they are more applicable for the applied computational mechanics, rather for practical civil engineering design. Thus, the Cone Modeling approach, which is based on a simple physical model with a small number of degrees of freedom, appears to be a favorable candidate to be utilized for better understanding of the aforementioned SFSI systems. Exploiting this approach, vibrations of a foundation on the surface of, or embedded in, a layered half-space using conical bars and beams (*i.e.*, cones), can be

analyzed (Wolf and Deeks 2004). In this method, as they stated, "the complicated exact formulation of three-dimensional elastodynamics is replaced by the simple one-dimensional truncated semi-infinite description of the theory of strength of materials."

In order to avoid the complicated analysis associated with wave propagation techniques that involve rigorous mathematical formulations, cone models were originally proposed several decades ago. Indeed, the spring-dashpot-mass model is a derivative of the cone modeling approach (Figure 33). Meek and Wolf (1992) state that it can be regarded as a first step towards developing a strength of-materials approach to foundation dynamics; analogous to beam theory in structural analysis with a restricted deformation behavior (*i.e.*, plane sections remain plane). In the spring-dashpot-mass (lumped-parameter) model, there are certain important assumptions; for example, the dynamic loads are assumed to be applied directly on the structure. Nevertheless, for earthquakes and other excitations introduced into the dynamic system via the soil, this approach can still be used with a few modifications.

Using the cone model, Wolf (1994) proposed that the half-space below the foundation to be modeled as a truncated semi-infinite rod with its area varying as in a cone with the same material properties. To model the soil with linear elastic behavior and hysteretic material damping, horizontal layers are usually characterized by elastic modulus E (or constrained modulus, E_c), shear modulus G, Poisson's ratio ν, mass density ρ, damping

coefficient ζ either overlying a half-space or fixed at its base, shear-wave velocity c_S, dilatational or P-wave velocity c_p and the rigid disk foundation equivalent radius r_{eq} (or half of the width of a square foundation), and apex height z_o as a function of ν. The angle of the cone depends on Poisson's ratio and on the wave velocities of the soil under the foundation. The aspect ratio represents the opening angle and can be computed for each degree of freedom such that the behavior of the foundation on the half-space and the cone on the low-frequency limit coincide.

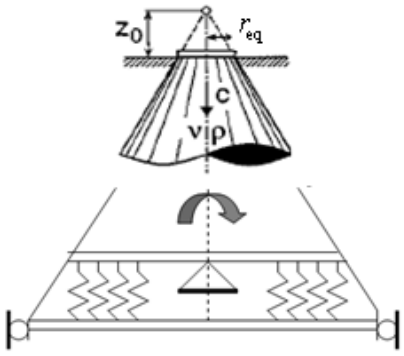

Figure 33: Truncated semi-infinite Cone Model (Wolf and Meek 2004)

By utilizing such a simplified physical model, the complicated three-dimensional wave propagation plus the body and surface waves could be represented by a one-dimensional model. Now, by looking at a harmonic excitation, this model can explain the physics of the problem and the rigorous mathematical solution.

For harmonic excitation with frequency of ω, the complex response $u(\omega)$ of a given dynamic system can be written as :

$$u(\omega) = \mathrm{Re}[u(\omega)] + i\,\mathrm{Im}[u(\omega)] \tag{13}$$

The corresponding force amplitude $P(\omega)$ is formulated as

$$P(\omega) = S(\omega)u(\omega) \tag{14}$$

where the stiffness matrix $S(\omega)$ can be formulated as:

$$S(a) = K[k(a) + iac(a)] \tag{15}$$

$k(a)$ and $c(a)$ represent frequency dependent stiffness and damping, respectively, while parameter a is introduced as the dimensionless frequency and formulated as follows:

$$a = \frac{\omega r_{\mathrm{eq}}}{c_{\mathrm{S}}} \tag{16}$$

where ω, r_{eq} and c_{S} are angular frequency, equivalent radius of the foundation and the shear wave velocity in the soil, respectively. If the foundation is square, use $r_{\mathrm{eq}} = B/2$ where B is the width of the foundation. The dimensionless spring coefficient $k(a)$ governs the force that is in phase (or 180 degree out of phase) with the displacement (real part), and the dimensionless damping coefficient $c(a)$ describes the forces that are 90 degrees out of phase (imaginary part).

The rocking static stiffness coefficient is introduced as K_{r}, relating the rocking motion of a square foundation to the moment applied to the foundation as follows:

$$K_r = \frac{GB^3}{2(1-\nu)} \tag{17}$$

where G, ν and B specify shear modulus, Poisson's ratio of the soil and the width of the square foundation.

Further, Wolf (1994) introduces a discrete-element models (Figure 35) representing foundations on surface of halfspace. The rotational cone's dynamic coefficients are obtained by a general strength-of-material approach using the approximate Green′s functions of the double-one models (Wolf, 1994). A bending moment with amplitude M_o is applied, resulting in a rocking equilibrium element, while horizontal motion is constrained as shown in Figure 33. The cone representing a beam with its moment of inertia increasing with depth z as

$$I(z) = \left(\frac{z}{z_o}\right)^4 I_o \tag{18}$$

where I_o is the area moment of inertial of the foundation, about an axis perpendicular to the page. The amplitude of the bending is

$$M(z) = \rho c_p^2 I(z)\theta(z)_{,z} \tag{19}$$

where $\theta(z)$ is the amplitude of the rocking motion and $()_{,}$ is the derivative notion.

By solving the he equilibrium equation for a massless foundation, and by writing dynamic stiffness coefficient as

$$S_r(a) = K_r\left[k_r(a) + iac_r(a)\right] \tag{20}$$

the dimensionless spring and damping coefficients are

$$k_r(a) = 1 - \frac{1}{3}\frac{a^2}{\left(\frac{Bc_p}{2}\right)^2 \Big/ \left(z_o c_s\right)^2 + a^2} \tag{21}$$

$$c_r(a) = \frac{2}{3}\frac{z_o}{B}\frac{c_s}{c_p}\frac{a^2}{\left(\frac{Bc_p}{2}\right)^2 \Big/ \left(z_o c_s\right)^2 + a^2} \tag{22}$$

To understand the effect of these frequency dependent terms as a function of dimensionless frequency, the spring and damping coefficient for a foundation on a dry sand is plotted in Figure 34. According to these plots, it is expected that the spring coefficient decreases drastically as the dimensionless frequency increases and remains constant for higher values of a (*i.e.*, for $a > 3$). In contrast, the damping coefficient tends to increase for dimensionless frequency up to $a < 3$, but then remains almost constant.

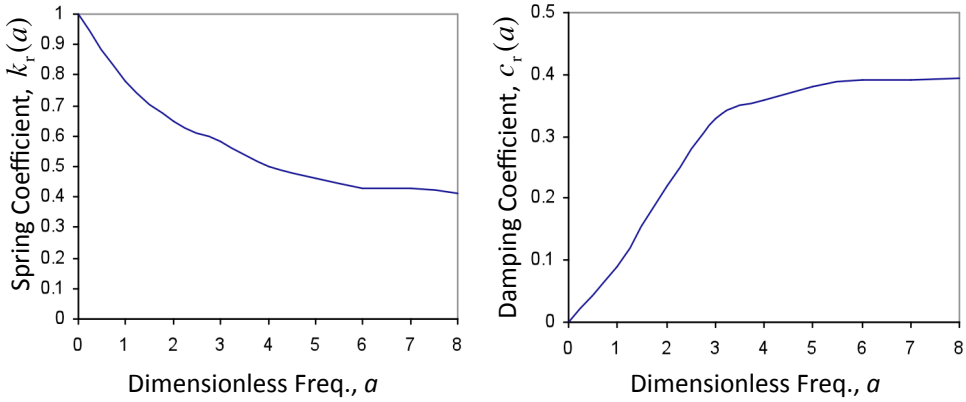

Figure 34: Frequency dependent spring and damping coefficients for rocking motion of dry soil.

In a practical sence, to convert a typical cone model to a spring-dashpot-mass model, Wolf (1994) introduced models for rocking motions as shown in Figure 35. His so-called Monkey-tail model (right) shows an equivalent spring-dashpot model (equivalent to Figure 35, left).

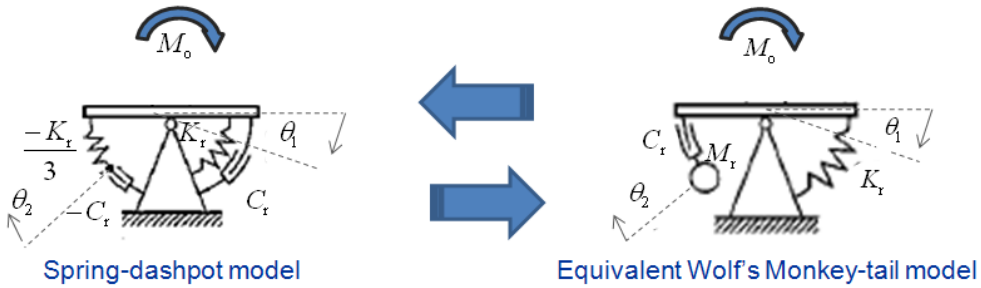

Figure 35: Equivalent Wolf's Monkey-tail model (right) derived from the Spring-dashpot model (left).

Considering the cone modeling approach, the corresponding rocking motion properties of this so-called Monkey-tail model are defined as follows:

$$K_r = \frac{3\rho c_p^2 I_o}{z_o} \qquad M_r = \rho I_o z_o \qquad C_r = \rho c_p I_o \tag{23}$$

where K_r, M_r, C_r are rocking stiffness, mass moment of inertia and damping coefficient of the soil, and z_o, known as the apex height. It can be shown that the models in Figure 35 are equivalent by writing the equilibrium equations for the monkey-tail model as follows:

$$M_o(t) = C_r\left(\dot{\theta}_1(t) - \dot{\theta}_2(t)\right) + K_r\theta_1(t) \tag{24}$$

$$M_r\ddot{\theta}_2(t) + C_r\left(\dot{\theta}_2(t) - \dot{\theta}_1(t)\right) = 0 \tag{25}$$

Considering the cone model properties, it can be concluded that

$$\frac{M_r}{C_r} = \frac{z_o}{c_p} \tag{26}$$

Substituting (26) in (25),

$$\frac{z_o}{c_p}\ddot{\theta}_2(t) + \dot{\theta}_2(t) = \dot{\theta}_1(t) \tag{27}$$

By solving this second-order differential equation, the following convolution integral, by using the impulse response function $h(t)$, can be written:

$$\dot{\theta}_2(t) = \int_0^t h(t-\tau)\dot{\theta}_1(\tau)d\tau \tag{28}$$

By substituting (28) in (24), the equilibrium equation can be written as:

$$M_o(t) = K_r\theta_1(t) + C_r\dot{\theta}_1(t) - \int_0^t h(t-\tau)C_r\dot{\theta}_1(\tau)d\tau \tag{29}$$

It can be verified that the result of the time domain formulation of the monkey-tail's model coincides with the spring-dashpot model in Figure 35 (left). Further in this current study, the equivalent monkey-tail model is used.

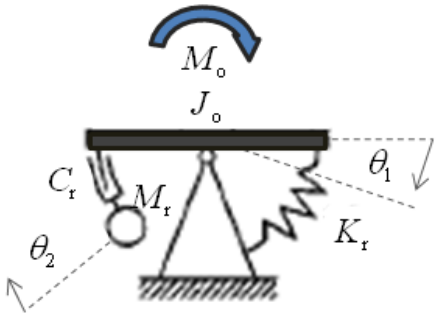

Figure 36: Monkey-tail model of a soil-foundation system; inclusion of the mass for the foundation.

Next, by including the mass of the foundation (Figure 36), a mass moment of inertia term is added to the equilibrium equations. Therefore, equations (30-31) can be re-written as follows:

$$M_o(t) = C_r\left(\dot{\theta}_1(t) - \dot{\theta}_2(t)\right) + K_r\theta_1(t) + J_o\ddot{\theta}_1(t) \tag{30}$$

$$0 = M_r\ddot{\theta}_2(t) + C_r\left(\dot{\theta}_1(t) - \dot{\theta}_2(t)\right) \tag{31}$$

where $J_o = m_f\left(\frac{B^2}{12} + \frac{D^2}{3}\right)$, m_f and D are moment of inertia about the rocking axis, mass and depth of foundation, respectively.

For harmonic excitation, these equations are transformed to:

$$M_o(\omega) = i\omega C_r\left(\theta_1(\omega) - \theta_2(\omega)\right) + K_r\theta_1(\omega) - \omega^2 J_o\theta_1(\omega) \tag{32}$$

$$0 = -\omega^2 M_r\theta_2(\omega) + i\omega C_r\left(\theta_1(\omega) - \theta_2(\omega)\right) \tag{33}$$

By eliminating $\theta_2(\omega)$,

$$M_o(\omega) = \underbrace{K_r\left[\overbrace{1 - \frac{\omega^2(M_r/K_r)}{1+\omega^2(M_r^2/C_r^2)} - \omega^2\frac{J_o}{K_r}}^{k_r} + i\omega\overbrace{\left(\frac{M_r}{C_r}\frac{\omega^2(M_r/K_r)}{1+\omega^2(M_r^2/C_r^2)}\right)}^{c_r}\right]}_{S_r}\theta_1(\omega) \tag{34}$$

It is noticed that the dynamic stiffness can be written as:

$$S_r(a) = K_r[k_r(a) + iac_r(a)] \tag{35}$$

where a is a dimensionless frequency:

$$a = \frac{B\omega}{2c_S} \tag{36}$$

By substituting the cone modeling parameters, the frequency-dependent terms of the dynamic stiffness, $k_r(a)$ and $c_r(a)$ can be formulated as follows:

$$k_r(a) = 1 - \frac{1}{3}\frac{a^2}{\left(\frac{Bc_p}{2z_oc_S}\right)^2 + a^2} - \frac{4}{3}\frac{z_oJ_o}{\rho I_oB^2\left(\frac{c_p}{c_S}\right)^2}a^2 \tag{37}$$

$$c_r(a) = \frac{z_o}{3\frac{B}{2}}\frac{c_S}{c_p}\frac{a^2}{\left(\frac{Bc_p}{2z_oc_S}\right)^2 + a^2} \tag{38}$$

Further, for a square foundation, the aspect ratio can be obtained by matching the static stiffness coefficient of the foundation to that of the corresponding cone.

$$\frac{3\rho c_p^2 I_0}{z_0} = \frac{GB^3}{2(1-\nu)} \tag{39}$$

Therefore the aspect ratio can be written as:

$$\frac{z_o}{B} = \frac{1}{2}(1-\nu)\left(\frac{c_p}{c_S}\right)^2 \tag{40}$$

where z_o as shown in Figure 33, is a function of the foundation's width and two important input parameters of a cone model, the pressure and shear wave velocity in the soil under the foundations. The relationship between Poisson's ratio and the elastic constants for soil with mass density ρ, wave propagation velocities c_S (shear waves) and c_p (dilatational waves) can be obtained from the formulas given in Table 4. Please note that the constrained modulus can be formulated in terms of Young's Modulus E, and shear Modulus G as

$$E_c = \frac{1-\nu}{(1+\nu)(1-2\nu)}E = \frac{1-\nu}{1-2\nu}G \tag{41}$$

Table 4: **Poisson's ratio and elastic constants for soil mechanics.**

Poisson's Ratio	Constrained Modulus	Shear Modulus
$\nu = \dfrac{\left(\frac{c_p}{c_S}\right)^2 - 2}{2\left(\frac{c_p}{c_S}\right)^2 - 2}$	$E_c = \rho c_p^2$	$G = \rho c_S^2$

As shown in Figure 37, the shear wave velocity is not impacted by the saturation level; however, the P-wave velocity increases as the air proportion decreases (saturation increases). In fact, an increase in saturation level, causes $c_p >> c_S$; as a result, according to the Poisson's Ratio formula in Table 4, as $\frac{c_p}{c_S}$ tends to infinity, the Poisson's ratio approaches 0.5.

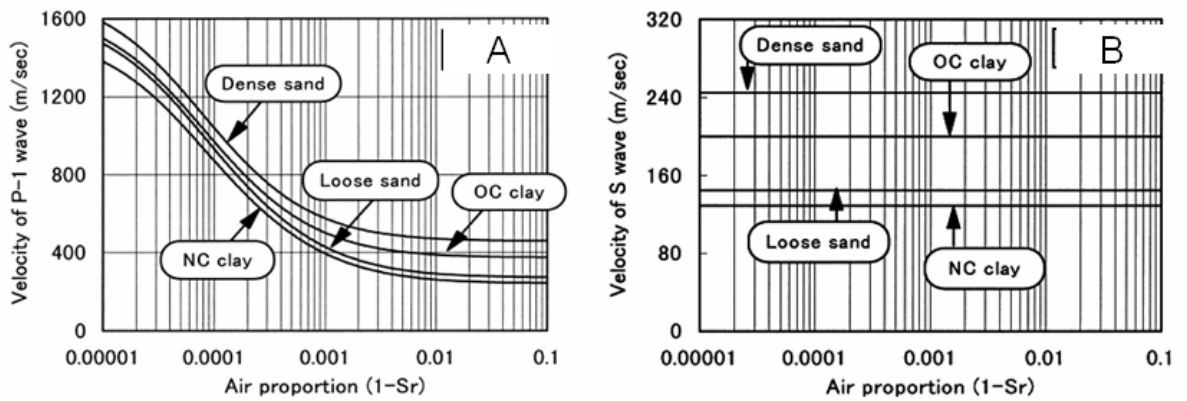

Figure 37: Effects of saturation on the wave velocities in different types of soils: (A) P-waves, (B) S (shear) waves . (Yang and Sato, 2002)

In the cone modeling approach, a saturated and un-drained soil (*i.e.*, when Poisson's ratio ν approaches 0.5) is considered to be nearly incompressible soil, requiring certain modeling considerations. Meek and Wolf (1993b) believe that as the P-wave velocity tends to infinity, it causes anomalous behavior, not only for cones, but for rigorous solutions as well. In such cases, a special technique for the Cone models has been offered by Meek and Wolf (1993a). Based on their calculations, they suggest that the axial-wave

velocity relationship $c_p = 2c_S$ should be enforced for the cone models. Thus, the aspect ratio formulation can be simplified as shown below:

$$\frac{z_o}{B} = 2(1-\nu) \tag{42}$$

Further, Meek and Wolf(1993b), particularly for nearly incompressible soils, suggest that the idea of a trapped mass under the foundation should be taken into account. To model the contribution of the mass of the soil under the foundation, they introduce a trapped mass of soil beneath the foundation, which moves as a rigid body in phase with the foundation (*i.e.*, ΔJ_r) with no additional degree of freedom (Figure 38).

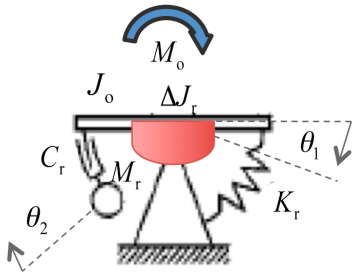

Figure 38: The conceptual notion of the trapped mass underneath the foundation of a monkey-tail model.

Thus, the corresponding equilibrium equations can be re-formulated as follows:

$$M_o(t) = C_r\left(\dot{\theta}_1(t) - \dot{\theta}_2(t)\right) + K_r\theta_1(t) + (\Delta J_r + J_o)\ \ddot{\theta}_1(t) \tag{43}$$

$$M_r\ddot{\theta}_2(t) + C_r\left(\dot{\theta}_1(t) - \dot{\theta}_2(t)\right) = 0 \tag{44}$$

For harmonic excitation, they can be written as

$$M_{\mathrm{o}}(\omega) = i\omega C_{\mathrm{r}}\left(\theta_1(\omega) - \theta_2(\omega)\right) + K_{\mathrm{r}}\theta_1(\omega) - \omega^2(\Delta J_{\mathrm{r}} + J_{\mathrm{o}})\theta_1(\omega) \tag{45}$$

$$-\omega^2 M_{\mathrm{r}}\theta_2(\omega) + i\omega C_{\mathrm{r}}\left(\theta_1(\omega) - \theta_2(\omega)\right) = 0 \tag{46}$$

By eliminating $\theta_2(\omega)$,

$$M_{\mathrm{o}}(\omega) = \underbrace{K_{\mathrm{r}}\left[1 - \frac{\omega^2(M_{\mathrm{r}}/K_{\mathrm{r}})}{1+\omega^2(M_{\mathrm{r}}^2/C_{\mathrm{r}}^2)} - \omega^2\frac{\Delta J_{\mathrm{r}} + J_{\mathrm{o}}}{K_{\mathrm{r}}} + i\omega\left(\frac{M_{\mathrm{r}}}{C_{\mathrm{r}}}\frac{\omega^2(M_{\mathrm{r}}/K_{\mathrm{r}})}{1+\omega^2(M_{\mathrm{r}}^2/C_{\mathrm{r}}^2)}\right)\right]}_{S_{\mathrm{r}}}\theta_1(\omega) \tag{47}$$

Consequently, it is expected that, for perfectly incompressible soil with Poisson's ratio exactly equal to 0.5, the real-valued mass term of the dynamic stiffness, $-\omega^2(\Delta J_{\mathrm{r}} + J_{\mathrm{o}})$, would dominate the response which would result in reduction of the dynamic stiffness of the discussed spring-mass-damper model.

For the rocking motion, the trapped mass moment of inertia is formulated as follows:

$$\Delta J_{\mathrm{r}} = \frac{1.2}{24}H\left(\nu - \frac{1}{3}\right)\left(\nu - \frac{1}{3}\right)\rho B^5 \tag{48}$$

where $H(x) = \begin{cases} 0, & x < 0 \\ 1, & x \geq 0 \end{cases}$.

It is clear that according to the dynamic-stiffness formulation the stiffness is decreased, proportional to the square of frequency, by a mass trapped under the foundation and moving in phase with it because the soil is nearly or perfectly incompressible. Practically speaking, this formulation implies the rocking frequency of saturated soil-foundation-structure system, at some point, is becoming less than the dry case frequency.

Including the trapped mass effect, the dynamic stiffness coefficient for the rocking motion can be written as follows:

$$k_r(a) = 1 - \frac{1}{3}\frac{a^2}{\left(\frac{Bc_p}{2z_o c_S}\right)^2 + a^2} - \frac{4}{3}\frac{z_o J_o}{\rho I_o B^2 \left(\frac{c_p}{c_S}\right)^2}a^2 - \frac{1.2}{3}H\left(\nu - \frac{1}{3}\right)\left(\nu - \frac{1}{3}\right)(1-\nu)a^2 \qquad (49)$$

It is obvious that the last term in (49) is the contribution of the trapped mass which would vanish for $\nu < \frac{1}{3}$ (dry sand). Again, according to this empirical formulation, the trapped mass contributes for $\nu > 1/3$ and increases linearly with ν.

5.3 Coupled Dynamic Model for SFSI Systems

To better understand the physics behind a coupled soil-structure system for rocking motions, a dynamic model is introduced as shown in Figure 39. In this model, the structure is represented with a mass *m* and a static spring with coefficient *k* (the lateral stiffness of the structure), which is connected to a rigid mass less bar of height *H*. Considering the foundation of width *B*, the soil dynamic stiffness has been modeled with the frequency dependent coefficient utilizing the cone model for the soil with the following properties: mass density ρ, shear wave velocity c_S, frequency dependent

stiffness coefficient $k_r(a)$, static stiffness K_r and dimensionless frequency parameter $a = \frac{1}{2}\omega B c_s^{-1}$.

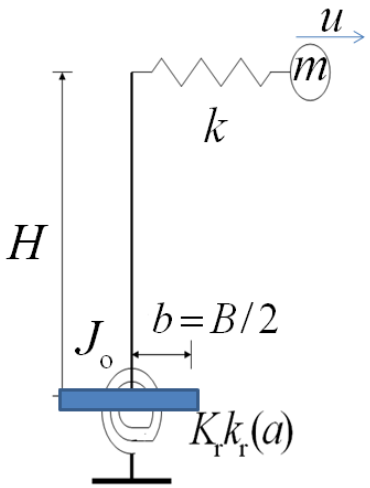

Figure 39: Coupled dynamic model of soil-structure system for rocking motion; representing SFSI test structure.

The equilibrium equation for the whole soil-foundation-structure system, can be written

$$\begin{bmatrix} m & mH \\ 0 & J_o \end{bmatrix} \begin{Bmatrix} \ddot{u} \\ \ddot{\theta} \end{Bmatrix} + \begin{bmatrix} k & 0 \\ -kH & K_r k_r(a) \end{bmatrix} \begin{Bmatrix} u \\ \theta \end{Bmatrix} = \begin{Bmatrix} 0 \\ 0 \end{Bmatrix} \tag{50}$$

To find the system eigenvalues $\lambda = \omega^2$, the *characteristic equation* can be obtained by solving an eigenvalue problem, which leads to the following equation

$$\det \begin{bmatrix} k - m\lambda & -m\lambda H \\ -kH & K_r k_r(a) - J_o \lambda \end{bmatrix} = 0 \tag{51}$$

Since the term $K_r k_r(a) - J_o\lambda$ is a function of a, above equation will yield to a frequency dependent equation as below:

$$(k - m\lambda)(K_r k_r(a) - J_o\lambda) - m\lambda kH^2 = 0 \tag{52}$$

Rearranging (52) by collecting terms of like powers of λ gives

$$mJ_o\lambda^2 - (mK_r k_r(a) + J_o k + mkH^2)\lambda - + kK_r k_r(a) = 0 \tag{53}$$

Solving (58) for λ gives

$$\lambda = \frac{mK_r k_r(a) + J_o k + mkH^2 \pm \sqrt{\left(mK_r k_r(a) + J_o k + mkH^2\right)^2 - 4mJ_o kK_r k_r(a)}}{2mJ_o} \tag{54}$$

The fixed-base natural frequency ω_s of the structure can be simply computed as

$$\omega_s = \sqrt{\frac{k}{m}} \tag{55}$$

The rocking natural frequency can be expressed, using the stiffness derived from the cone model in section 5.3 and ignoring any base mass, as

$$\omega_r = \sqrt{\frac{K_r k_r(a)}{mH^2}} \tag{56}$$

Using the fixed base frequency and the massless foundation rocking frequency, (61) can be simplified and re-written as follows:

$$\lambda = \frac{T \pm \sqrt{T^2 - 4J_o m^2 \omega_s^2 (J_o + mH^2)\omega_r^2}}{2mJ_o} \tag{57}$$

where $T = m(J_o + mH^2)\omega_r^2 + J_o m\omega_s^2 + m^2\omega_s^2 H^2$. Let $J_o = \varepsilon mH^2$

$$\lambda = \frac{T \pm \sqrt{T^2 - 4m^4 H^4 \varepsilon(\varepsilon+1)\omega_s^2\omega_r^2}}{2\varepsilon m^2 H^2} \tag{58}$$

where $m^2H^2(\varepsilon+1)\omega_r^2 + \varepsilon m^2 H^2 \omega_s^2 + m^2\omega_s^2 H^2$ and the m^2H^2 terms cancel out, giving

$$\lambda = \frac{(\varepsilon+1)(\omega_r^2 + \omega_s^2) \pm \sqrt{(\varepsilon+1)^2(\omega_r^2 + \omega_s^2)^2 - 4\varepsilon(\varepsilon+1)\omega_s^2\omega_r^2}}{2\varepsilon} \tag{59}$$

In some analyses, the rotational inertia of the foundation is ignored. For example, Todorovska and Al Rjoub (2006) assume the fundamental frequency of the coupled system is related to the rocking and fixed base frequencies, by $\omega^{-2} = \omega_s^{-2} + \omega_r^{-2}$. To verify this, the limit of $(\varepsilon+1)$ as ε tends to zero can be considered. As $\varepsilon \to 0$ (*i.e.*, massless foundation), the right-side tends to infinity for the "+" solution and to $\frac{0}{0}$ for "–" solution. Since the first mode is of interest here, only the "–" solution needs to be considered. Using L'Hôpital's rule, the limit, as ε approaches zero is

$$\lambda = \lim_{\varepsilon \to 0} \frac{1}{2}\left[(\omega_r^2 + \omega_s^2) - \frac{2(\varepsilon+1)(\omega_r^2 + \omega_s^2)^2 - 4(2\varepsilon+1)\omega_s^2\omega_r^2}{2\sqrt{(\varepsilon+1)^2(\omega_r^2 + \omega_s^2)^2 - 4\varepsilon(\varepsilon+1)\omega_s^2\omega_r^2}}\right] \tag{60}$$

$$\lambda = \frac{1}{2}\left[(\omega_r^2 + \omega_s^2) - \left\{(\omega_r^2 + \omega_s^2) - \frac{2\omega_s^2\omega_r^2}{(\omega_r^2 + \omega_s^2)}\right\}\right] = \frac{\omega_s^2\omega_r^2}{\omega_r^2 + \omega_s^2} \tag{61}$$

Or, more simplified, can be written as:

$$\lambda^{-1} = \omega^{-2} = \omega_s^{-2} + \omega_r^{-2} \tag{62}$$

Thus, the fundamental frequency ω of the coupled soil-structure system with a massless foundation, which is a combined rocking and structural bending mode, can be obtained in terms of the fixed-base bending frequency of the structure ω_s and the rocking frequency ω_r of a rigid structure and foundation on the soil. This equation also implies that the equivalent fundamental frequency ω of the soil-structure system is always smaller than that of the fixed-base frequency of the structure ω_s. Nevertheless, for the modeling of the SFSI test structure, the mass moment of inertia of the foundation is considered (*i.e.*, J_o). For the SFSI test structure $B = H$, $B = 8D$ and $m = 0.8m_f$; thus $\varepsilon \cong 0.11$.

Since the dynamic stiffness of the foundation for the rocking motion includes frequency-dependent term, cannot be solved by a straight hand calculation; instead, it requires a numerical iterative solution. By utilizing a program in MATLAB, a symbolic formulation is created. Then, by substituting the parameters of the SFSI test structure problem, the characteristic equation can be solved for λ.

Further, to perform a parametric study, it is convenient to introduce a set of dimensionless parameters as follows that relate the properties of the structure to itself and to the soil:

$$\bar{s} = \text{normalized structure frequency} = \omega_s H / c_S \tag{63}$$

$$\bar{h} = \text{slenderness ratio} = H/b \tag{64}$$

$$\bar{m} = \text{mass ratio} = m/\rho b^3 \tag{65}$$

The ratio of the natural frequency of the fundamental vibration mode of the coupled system to that of the fixed-base structure (*i.e.*, ω/ω_s) is called the *SFSI stiffness factor*, which, depending on the extent of the SFSI effect, would vary between zero and one. Note that, due to complexity of the (59) and its dependence on several soil-structure parameters, the SFSI stiffness factor is very crucial for SFSI analysis, yet is not easily obtained.

5.4 Parametric Study

This modeling approach is capable of estimating the SFSI effect on the rocking motion of any soil-structure system that can be modeled as described in the previous section (*e.g.*, water towers, telecommunication towers, etc.). In particular, it is employed for characterizing the effect of the soil saturation on the identified rocking mode frequency of the SFSI test structure and of the small-scale prototype. To better understand and explain the SFSI rocking frequency variation of both SFSI systems, a parametric study is

performed. Based on the properties of the SFSI test structure given in Table 5 and the soil characteristics at the site, given in Table 6 (discussed in Chapter 3), the dimensionless parameters are evaluated; $\bar{s}$ (normalized structure frequency) = 2.68, $\bar{h}$ =2 and $\bar{m}$ =1.25 for dry soil or $\bar{m}$ =1.05 for saturated soil.

Table 5: Properties of the SFSI test structure.

SFSI test structure Properties			
H [m]	m [kg]	b [m]	m_f [kg]
4	16000	2	20000

Table 6: Saturated vs. Dry characteristics of the soil at the site.

		Soil Properties			
		ρ [kg/m^3]	c_p [m/s]	c_S [m/s]	ν
SFSI Site	Dry	1600	300	150	0.33
	Saturated	1900	1600	150	0.50

The fundamental frequency of a soil-foundation-structure system, relative to the fixed base frequency, is illustrated in Figure 40 as function of normalized structure frequency

for both dry and saturated soil. The specific normalized structure frequency $\bar{s}$= 2.68 of the NEES SFSI test structure is indicated with an arrow on Figure 40.

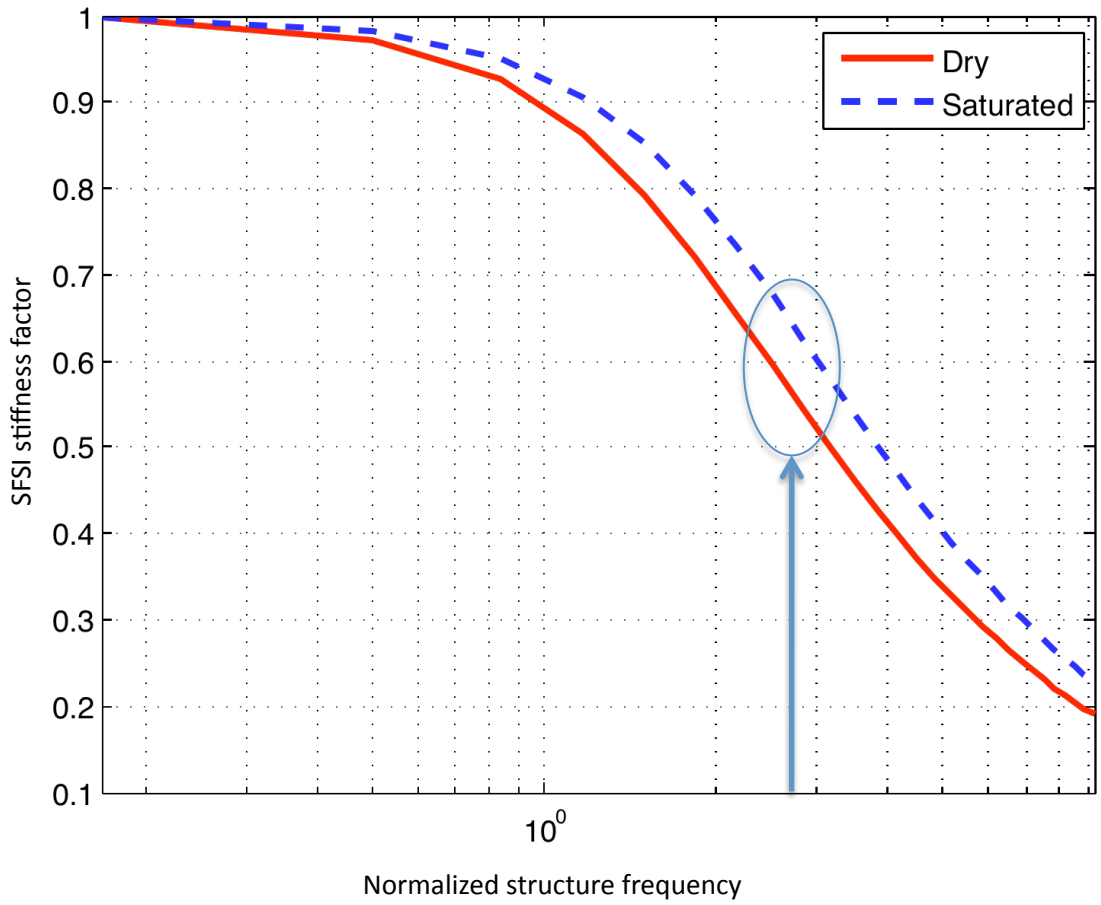

Figure 40: The rocking frequency for a SFSI system ($\bar{h}$ =2, $\bar{m}$ =1.25 (1.05) and Poisson's ratio=0.33 (0.5) for dry (saturated) soil. (Normalized structure frequency = 2.68).

The SFSI test structure has parameters and solution as shown in Table 7, which causes different SFSI effects for the dry and saturated cases. The first bending mode frequency of the fixed-base SFSI test structure is about 16 Hz — computed with the finite element

analysis described in Chapter 3. Thus, the model here predicts that the first mode of vibration for the SFSI system (rocking + bending) should be 8.9 Hz, which should increase to about 10 Hz upon the full saturation of the soil. The SFSI stiffness factor for the dry case is predicted to be about 0.56, as opposed to 0.63 for the saturated case. The results of the numerical solution for the dry and saturated cases of the SFSI test structure are tabulated in Table 7. According to the results of the modeling, it can be concluded that the rocking mode frequency of the SFSI test structure, from a dry soil to fully saturated soil, is predicted to increase by about 10%, which is in contradiction with the trend of identified rocking frequencies variation of the SFSI test structure as described in Chapter 4.

Table 7: Results of the rocking motion estimation of the SFSI test structure.

	$f_{\text{fixed-base}}$ [Hz]	$\bar{s}$	$\bar{h}$	$\bar{m}$	$\omega_s [s^{-1}]$	$\omega [s^{-1}]$	ω / ω_s	f_{SFSI} [Hz]
Dry	16	2.68	2	1.25	100.5	56.10	0.56	8.93
Saturated	16	2.68	2	1.05	100.5	63.31	0.63	10.08

As illustrated in Figure 40, it is obvious that relative soil-structure stiffness $\bar{s}$ has a very important role in the effect of soil-structure interaction. With increase of $\bar{s}$, the effect of the soil (in lowering the rocking stiffness of the system) also increases. Also, it is important to remember that those predicted modeling results are highly dependent upon

the other presumed characteristics of the soil relative to those of structure. For instance, as illustrated in Figure 41, for a SFSI system with wider foundation, say twice as much as that of the SFSI test structure (*i.e.*, B = 8m), the predicted SFSI stiffness factor — as a function of normalized structure frequency — would be of different trend. That is, the SFSI stiffness factor for a saturated soil case starts to be lower than that of the dry case for normalized structure frequency greater than 3.

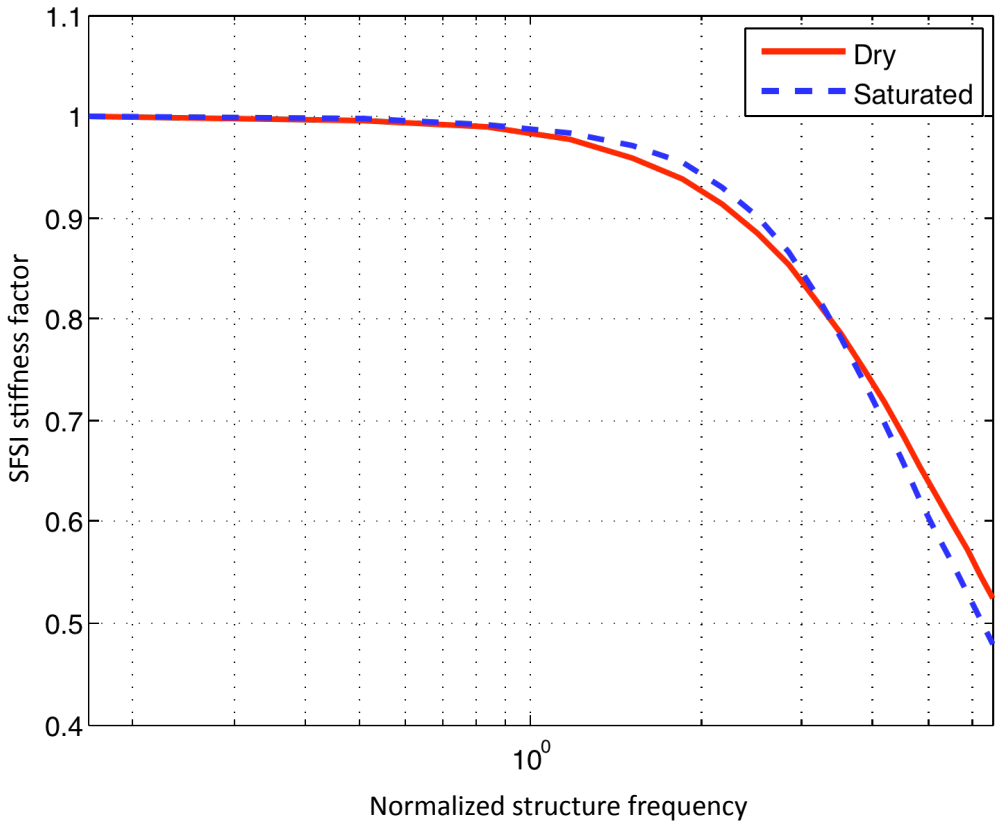

Figure 41: The rocking frequency for a SFSI system ($\overline{h}$ =1, $\overline{m}$ = 0.16 (0.13) and Poisson's ratio=0.33 (0.5) for dry (saturated) soil.

It is also believed that the observation and modeling reported on the Millikan Library published by Todorovska and Al Rjoub (2006) could be similarly justified. The hypothesis postulated in their work is that the observed increases in frequency are due to the water saturation of the soil. The Millikan library is a 9-story reinforced concrete structure on an embedded foundation; however, the dynamic coupled SFSI system is the simplest representation of a structure modeled as a SDOF structure with a surface foundation that can be exploited for the modeling of the similar structural systems and structures with shallow foundation. The speculation is that there might be other environmental variables (*e.g.,* soil moisture) that could affect on the soil stiffness and consequently on the rocking mode of the SFSI systems, which are out of the scope of this research.

5.5 Summary

The prediction of dynamic behavior of SFSI systems is very complicated; the presence of the soil and its interaction with the structure are the main contributors to this complexity. In order to properly model the soil's behavior, various material and environmental parameters need to be taken into account.

In this current study, Wolf's Cone Model was utilized to explain the effect of soil structure interaction and saturation of the soil on the observed variability in the rocking

frequency of the SFSI test structure. Further, a model representing the coupled SFSI system was developed. The saturated soil has been modeled with higher P-wave velocity and, consequently, higher Poisson's ratio in the soil model. Further, by introducing the empirical concept of the trapped mass under the foundation (moves in-phase with the foundation), the rocking frequency of SFSI systems as a function of soil saturation was parametrically studied. It was shown that the shift (increase or decrease) of the rocking frequencies of SFSI systems were strongly dependent on the characteristics of structure relative to the soil under its foundation. In addition, the sensitivity analyses (by changing the input parameters value) were carried out to study the sensitivity of some of input parameters. The width of the foundation, for instance, was shown to have significant effect on the rocking frequency of a SFSI system on the saturated soil.

Unfortunately, this model does not predict the observed decrease in the SFSI test structure's fundamental rocking frequency as the water table increases. The effects of other environmental parameters (*e.g.*, moisture in the soil, etc.) or soil behavior — such as cohesion or expansion — are speculated to be significant enough that they should be investigated further for this particular case. Suggested investigations might include soil sampling and laboratory testing for cohesion and expansion, better soil moisture measurements, and localized in-situ soil property measurements underneath the structure. Future research attempting to model the observed behavior should perhaps look at a more complete physics-based approach to this particular soil.

6 Effect of Water Table Variation on the Rocking Frequency of a SFSI system: Small-Scale Experiment

In order to characterize and reproduce the observed variation in structure's identified rocking frequency and its correlation with the ground water-table under the foundation, a small-scale laboratory-size experiment was designed. Since the SFSI test structure might not experience a full range of different water-table levels during a reasonable monitoring period, the key advantage of a scaled model in the laboratory is that the system identification of the prototype could be performed under certain artificially created and controlled water table conditions. The main challenge, however, is to ensure that the prototype has dynamic properties similar to the original SFSI test structure for the intended testing purposes while still easy to set up for various configurations for studying different aspects of interest. The most important step in designing the experiment was to determine an appropriate scale factor for the specific scope of experiment (*e.g.*, rocking mode frequency and relative stiffness with respect to the soil).

6.1 Testing Procedure

The main intention here is to identify the modal properties of a scaled model while the water level is changing in a controlled fashion. The scaled prototype must provide a soil-

foundation-structure system with appropriate laboratory-size layout. The layout of the experiment includes a simple single-degree-of-freedom (SDOF) fixed-base structure with concrete foundation sitting on top of a sandy/silty soil as illustrated in Figure 42. The water table and saturation of the soil are controlled by adding water through the funnel. The water level in the soil is measured by simply reading the water level in the transparent tube installed at the bottom of the drum.

The response of the system can be recorded for identifying the rocking mode frequency. The impulse response of the stick model, created by the hammer test excitation, is recorded by an accelerometer on top of the structure while the water-level under the foundation is gradually changed. Indeed, as the water is added gradually through the funnel, it was possible to control the water-level to any desired level for performing a system identification. In contrast with a real-world experiment, water can be easily added all the way up to the ground level.

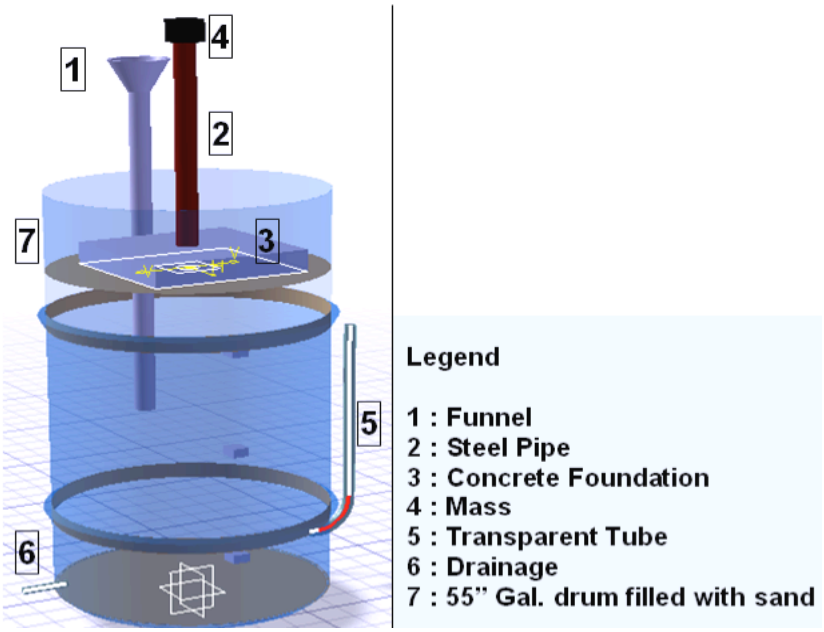

Figure 42: 3D rendering of the conceptual layout of the scaled prototype.

To make sure that the soil, after full saturation, is readily reusable for more testing, a small drainage pipe was put in place at the bottom of the drum to provide water drainage. Note that full drainage of the water might not return the soil back to its normal dry condition; in fact, damp soil has different dynamic characteristics compared to the dry soil, the effect of which will be discussed later in this chapter.

6.2 Hypothesis

The hypothesis of this experiment is that the identified first frequency (rocking mode) of the small scale model would be changed due to the variation of the water table under the

foundation, with the same trend as observed for the SFSI test structure. Based on the observations discussed in Chapter 4, it is speculated that the identified rocking frequency of the simplified experimental structure, will change as the water level varies under the foundation. The change trend is expected to be in negative correlation with the identified frequency, meaning that when the water table goes down the identified frequency would increase (Figure 43).

Figure 43: Schematic hypothesis in illustration: Water-level vs. Rocking Frequency.

6.3 Test Specifications and Design

Due to the presence of the soil-foundation-structure interaction, it is expected that the small scale prototype model will respond with a combination of the rocking of the foundation as well as the bending of the structure (Figure 44).

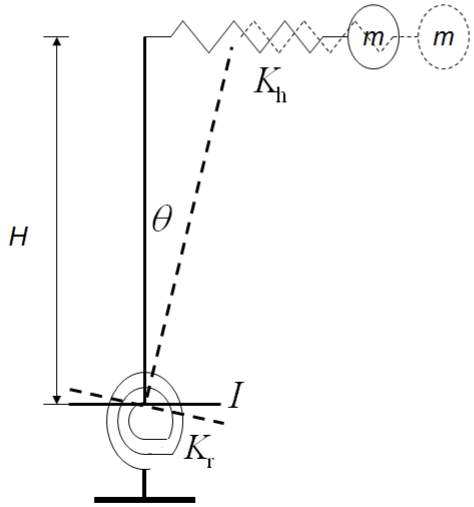

Figure 44: Small-scale stick model (2DOF) of the SFSI test structure.

In addition to the shape and type of the foundation, the stiffness of the soil relative to the structure is the dominating factor that governs the soil-structure interaction effect. Hence, to design the foundation of the prototype model, the properties of the soil relative to the SFSI test structure should be replicated in the small scale experiment. That is, about half of the rocking flexibility of the soil-structure system is to be provided by the soil and the other half by the structure through bending.

Since the small-scale prototype is considerably smaller than the SFSI test structure, some modifications on the test configuration as well as on the instrumentations is inevitable. Finding a proper *scale factor* for the prototype model is of great importance; it will affect the natural frequency of the model and needs to be addressed carefully. For instance, as stated by Powrie (2004), if the model is scaled with linear dimensions N (*i.e.,* full size

model length is *N* times larger than the small-scale length), the frequency of the small scale prototype would be larger by a factor of *N*. For measuring the dynamic response of such systems properly, the sensitivity of the instruments and potential sampling rate limitations of data acquisition (DAQ) systems must be known prior to the design of the experiment.

The optimal value of the scale factor, depending on the available instruments and DAQ system as well as experiment setup, is obtained after some heuristic iteration. For instance, the data acquisition system might not be capable of recording data with a very high sampling rate; if the sampling rate is not more than twice the natural frequency, aliasing will distort the data. Aliasing is a phenomenon that occurs whenever a signal has frequency content above Nyquist frequency of the sampling.

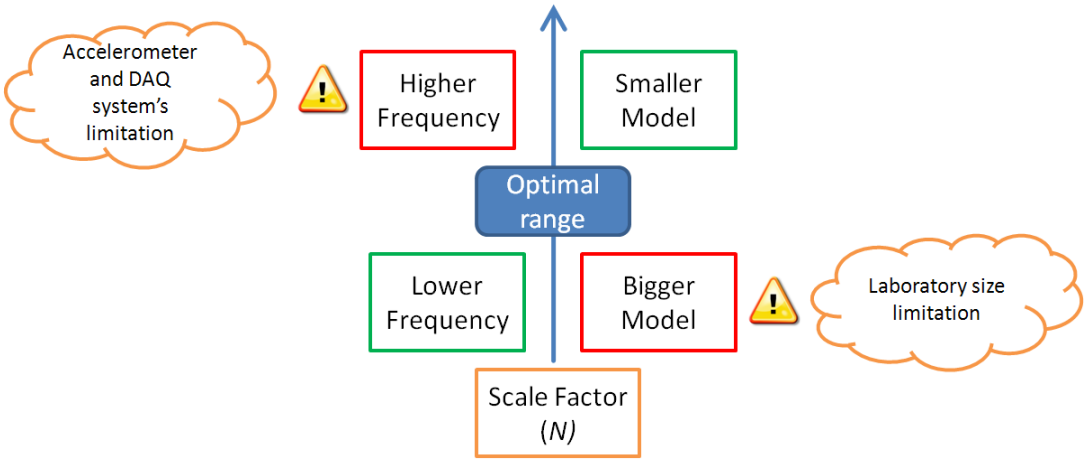

Figure 45: Schematic constraints for finding an optimal scale factor, illustrates the trade-off between higher vs. lower value of *N*.

As illustrated in Figure 45, practical laboratory limitations must be considered in the dimensions of the experiment. For example, to ensure that the possible disturbance induced by the boundary conditions on the rocking mode frequency is negligible, the scaling factor needs to be big enough to ensure that enough clearance from the edge of the space that contains the soil.

Another concern for the context of current study is to ensure that, compared to the original model, the same level of soil-structure-interaction exists. Thus, the relative soil-structure properties (*e.g.*, mass and slenderness ratio) for the small scale prototype model should be similar to the NEES SFSI structure. It is convenient to introduce a set of dimensionless parameters as follows that relate the properties of the structure to those of the soil: Let the slenderness ratio $\overline{h} = H/b$ and mass ratio $\overline{m} = m/\rho b^3$, where H, m, ρ and b are the height of the structure, the top mass, the density of the soil and half of the width of the foundation, respectively. Based on the dimension of the original SFSI test structure, regardless of the scale factor, the slenderness ratio and the mass ratio of the prototype should be 2 and 1.25, respectively. $\overline{h} = 2$ implies that the height of the structure should be about equal to the width of the foundation. Given that the diameter of the 55 gallon drum that will contain the soil specimen is around 60 cm, to have enough clearance, the width of the foundation should not exceed 30 cm.

With all these practical and technical constraints, particularly the foundation dimension and the DAQ sampling rate, the scale factor $N = 14$ was chosen and used to compute the foundation dimension, the height of the structure and the top mass. A square concrete foundation (28 cm × 28 cm × 3.5 cm) reinforced by a layer of a steel mesh at the bottom, was poured (Figure 46). The mesh was a stainless steel wire mesh (25 cm × 25 cm) with 10 mesh/inch and wires 0.5 mm in diameter. As illustrated in Figure 46, a steel pipe, representing the columns of the test structure, was screwed into a steel flange and fully embedded within the concrete to create a fixed-base connection at the bottom. Knowing the equivalent area moment of inertia of the four columns of the SFSI test structure (*i.e.*, $I_{eq} \cong 3.8e5\ \text{cm}^4$) and scaling factor $N = 14$, the area moment of inertia of the prototype model needs to be around $10\ \text{cm}^4$. Off-the-shelf steel pipes are usually found with threads on both ends with various length and various standard diameters. The closest size matching the design (to provide equivalent bending stiffness), was the 12 in (30.45 cm) long pipe with 1 inch internal diameter. Some shorter pipes (same diameter) were also procured to allow for testing with other columns length.

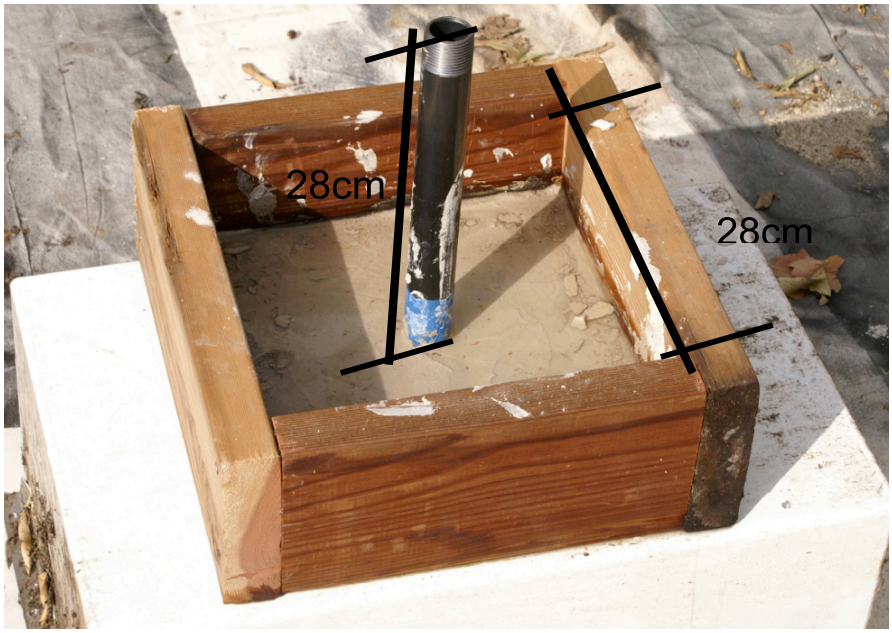

Figure 46: Picture of the poured concrete and the steel pipe to represent a SDOF system

To contain the soil, a 55-gal drum was filled two-thirds with sand so that it would provide sufficient height (h ≈ 60 cm) of soil which is almost twice the width of the foundation of the scaled stick model to make sure enough clearance from the bottom of the drum has been provided. The water-table level in the soil will be manually controlled and measured via a PVC pipe and a flexible transparent tube, respectively. Figure 47 illustrates the experiment layout. The top mass, analogous to the top slab of the SFSI test structure, must be firmly fixed to the pipe so that there would be no noise due to the vibration of the mass itself. Further, the top mass must provide a flat surface allowing a firm attachment of the accelerometer for reading in any desired direction. Thus, an 8 lb (3.6 kg) piece of metal (trailer hitch) was attached on top of the steel flange as depicted in Figure 47.

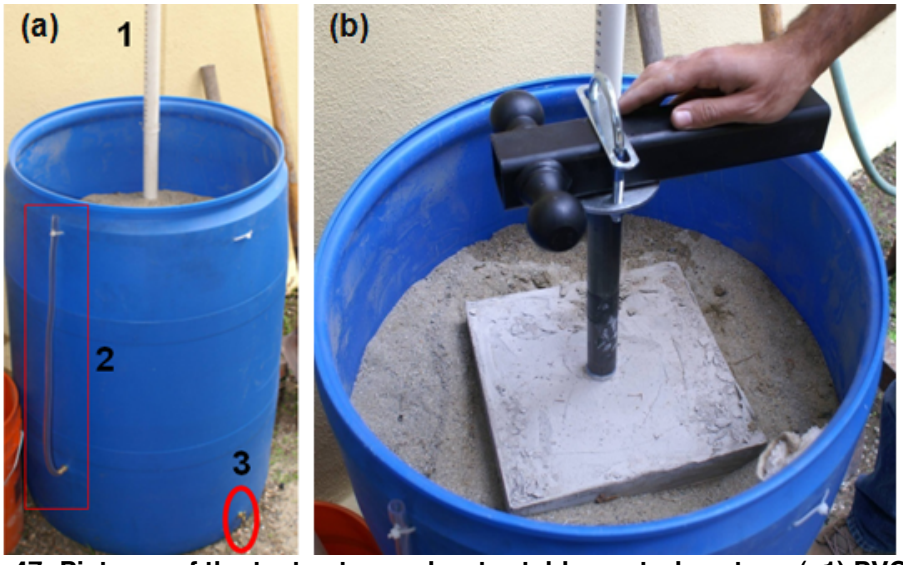

Figure 47: Pictures of the test setup and water-table control system: (a1) PVC pipe through which water can be directed inside the soil; (a2) A flexible transparent tube for water-level measurement purposes; (a3)Drainage system to let the water out. (b) small scale model sitting on a rigid foundation with a mass on top.

6.4 Experimental System Identification (Impulse Response)

In order to identify the rocking/bending frequency, the impulse response of the small scale prototype model can be measured and the frequency of the system can be estimated in either frequency or time domain. Since it is not possible in practice to create a perfect unit-impulse excitation, it can be approximated with a pulse of sufficiently short duration relative to the impulse response that excites the desired mode(s) of interest. The impulse excitation of small and medium size structures usually can be performed by a hammer test (swift hammer blow).

For experimental impulse excitation, depending on the size and configuration of the structure, a proper hammer (weight, type, etc.) must be selected. Often, by looking at the (time domain) impulse response induced by a given hammer, a suitable hammer, that could produce reasonably neat and clean signals for a given mode of vibration, would be selected.

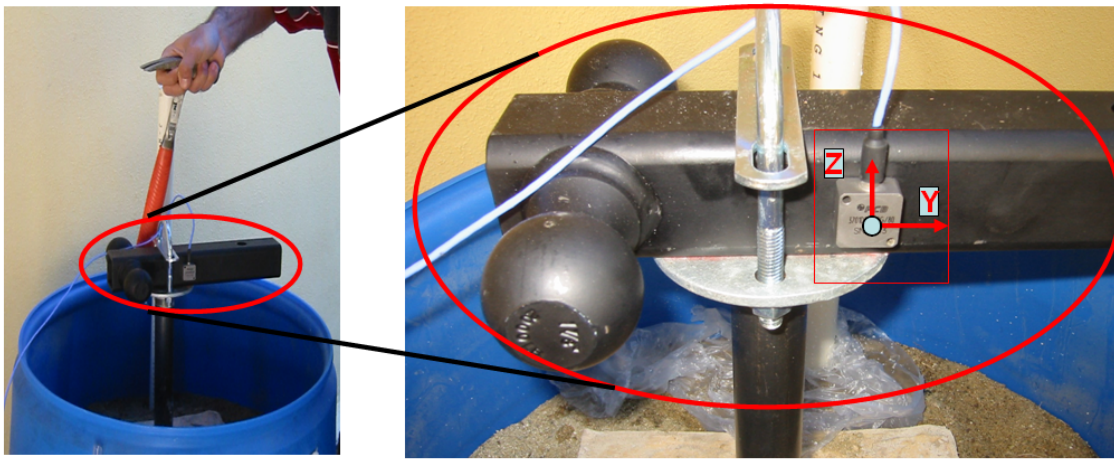

Figure 48: Illustration of the details of the hammer test configuration, including the sensor which reads the acceleration normal to the YZ plane shown above

The experimental system identification of the small-scale prototype was carried out by measuring its impulse response (time domain) for two configurations: fixed base and sitting on the soil (presence of the soil-structure-interaction). For measuring the impulse response, an accelerometer was attached on the top of the trailer hitch (sensing normal to the YZ plane) as shown in Figure 48. The sensor was made by the Vellman Oscillator Company, model # APS 230, with a sensitivity of 0.1 Volt/*g*.

After a number of impulse excitations tests and measurements, the apparent rocking frequency of the scaled model for the fixed-based and on the dry-sand are identified as 50 Hz and 30 Hz respectively. Thus, the presence of soil-foundation-structure-interaction has reduced the fundamental frequency as much as 40%; that is, the SFSI stiffness factor is $\omega/\omega_s = 2\pi 50/2\pi 30 = 0.6$ for the dry soil case.

6.5 Finite Element Modeling of the Prototype SFSI System

To better understand and study the small-scale model (Figure 47, right), a solid finite element model of the soil-foundation-structure system was developed (Figure 49A). For performing a series of frequency analyses, a linear (small-strain) FEM was modeled and analyzed with he CATIA and ELFINI programs, respectively. Both programs are products of Dassault Systemes Company (http://www.3ds.com).

The analysis of soil-foundation interaction, especially in the case of embedded foundation, is very complicated and requires careful modeling of the interface between the foundation and the soil. Thus, a complete real-world soil-foundation-structure system usually would be partitioned into two substructures (*i.e.*, the soil-foundation and the structure) to account for the excavated site vs. free field. The introduced scaled model however, is a fixed-based structure on a surface foundation; therefore, the interface between the foundation and the soil was simply modeled as a rigid connection between

the two media which are meshed by linear 4-node tetrahedral finite elements. To model the boundary condition of the soil, since the soil was contained inside the drum, the degrees of freedom on the outer periphery of the cylindrical-shape meshed solid (representing the soil) were constrained to have no outward radial motion while free for all other degrees of freedom.

The properties of the steel pipe with the 8 lb mass on top and the concrete (foundation) were assigned (Compressive strength of the concrete: 30 MPa, Density : 2300 kg/m^3, Poisson's ratio : 0.2) through the standard library of existing materials offered by the software. As for the soil, the physical properties of sand, such as shear modulus, are obtained for the density $\rho = 1600\ kg/m^3$, shear wave velocity at the site, $c_S = 150$ m/s, and Poisson's ratio $\nu = 0.33$.

Utilizing the Lanczos eigensolution technique, a frequency analysis was carried out on the model; the first 1st and 2nd modes of the vibration (bending plus rocking motion in two perpendicular directions), for the fixed-base and the SFSI case, were computed to be 50 Hz and 30 Hz, respectively, which were in agreement with the experimental identification. The result of the frequency analysis and the Von Mises stresses associated with the 1st mode of vibration (Figure 49 B,C) demonstrate that the bending of the pipe along with the rocking of the soil-foundation system contributes to the 1st natural frequency of the SFSI system.

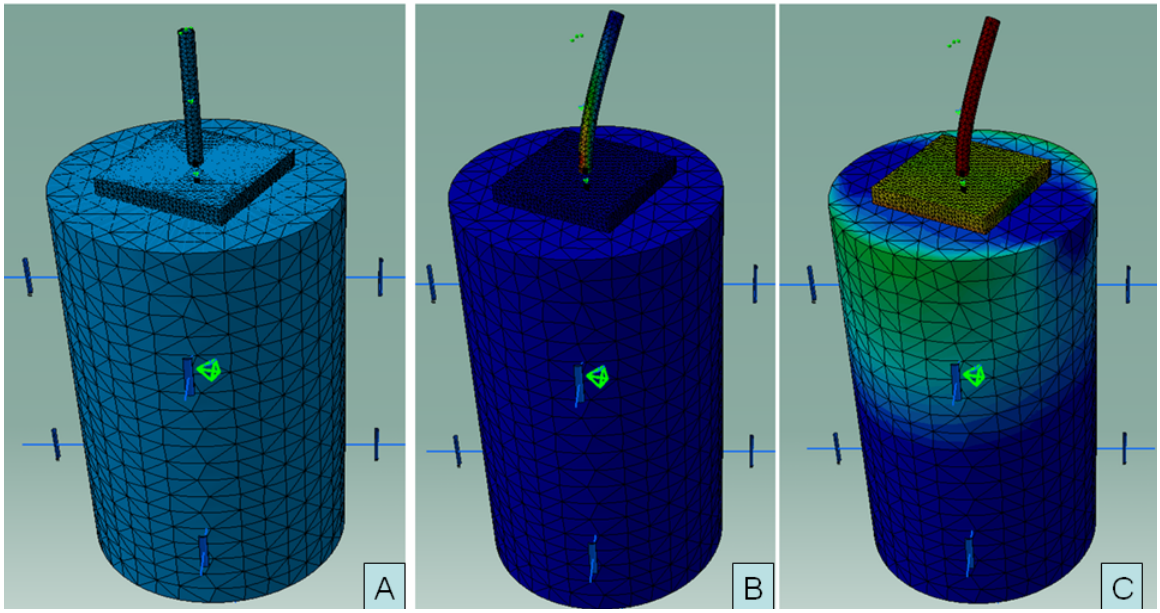

Figure 49: Finite Element Analysis illustration : A) The meshed model, B) Von Mises stress of the 1st bending/rocking mode , C) 1st bending/rocking mode with adjusted color to show the rocking/bending phenomena

The fixed-base bending frequency of the steel pipe was identified, both experimentally and by FEM frequency analysis, to be around 50 Hz. From beam theory, however, the lateral stiffness of a (fixed-based) steel pipe, with area moment of inertia about 10 cm^4 with known Young's modulus (E=210 GPa), and length l = 28 cm, is computed from $k = \frac{12EI}{l^3}$. and with an 8lb mass on top, the bending frequency would be expected to be about 60 Hz, which is around 20% higher then the FEM fixed-base result. Since the pipe that was used in the experiment had threads at both ends, which can be seen on the top of

the pipe in Figure 46, it was speculated that the difference between the identified first mode frequency of the fixed-based and the theoretical expected frequency might be due to reduction of the wall thickness of the pipe where the threads are located. To validate this speculation, two finite element models of the pipe were created. The two models are: a) steel pipe with threads at both ends (*i.e.*, an effective thickness of 0.12 cm over the two top and bottom 2 cm at each end) shown in Figure 51-left, and b) steel pipe with no threads (0.24 cm effective thickness) and fixed at the bottom (Figure 51-right). Similar frequency analyses of these two cases show that thinner cross-section at the bottom of the pipe can cause different rocking frequency of the fixed-base cases.

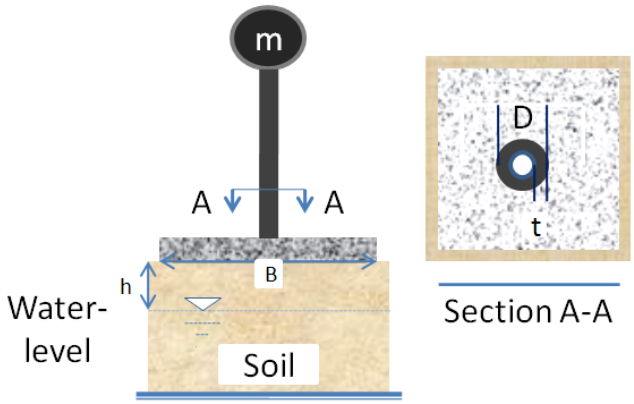

Figure 50: Stick model of a fixed-base SDOF model; representing the steel pipe (outside diameter D = 2.67 cm and wall thickness t = 0.24 cm) used in the experiment.

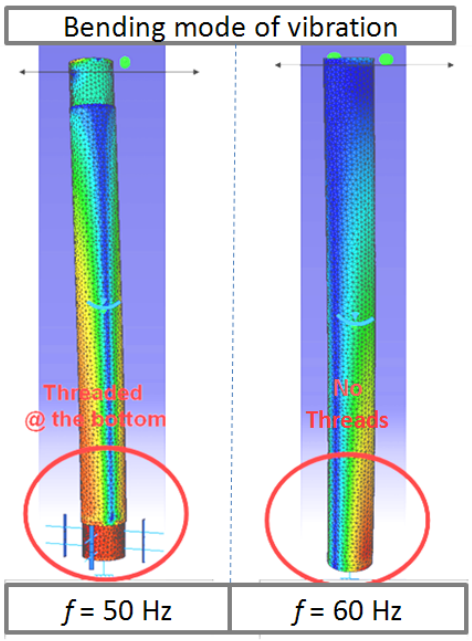

Figure 51: Frequency analysis of the pipe for two cases: Threaded pipe has bending frequency of 50 Hz (Left), compared to the pipe with no threads with 60 Hz.

6.6 Boundary Condition of the Prototype SFSI System

For a real-world structure, the soil horizon is continuous; a physical model must endeavor to provide a lateral boundary as far away as possible that the free field condition is simulated with reasonable accuracy. In the present experiment, the wall of the drum is a physical boundary, and must provide enough clearance to minimize the distortion induced by the boundary on the soil stress field, the soil strain field and, most importantly, the rocking frequency of the SFSI model. The Von Mises stress distribution

inside the soil corresponding to the rocking motion of the SFSI system is shown in Figure 52.

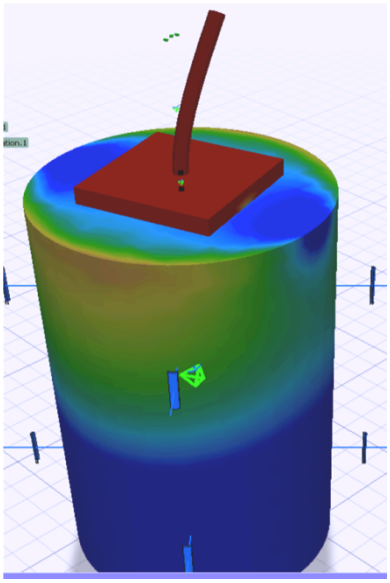

Figure 52:Stress distribution for the soil-foundation-structure model; result from the Finite Element Analysis (color represents the stress levels, adjusted so that the stress inside the soil stands out).

To make sure that enough clearance from the edge of the drum has been provided (*i.e.*, no impact on the rocking mode frequency of the prototype), a frequency analysis of the finite element model was performed with varying drum radius. The resulting rocking frequency is shown in Figure 53 as a function of drum radius. The effect of the edge of the drum on the rocking mode starts to fade away for a drum radius larger than 250 mm. Thus, the boundary condition in this experiment (260 mm radius) causes negligible error in the estimation of the roc.

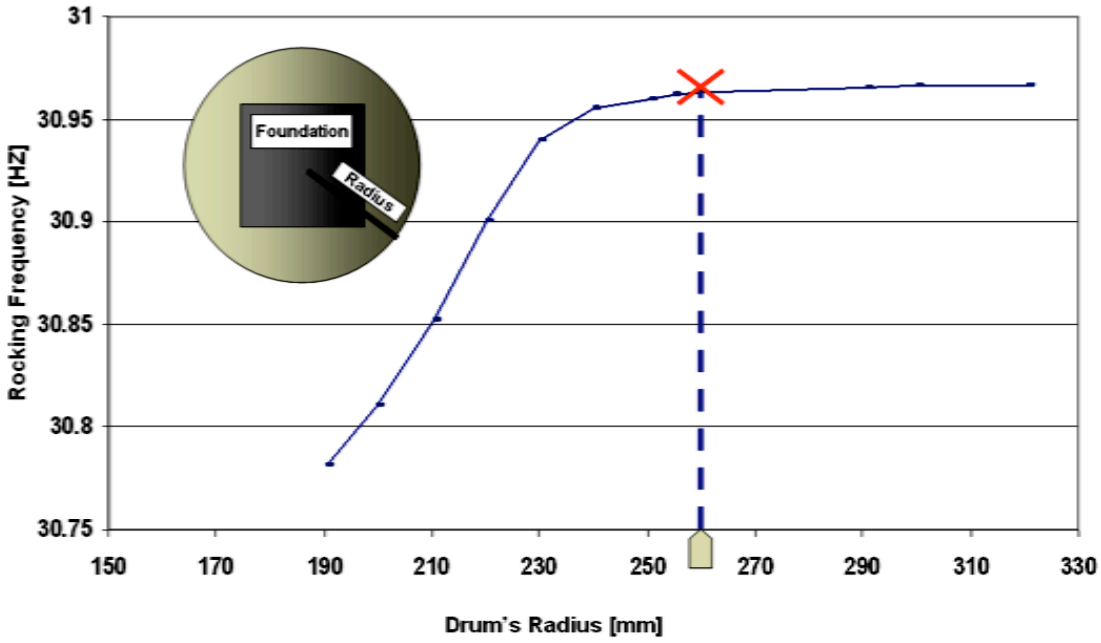

Figure 53: The edge effect analysis of the rocking mode of the prototype model; the estimated frequency by the FEM vs. the drum's Radius.

6.7 Water-level Variation Effect on the Prototype SFSI System

The main objective of this experiment is to verify that the observation made on the variability in identified rocking frequency of the SFSI test structure due to change in the ground water-level could be reproduced in a small-scale prototype in a controlled laboratory condition (*i.e.*, by raising the water-level under the foundation). The experiment was expected to confirm that the identified rocking frequency for the saturated soil would slightly drop compared to the dry case.

The water-level under the foundation is manually increased by adding water via a funnel inserted deep into the soil as illustrated in Figure 42. The water-table level is measured by the transparent tube as illustrated in Figure 54, and is adjusted to a certain depth either by adjusting the input water or by controlling the output via the drainage valve. Water-level distance from the foundation is marked on the drum's wall (Figure 54). A series of experimental impulse response (hammer) tests were carried out to identify the rocking frequency of the soil-structure system at certain desired water levels.

To facilitate comparison of dynamic characteristics for various structure scales, it is convenient to introduce a dimensionless water table depth (*i.e.*, $\eta=h/B$) where h is water-level distance under the foundation and B is the width of the foundation. The water-table depth under the original SFSI test structure, during the monitoring period fluctuated from 3 to 4 feet under the foundation. Since the foundation is a square shape of 4 meters (13 ft) in width; therefore, the normalized water-level depth was around $\eta = 0.3$. The small-scale prototype sits on a foundation of 0.28 meter width. The experimental system identification was performed for various water table depths, much deeper all the way up to grade level (*i.e.*, fully saturated soil).

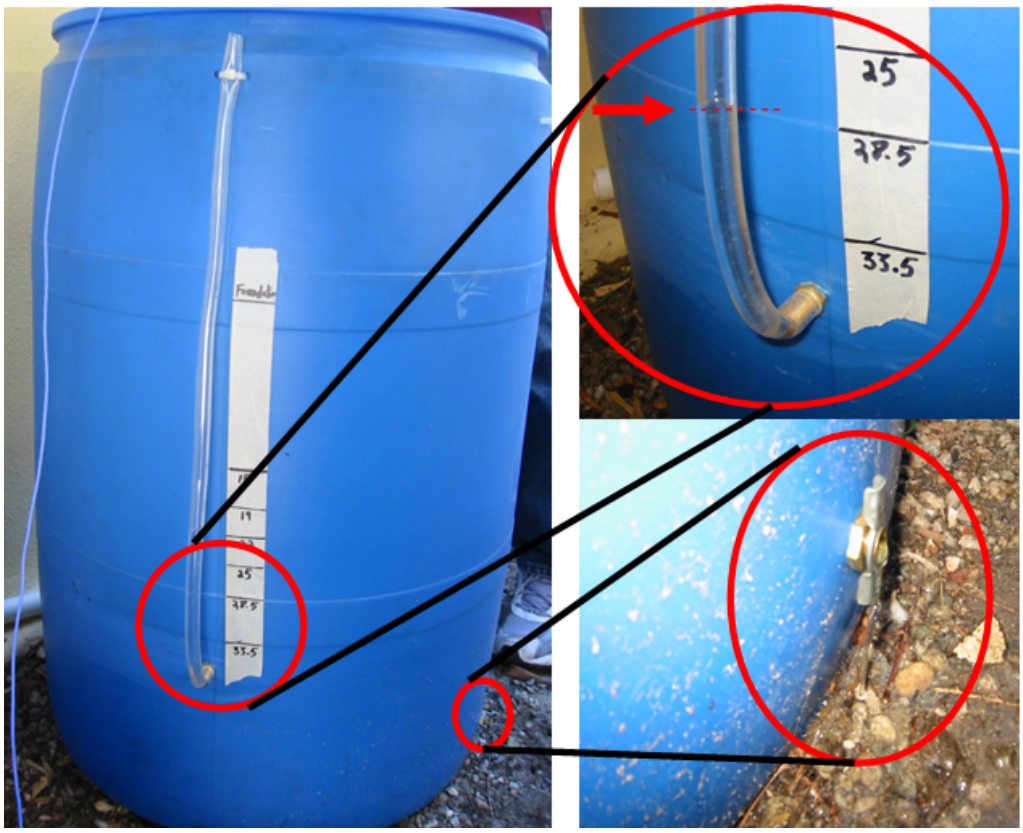

Figure 54: Illustration of the details of the water-level measurement and the drainage valve.

Starting from a totally dry soil three impulse response experiments (hammer test) are performed at each desired level of water in the soil. In Figure 55 and Figure 56, the result of the averaged identified rocking frequency and the normalized water depth for the scaled model tests for $\eta < 0.45$ are graphed. The results are comparable to the observed behavior of the SFSI test structure, with shallower water table resulting in lower identified rocking frequency. To determine the effects of deepening water table level,

several experimental system identifications were performed at several water-levels after draining some water from the drainage valve. The identified frequencies were observed to be of similar trend, (deeper water level increased rocking frequency), but when water depth η grew larger than about 0.20, the rocking frequency were larger while draining than while filling. As Tayabji *et al*. (2000) suggest the change in moisture can cause changes in soil stiffness properties, here it is likely that the significant moisture caused this frequency increase (higher damping was also observed).

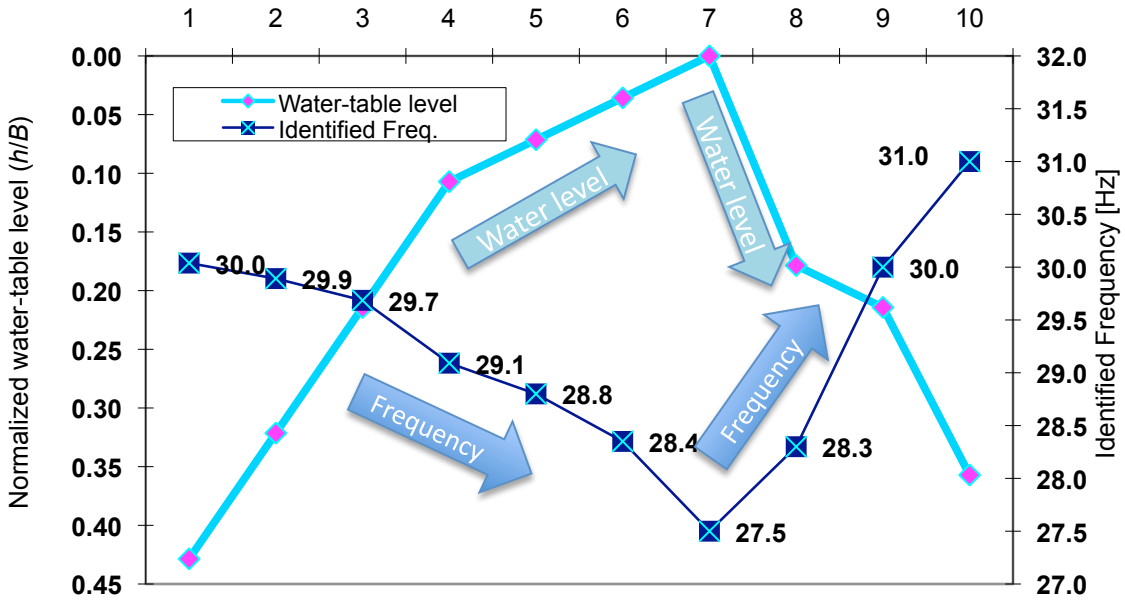

Figure 55: The trend of the identified rocking mode frequency variation in correlation with the water-table fluctuation (fixed-base frequency = 50 Hz).

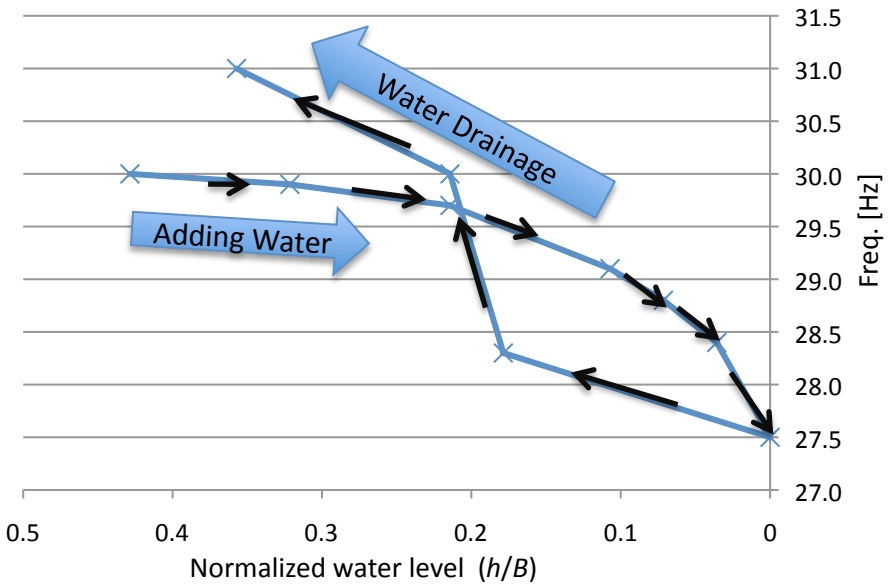

Figure 56: The Identified rocking frequency variation in correlation with the normalized water level fluctuation; water level is raised and then drained as shown by the arrow.

6.8 Summary

In order to characterize the water table effects on the dynamic properties of the SFSI test structure and to reproduce the observed variation in structure's identified rocking frequency and its correlation with the ground water table under the foundation, a laboratory-size model was designed and constructed. The results from tests on this small scale model confirm the trends seen in the large-scale SFSI test structure. The major technical challenge that was encountered during the experiment — which needs to be investigated in future related work — was the behavior of the soil-structure interaction due to presence of moisture in the soil.

7 Pattern Recognition and Regression Analysis Applied to the SFSI Data Set

7.1 Introduction

It is commonly known that the Structural Health Monitoring (SHM) process requires the extraction of a number of damage-sensitive feature(s) from measurement of dynamic response of a system over time. Therefore, it is recognized that SHM and damage detection are, in fact, applications of pattern recognition that are focused primarily on the identification of damage sensitive features.

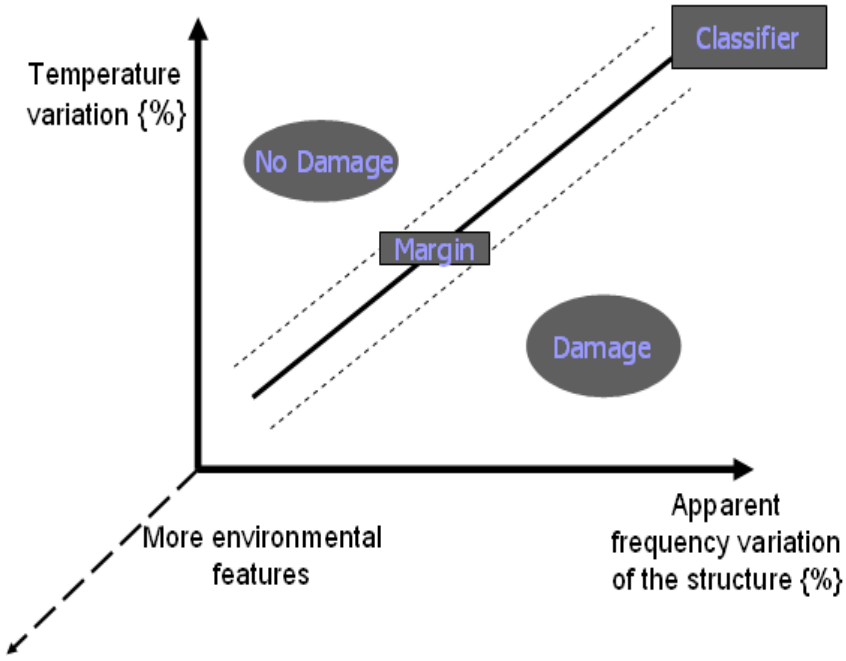

Figure 57: Proposed conceptual schema for the pattern recognition process upon the environmental effects on structural dynamic properties for SHM purposes.

As conceptually illustrated in Figure 57, the main objective of classifying a damaged structure is to ascertain, based on measured dynamic characteristics, if damage is present or not. After defining the sensitive features and training the system based on a given existing data set, the equation of the classifier — often with certain margin — must be mathematically determined. Then the trained system can classify that a new data set would belong to a damaged or undamaged class. Even though the implementation of statistical pattern recognition procedures on damage-sensitive features is not widely practiced (Farrar *et al*., 1999), the development of an automated health monitoring system often engages some statistical approaches. To statistically identify and quantify sources of feature variability for each classification problem, intensive research with sufficient samples is required. The type and location of the sensors and other hardwares (*e.g*., data acquisition/transmittal/storage) need to be determined as well.

7.2 Data Cleansing for Robust Pattern Recognition Process

In general, all sources of variability cannot be extracted out of the pattern recognition problem. Usually to be able to quantify such uncertainties, proper measurements and grounding are necessary. Obviously the data cleansing process, depending on the nature of each application, requires adequate experience and pertinent knowledge.

For structural monitoring purposes an important question would be as to how frequently the data is to be collected in order to train a robust pattern recognition system? Since the environmental/operational effects are widely-known as sources of noise/distortion in monitored data, it is necessary to collect data almost continuously for relatively long time intervals to be able to cleanse the data accordingly. One of the most common procedures for cleansing data is to normalize the measured responses by the operational/environmental inputs. Farrar *et al*. (1999) believe that damage produces changes in the feature distribution with a correlated trend produced by environmental variability. Worden *et al*. (2002) recommend that the normalization process should also include some measure of the environmental parameters. Thus, several features need to be identified and assembled into feature vectors; however, usually a low dimensional feature vector is more desirable, and sometimes a combination of two or more features would be assembled into one feature vector.

7.3 Novelty Detection for Structural Damage Detection

It is important to be reminded that the main well-known disadvantage of the pattern recognition approach for structural damage detection purposes is that, data from both damaged and undamaged systems might not be available. To address this issue, one of the *unsupervised learning* techniques (*i.e*., the *novelty detection*) has been discussed and

employed in this work. The *novelty detection* which is a specific (2-class) unsupervised learning is well recognized as the fundamental requirement of a good classification when the test data contains information about objects that were not known at the time of training.

In the realm of the Novelty Detection, there exist several approaches among which the statistical models have shown very promising results in practice. These models implement the algorithms that operate on the damage-sensitive features to detect damage(s). During training the system, if enough samples for each feature are not collected, the possibility of false indications of damage increases. The False indications of damage may fall into two categories: 1) False negative: the damage exists but cannot be detected. 2) False positive: the damage doesn't exist, though the classifier would indicate the existence of damage. Obviously, each false declaration would lead to different applicative ramifications. While the false negative case implies that a damaged structure has been missed to be detected, the latter case can be considered as a conservative option; with potentially several socio-economical impacts.

The novelty detection approach provides an indication only about the presence of damage in a system of interest; that is, the novelty detection is only a level 1 approach which implies that just the existence of abnormality is supposed to be detected but still there are many situations where this suffices, *i.e*. safety critical systems where any fault on the system would require it to be taken out of service.

7.4 Methodology

In the technique that is presented in current work, the values of particular monitored parameter(s) (*e.g.*, temperature, etc.) during normal behavior of the system are used to establish statistics for the variation of a given structural characteristic (*e.g.*, identified frequency). And subsequently, the variation of a given structural parameter can be virtually reduced by inverse projection of the 1 dimension scattered data onto a 2 (or higher) dimension space as illustrated in Figure 58.

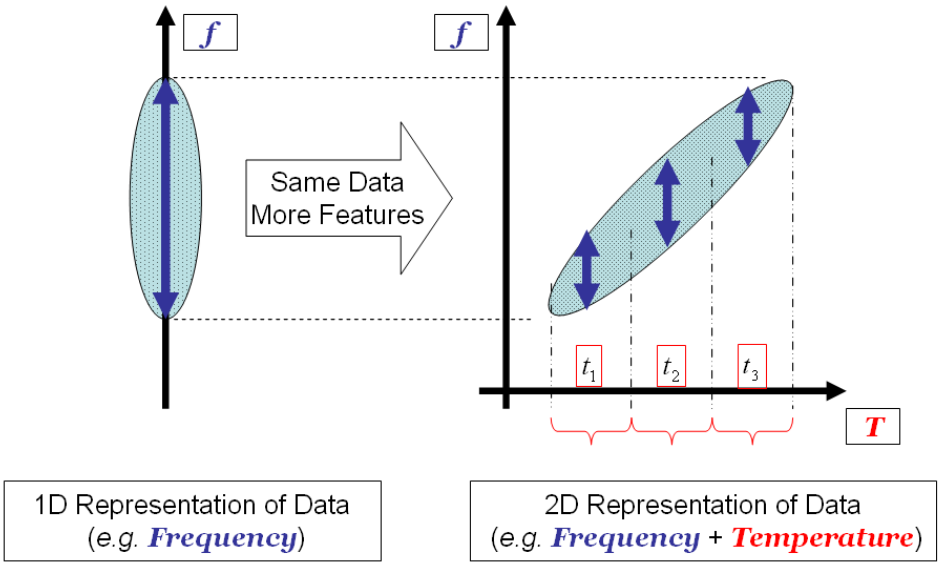

Figure 58: Conceptual representation of a structural parameter variation in one-feature space versus the same data with an additional environmental feature (*e.g.* Temperature).

Then, by discretization of the newly introduced monitoring feature (*e.g.*, temperature) into finite intervals (horizontal axis in 2D space of Figure 58), new subspaces are created.

As a result, a new subsequent test data would require to be compared merely with the data of "normal condition" within its corresponding subspace ($e.g., t_1$ subspace in Figure 58), that has been monitored along with the structural feature(s).

This process which assist reducing the effect of environmental variation in the observed data is considered as part of the larger spectrum of normalization as explained by Worden et al. (2002). The idea is to create a novelty indicator which has been normalized with respect to changes in the structure. In the other words, the statistical properties of the structural variation can actually be expressed as a function of defined environmental feature(s).

For the purpose of the structural damage detection, especially when the soil/environmental effects are also taken into account, the problem would often involve more than just one feature and thus lead to the multivariate analysis which is essential to precisely define the so-called "normal condition". The multivariate data set consisting of *s* observations in *n* variables can be represented as *s* samples in *n*-dimensional space which is more complex compared to a univariate statistics.

The Mahalanobis distance, for instance, can be utilized as an appropriate statistical measure to facilitate a multivariate outlier analysis. Given the mean value μ and the standard deviation σ, mathematically the threshold can be expressed as $\mu \pm \alpha\sigma$; in which α would be an applicative factor that represent statistical confidence level upon which

the alarm level would be determined. Assuming a normal distribution for the data, and by allowing for α being 1 or 2 and etc., different confidence level, *i.e.*, 68.2%, 95.4%, etc. can be reflected respectively. The threshold level therefore, is a quantity its value at a given time being dependent on the estimated mean and definite deviation away from the mean point. This being said, the Mahalanobis distance notion can be used to detect and declare a possible novelty situation. Since the computation associated with the eigenvalue decomposition (Basis transformation) might be very complicated, a methodology has been suggested in this work.

The gist of the proposed approach is to eliminate the eigenvalue decomposition step by discretizing the dataset over finite interval with respect to a given random variable(s) ($e.g., X_1$) which could create discretized subspace as illustrated in Figure 59.

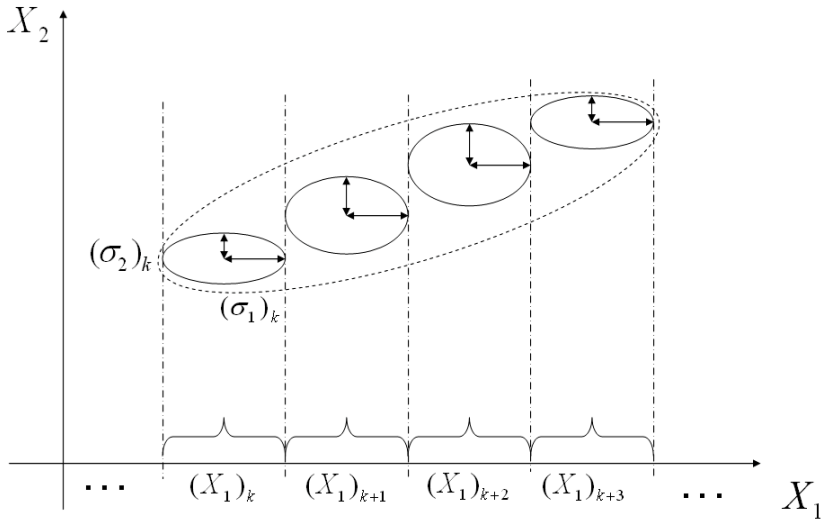

Figure 59: Conceptual schema on the proposed Finite Eigen-space approximation model on a 2-feature novelty detection problem.

Then, each subspace approximately can be represented by a finite eigen-space; as a result, the Mahalanobis distance (and corresponding threshold) would be simply defined just upon each sub-space and independent from the rest of the training data. This approach would clearly have certain advantages when it comes to dealing with a structural feature with *variable standard deviation* on each sub-space; for example due to a non-linearity phenomenon in different mode-shapes. Consequently the standard deviation would not require to be estimated over the whole range of the data and instead, it would be counted for in the Mahalanobis distance definition of each approximated eigen sub-space accordingly as shown in Figure 60.

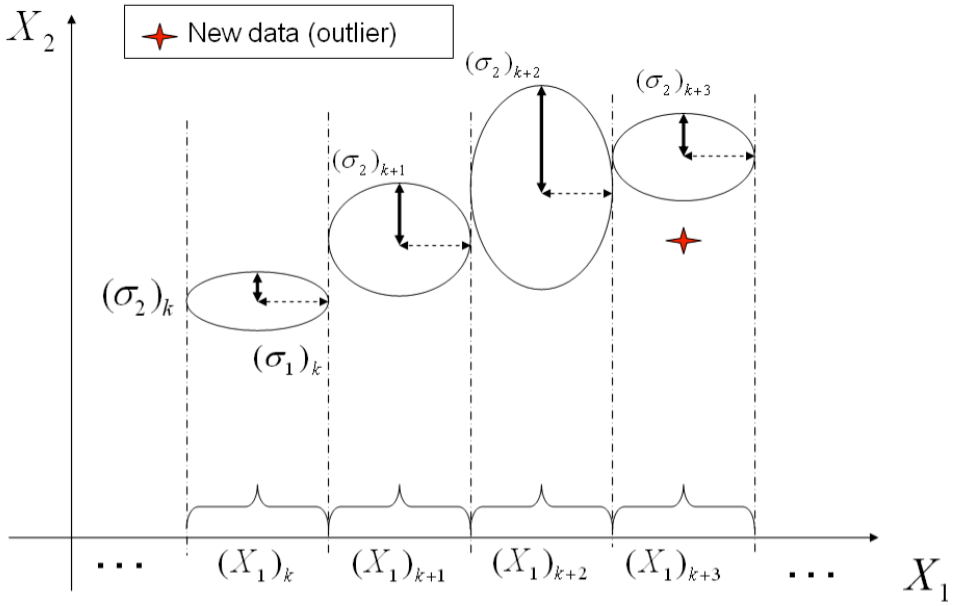

Figure 60: A potential outlier to be detected in a dataset with variable standard deviation in a 2-feature novelty detection problem.

For instance, if X_1 and X_2 are two random variables representing two predefined features, then any data point (a potential outlier as shown in Figure 60) which falls into a given subspace $(e.g.(X_1)_{k+3})$, would be exclusively analyzed and its (Mahalanobis) distance would be compared with the data representing the system's "normal condition" within that subspace, only.

With similar approach, when the environmental variability is present, the statistics of the normal conditions, in a changing environment, simply can be expressed as functions of the environmental parameters. In case of civil structures, however, the "normal condition" due to environmental variability might be represented with constant standard deviation; that could be also verified by observing the collected data from the SFSI Test Structure.

7.5 Statistical Novelty Detection Model for SFSI Test Structure

In a sense, the novelty detection approach can be considered as a statistical outlier problem. It implies that similar to a typical outlier analysis, after defining the "normal condition", the subsequent data is analyzed to see how significantly it departs from the rest of population; the postulation is that the outliers are generated from an abnormal (damaged) condition. Often by assuming a Gaussian distribution for the samples, a

decision boundary (threshold) value needs to be established as well. And the idea is that only training data from the normal operating condition of the structure or system is used to establish this diagnostics. Often the potential outlier can be tested based on deviation statistics which is the distance from the estimated mean of the data set while normalized with respect to the estimated standard deviation. Thus by determining a threshold, the level of disagreement of a candidate outlier is essentially compared against certain predefined criteria. That would allow the outlier to be judged as statistically likely or unlikely to identify abnormal condition. Consequently, depending on the importance and sensitivity of each structural system, an applicative statistical distance from the norm requires to be characterized. Depending on each application, the potential outlier itself may or may not be included (inclusive vs. exclusive) in the training data set. For damage detection processes, however, it is not usually included. The threshold value depends upon whether an inclusive or exclusive strategy has been utilized. For the SFSI test structure, an exclusive approach has been proposed.

To develop a statistical pattern recognition model for the data collected from the SFSI test structure, the statistical novelty detection approach is deployed. It is observed that the identified modal properties of SFSI test structure have been subject to variation that is usually due to changing environment. Therefore, the novelty detector must be able to distinguish between a statistical fluctuation in the data and a real deviation from normality, which would lead to including more features. Even though relatively large

feature vector is not desirable, yet the inclusion of environmental features along with the structural features seems to be inevitable.

To compare new data only with reference data from the same environmental conditions, two possible situations can be perceived: (a) the environment is uniquely characterized by a group of measurable parameters (temperature, ground water-level, etc.); (b) due to some limitations the environmental variations cannot be characterized. The current work is an attempt to mainly address the former situation. The idea is that (during structural monitoring of SFSI test structure) to build a set of reference models parameterized by the environmental variables. The algorithm proposed in this work, is an outlier analysis and outlines how it can be adapted to deal with soil and environmental variations. A case study is carried out which implemented the introduced procedure on the monitored data collected from the fully instrumented SFSI Test Structure over 18 months (for more details see Chapter 3). The data included the output of the accelerometer under the top-slab of the structure subject to ambient vibration (from which the rocking mode frequency can be identified), measured ambient temperature and the ground water-level under the foundation. The data is illustrated in three dimensions in Figure 61. The plots in Figure 62 and Figure 63 are showing the identified rocking mode frequency versus measured water-table and versus the ambient temperature, respectively.

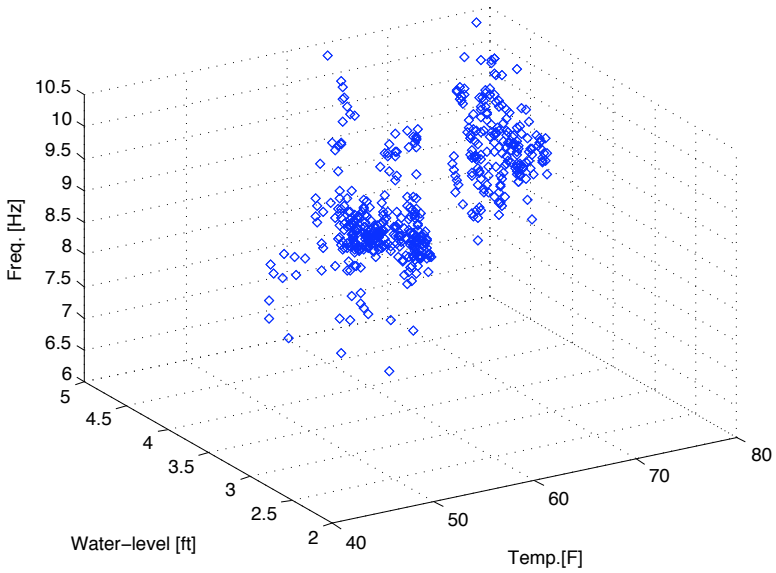

Figure 61: Three dimensional representation of the SFSI data; identified rocking frequency versus the ground water-level and the ambient temperature.

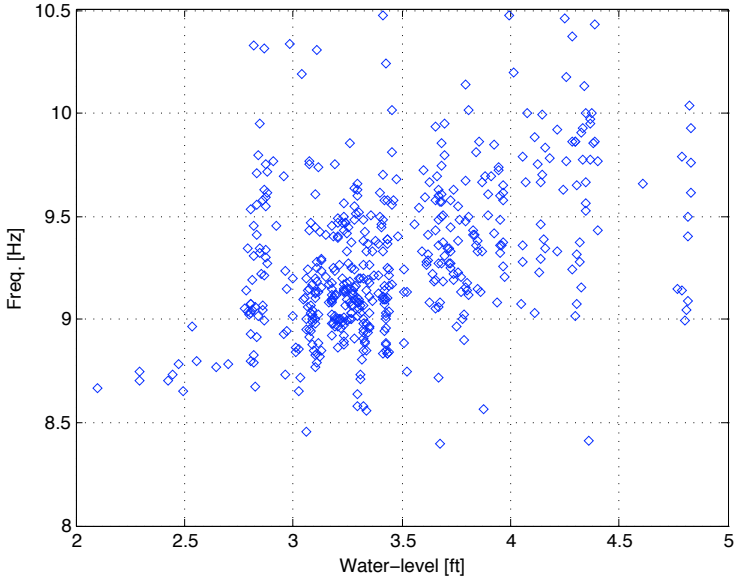

Figure 62: Identified rocking frequency versus the ground water-level under the SFSI foundation.

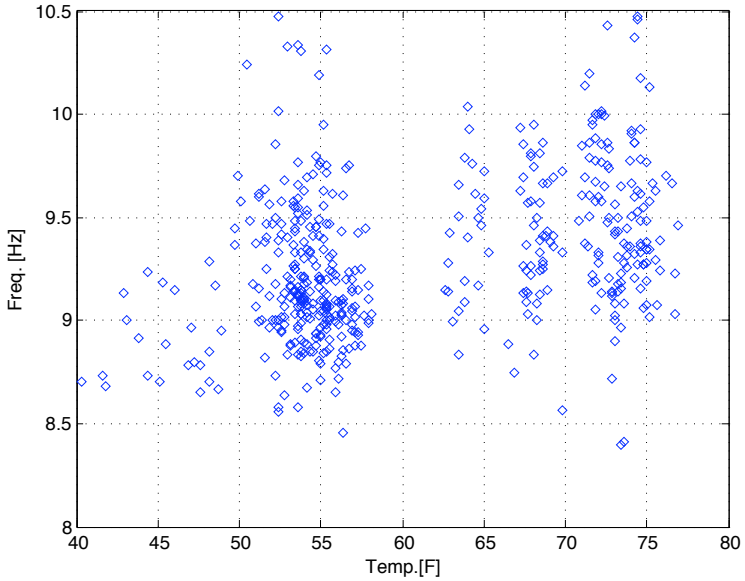

Figure 63: Plot of identified rocking mode frequency of the SFSI Test Structure versus the ambient temperature.

The collected environmental data from the SFSI Test Structure is parameterized by two measurable variables (*i.e.*, ambient temperature *t* and water-level under the foundation *w*), in addition to the structural variable (identified rocking frequency) *f*.

For each sub-space confined within the intersection of the two environmental variables t_i and w_j (see Figure 64), while the environmental effects have been taken into account, the statistical parameters for such a sub-space would be function of environmental variables (*i.e.*, *t*, *w*) and can be written as follows: $\mu_{T_i \cap W_j} = \mu(T_i, W_j)$ and $\sigma_{T_i \cap W_j} = \sigma(T_i, W_j)$.

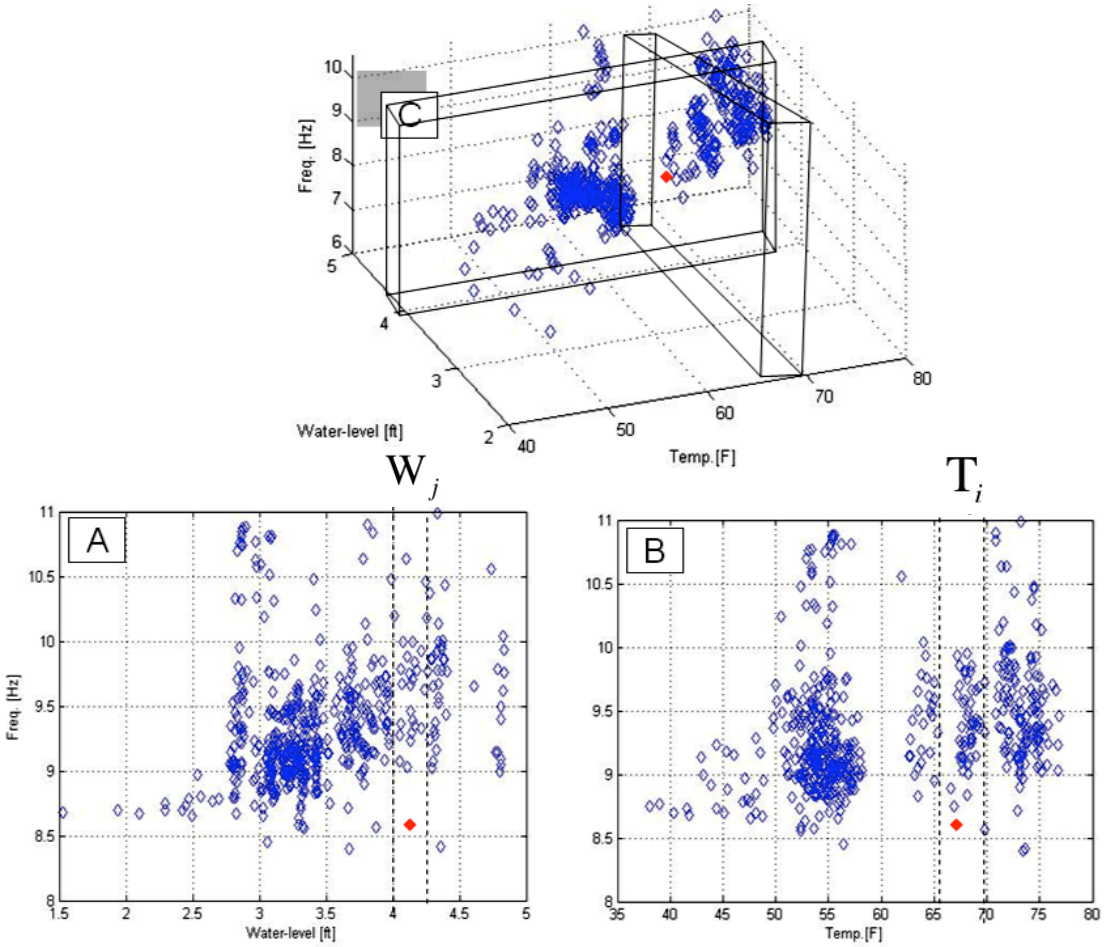

Figure 64: Conceptual representation of the $T_i \bigcap W_j$ sub-space created by the intersection of two finite environmental variables, and a new subsequent test data (solid diamond).

Consequently, the test data, $\mathbf{x}_\xi = \left[t_i \;\; w_i \;\; f_i\right]^T$, with measured temperature t_i, water-level w_i, and identified frequency f_i, can be analyzed upon the corresponding $T_i \bigcap W_j$ eigen-space with univariate mean and standard deviation (*e.g.*, $\boldsymbol{\mu} = \left\{\mu_{T_i \cap W_j}\right\}$). That implies that

with a single structural variable, the Mahalanobis distance could be reduced to a univariate case:

$$D_{\mathrm{M}(\mathrm{T}_i \cap \mathrm{W}_j)}(x) = \frac{\left| f_i - \mu_{\mathrm{T}_i \cap \mathrm{W}_j} \right|}{\sigma_{\mathrm{T}_i \cap \mathrm{W}_j}} \tag{66}$$

Thus, a new subsequent data, say the solid diamond in Figure 64 (identified frequency, water-level and temperature are 8.6 Hz, 4.13 ft and 67° F, respectively), is tested merely against the so-called "normal condition" within that specific region depicted in the plot. As discussed above, depending on the distance (Mahalanobis) and the defined confidence level ($\alpha\sigma$), the novelty in the system can be detected.

In this example, the width of each sub-space has been uniformly, yet arbitrarily chosen. The narrower the sub-spaces are, the more discretized spaces, but of course with less data point would be created. Therefore, depending on the number of existing samples and desired precision, different widths are selected. Herein, μ and σ for the $\mathrm{T}_{65\sim70} \bigcap \mathrm{W}_{4\sim4.25}$ subspace can be estimated as follows: $\mu_{\mathrm{T}_{65\sim70} \cap \mathrm{W}_{4\sim4.25}} = 9.52$ Hz and $\sigma_{\mathrm{T}_{65\sim70} \cap \mathrm{W}_{4\sim4.25}} = 0.35$ Hz. Suppose that the alarm level (threshold) has been defined such that for the Mahalanobis distance greater than, say 2, the abnormality warning or alarm will be set off. Statistically, that means that for the test point more than $2\sigma_{\mathrm{T}_{65\sim70} \cap \mathrm{W}_{4\sim4.25}}$ away from the mean (corresponding to approximately a 95% confidence level), a novelty in system

would be detected. The Mahalanobis distance of the test data (*i.e.*, f = 8.6 Hz) can be calculated as following:

$$D_{M(\mathrm{T}_{65\sim70}\cap\mathrm{W}_{4\sim4.25})}(x)=\frac{|8.6-9.52|}{0.35}=2.63 \tag{67}$$

In other words, the test data resides a distance 2.6σ from the sample mean within that subspace. Thus, depending on the designated alarm or warning level, it can be declared as a novelty in the structure.

The proposed procedure was also used to see if the second configuration in which all the bracings were removed would represent a damaged case compared to the first configuration. As a matter of fact, the SFSI Test Structure with no bracings is of significantly lower rocking frequency and should be confidently detected as a novel condition compared to the braced configuration.

A data point from the unbraced configuration was randomly selected which carries information on the identified frequency, temperature and ground water-level at the site collected in January 2007. As illustrated in Figure 65, the selected potential outlier (shown as a solid diamond) has an identified frequency of 6 Hz, while the ambient temperature and the water-level are logged as 48° F and 4.2 ft under the foundation, respectively. Again, the environmental features (*i.e.*, t and w) are divided into certain sub-spaces within which the structural feature would be compared with the normal condition.

The t_i and w_j sub-spaces corresponding to the testing data points are illustrated in Figure 65.

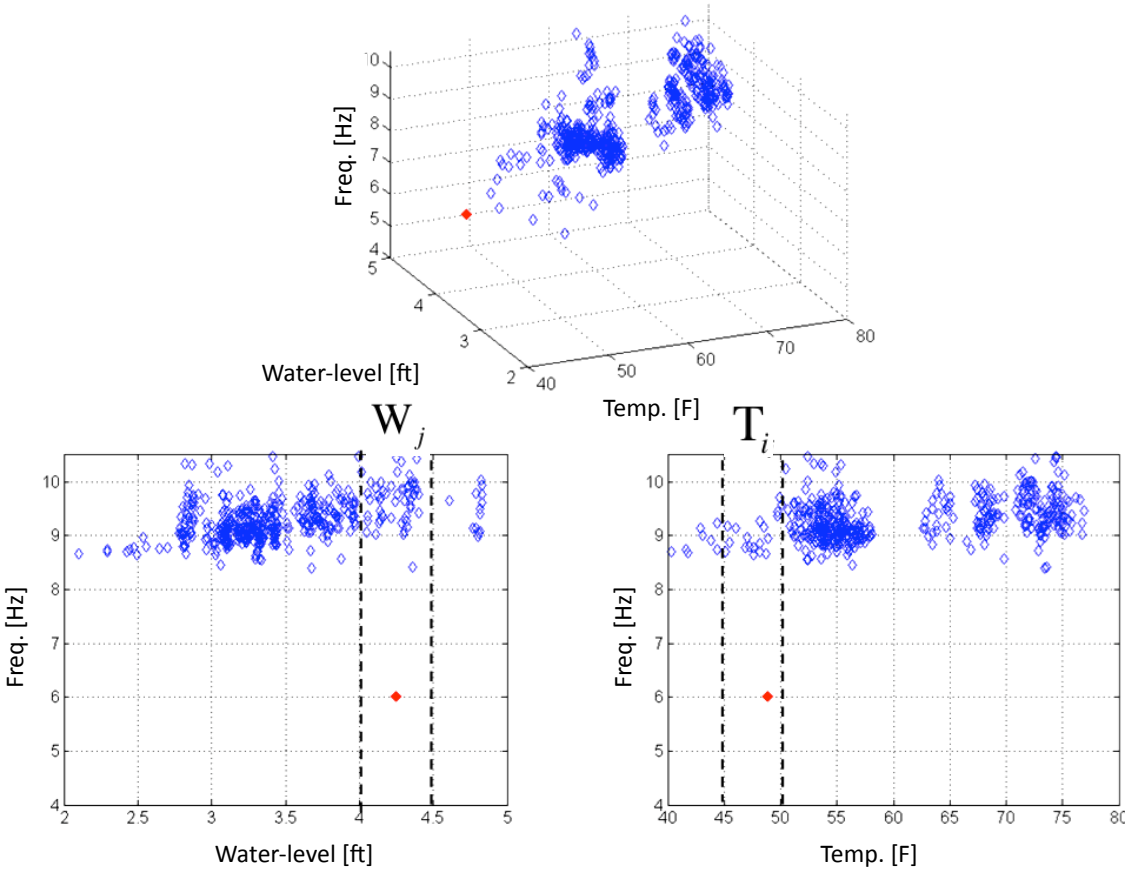

Figure 65: The novelty detection of the SFSI Test Structure with no bracings (solid diamond) against the same structure with bracings.

Similarly the mean, the standard deviation and the Mahalanobis distance can be estimated for the intersection of these sub-spaces as follows:

$$\mu_{T_{45\sim50} \cap W_{4.0\sim4.5}} = 9.02 \text{ Hz}$$

$$\sigma_{T_{45\sim50} \cap W_{4.0\sim4.5}} = 0.2 \text{ Hz.}$$

$$D_{M(T_{45\sim50} \cap W_{4.0\sim4.5})}(x) = \frac{|6 - 9.02|}{0.2} = 15.1$$

As expected, the testing data is significantly ($15\sigma_{T_{45\sim50} \cap W_{4.0\sim4.5}}$) away from the mean of the normal condition in that sub-spaces; therefore, it would be declared as a novelty case for the original SFSI Test Structure.

7.6 Data Cleansing of the SFSI Data Set

The primary statistical analysis on the collected data set in Chapter 4, showed significant variability (*i.e.*, 10%) in the identified rocking frequencies of the SFSI test structure. In addition to the identified frequency of the test structure, the temperature and water table level at the site from 6/17/05 through 9/4/05 were also collected. Then, it was shown (Figure 22, Figure 29) that the variation of the identified frequencies and those environmental parameters were correlated.

The data analysis by utilizing statistical approaches — compared to deterministic methods — requires several validation and cleansing processes before being able to provide any strong assertions. Therefore, to achieve a higher level of certainty upon the quantitative correlation between the identified frequencies of the SFSI test structure and the measured environmental parameters, more investigation is needed. First, to separate

the effects of the temperature and the water level on the frequency variation of the SFSI test structure, herein some data cleansings in conjunction with the correlation analyses are applied to the SFSI data set. Subsequently, to study the combined effects of temperature and water table variation on the identified frequencies, a three dimensional regression analysis is performed.

By examining the variability trend of the two environmental parameters in the data set, one can easily notice that while temperature has a daily and seasonal fluctuation, the water level changes only in a seasonal basis. That is said, the temperature effect on the identified frequencies can be normalized and isolated from the water-level-variation effect. To cleans the data from the temperature effect — assuming that the effect is linear — the normalized identified frequencies with respect to an arbitrary temperature, say T = 55° F, is computed. As a result, a temperature-effect-free measure of correlation between the identified rocking frequencies of the SFSI test structure and the depth of the water level under the foundation is obtained.

To have a quantitative measure of the daily effect of the temperature, a linear curve is fit to the data for those days that enough identified frequencies and measured temperatures are available. For example, in Figure 66 a linear fit (and the residuals) to the scattered plot of identified frequencies for a given day (*i.e.*, 16 Oct. 2005) versus the measured temperature is shown. The regression coefficient (0.19 Hz/ºF) indicates the slope of the line resulted from the linear least square fitting to the data for that day.

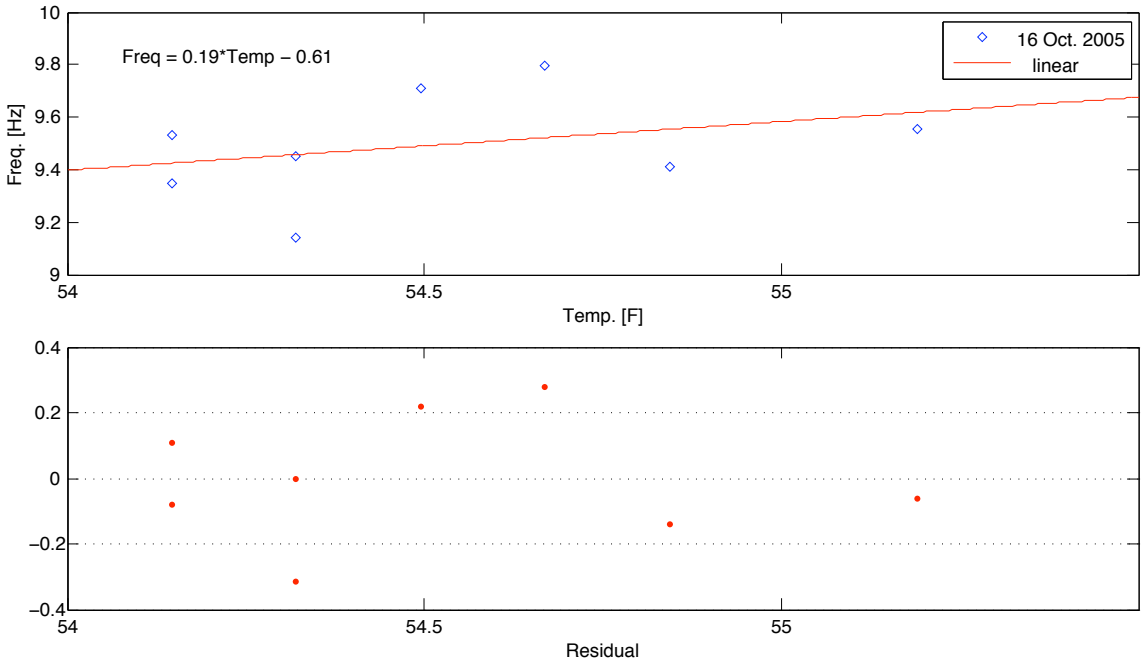

Figure 66: Linear regression of identified frequencies dated 16 Oct. 2005 versus measured temperatures on that day (top) and the residual results of the fit (bottom).

To obtain more precision, this process is repeated for several days and the histogram of the estimated regression coefficients has been plotted in Figure 67. The estimated mean and standard deviation for all these coefficients are 0.16 Hz/ºF and 0.02 Hz/ºF, respectively. Consequently, the data can be normalized with respect to daily temperature variation, by 95% (2σ) confidence interval as is shown in Figure 68. The equation of the normalized data set can be written as

$$f_{55^\circ} = 0.16\left[\mathrm{Hz}/{}^\circ\mathrm{F}\right](\pm 0.04).\,(t - 55^\circ[\mathrm{F}]) + 8[\mathrm{Hz}] \tag{68}$$

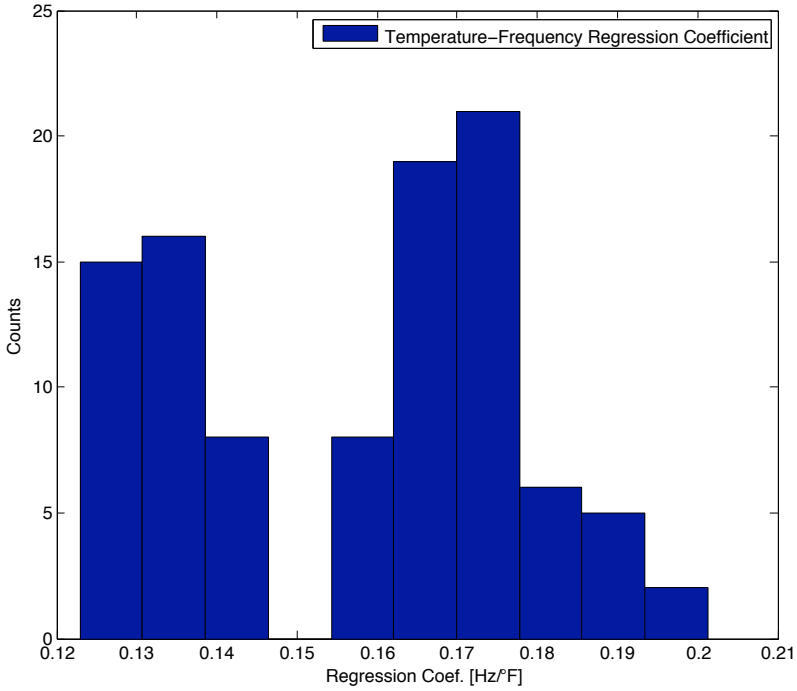

Figure 67: Histogram of regression coefficients of daily temperature-frequency analysis.

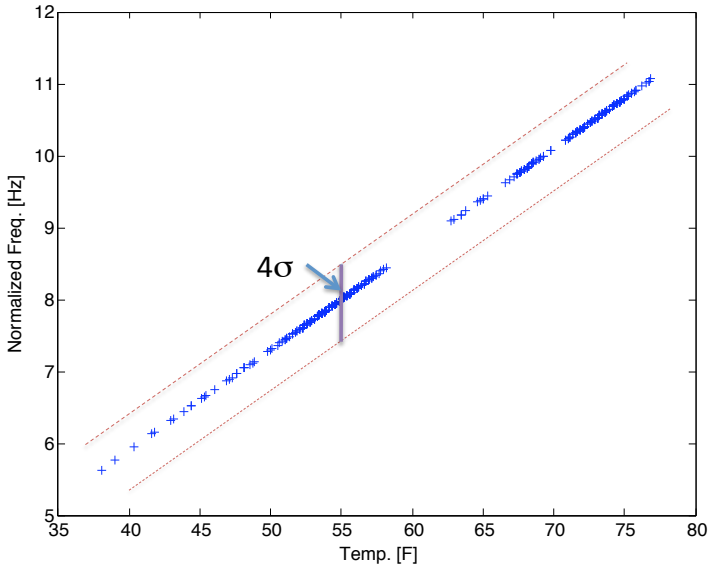

Figure 68: Linearly normalized frequencies with respect to the *T*= 55° F.

Further, the normalized (temperature-effect-free) identified frequencies are plotted versus the water level depth in Figure 69 (bottom) and is compared with the original data (top). It is noticeable that the normalized frequencies have significantly decreased, while the ground water level has raised (*i.e.*, lower water level).

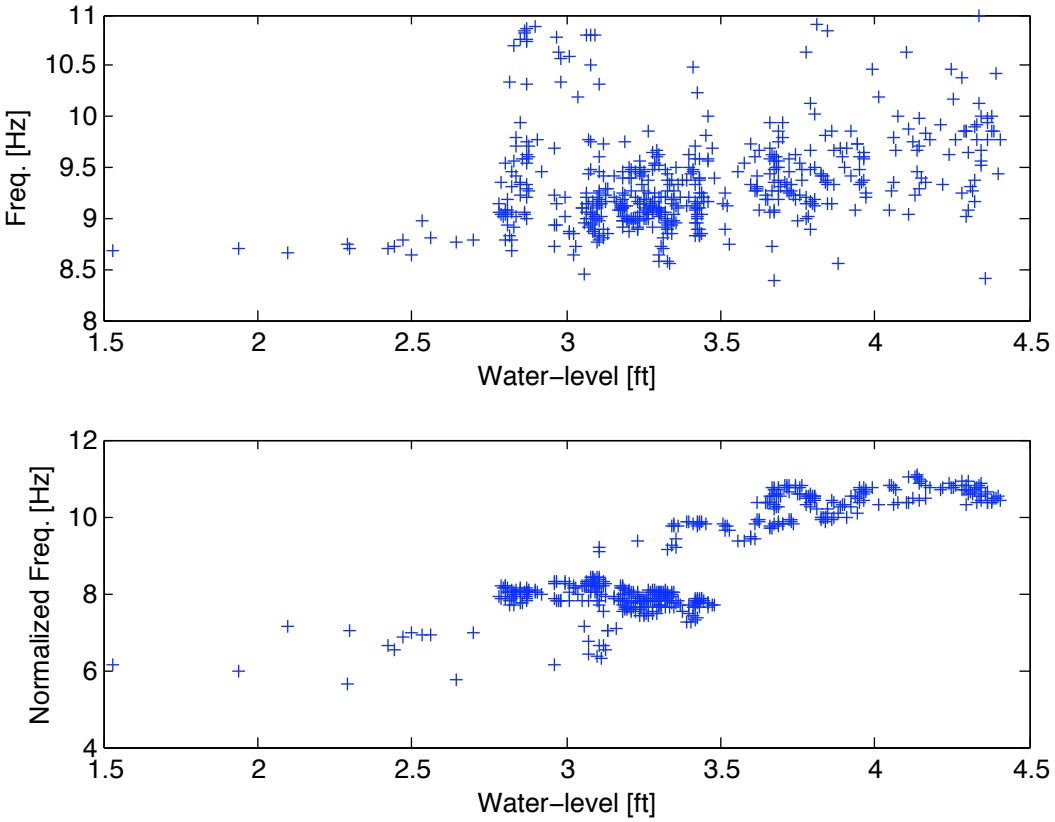

Figure 69: The comparison between the identified frequencies versus the water level; before (top figure) and after normalization (bottom figure).

To better understand the correlation between these environmental parameters and the identified rocking frequencies of the SFSI test structure, the data is divided into two sub-

categories; summer vs. winter. First, the correlation coefficients between the temperature and the water level for the winter and the summer data are computed as 0.8 and 0.04, respectively. That implies that the decoupling of the temperature and the water level effects on the identified frequencies would be more intricate for the summer data set. The high correlation between these two parameters can be explained based on the fact that there was almost no precipitation at this site during summer 2005. The normalized frequencies vs. the water level data for both summer and winter are shown in Figure 70.

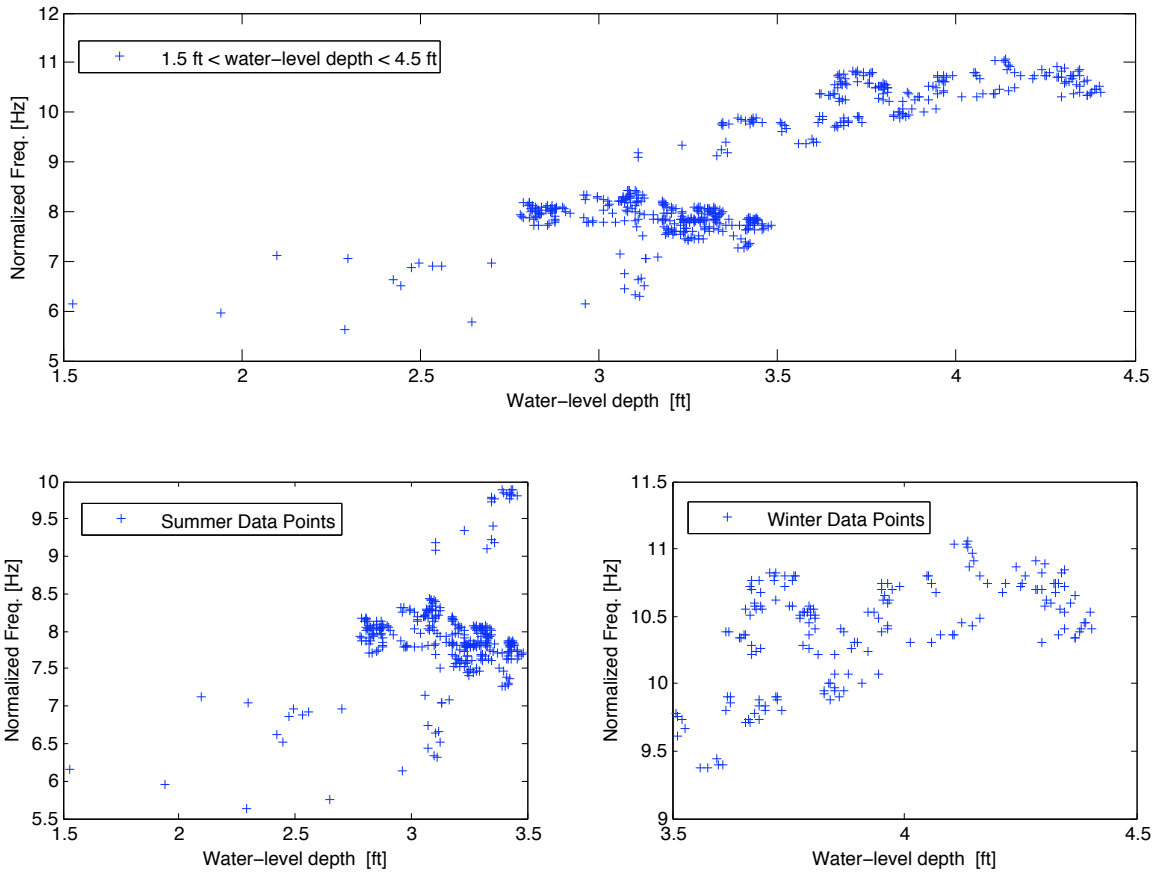

Figure 70: The normalized frequencies variation versus the water level fluctuation at the site for the summer (bottom left) and the winter (bottom right), respectively.

It is also important to note that while the identified frequencies and the temperature are pretty correlated (Correlation Coef. ≅ 0.3), overall the normalized frequencies and the water level data are highly correlated (Correlation Coef. ≅ 0.8). The normalized frequencies and the water level variation are plotted in Figure 71. It can be seen that as the depth of the water level increases the normalized frequencies increase as well. In Figure 72, the result of a linear regression and the residuals of the fit are plotted.

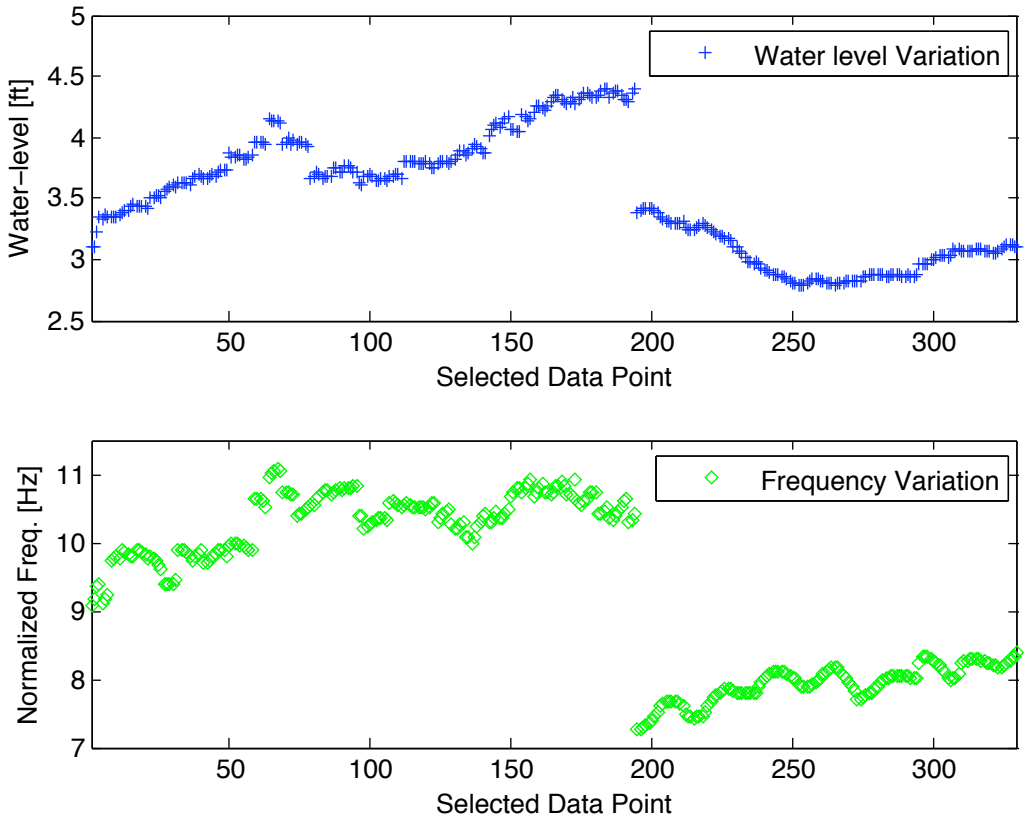

Figure 71: Comparison between the water level variation at site and the identified frequencies of the SFSI test structure in the top and bottom figure, respectively.

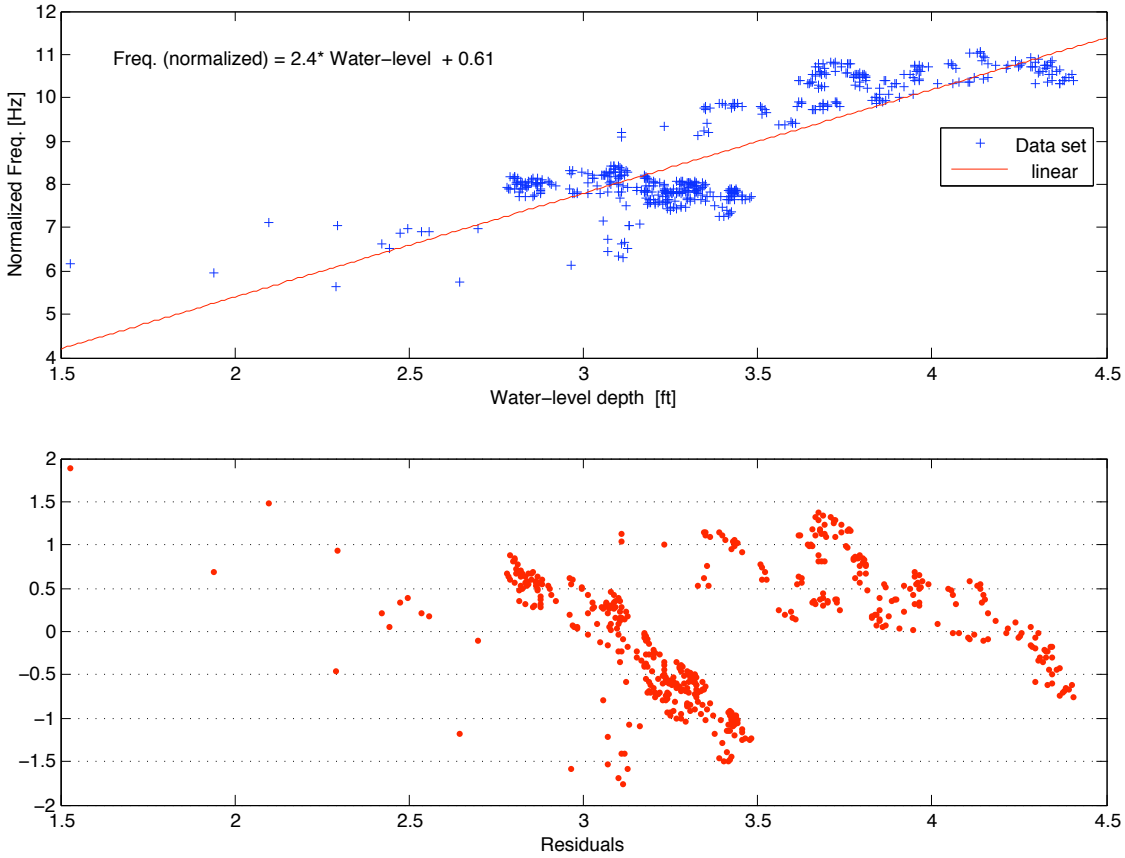

Figure 72: Linear regression result of a fit to the Normalized frequencies versus the water level variation (top figure) and the residuals (bottom figure).

Further, to improve the regression result, a non-linear curve is fit to the normalized frequencies data set. By utilizing MATLAB's curve fitting toolbox, a power function ($e.g.,\ f(x) = ax^b + \varepsilon$) for the prediction of the normalized frequencies is tried, where x would represent the water level depth, a and b are the parameters to be estimated and ε is the associated error. The result of the fit along with the 95% prediction bounds are plotted in Figure 73. The a, b parameters of the fit are estimated as 5.23 and 0.42, respectively.

The goodness of the fit is computed as $r^2 \cong 0.7$, which is very close to the result of the linear fit.

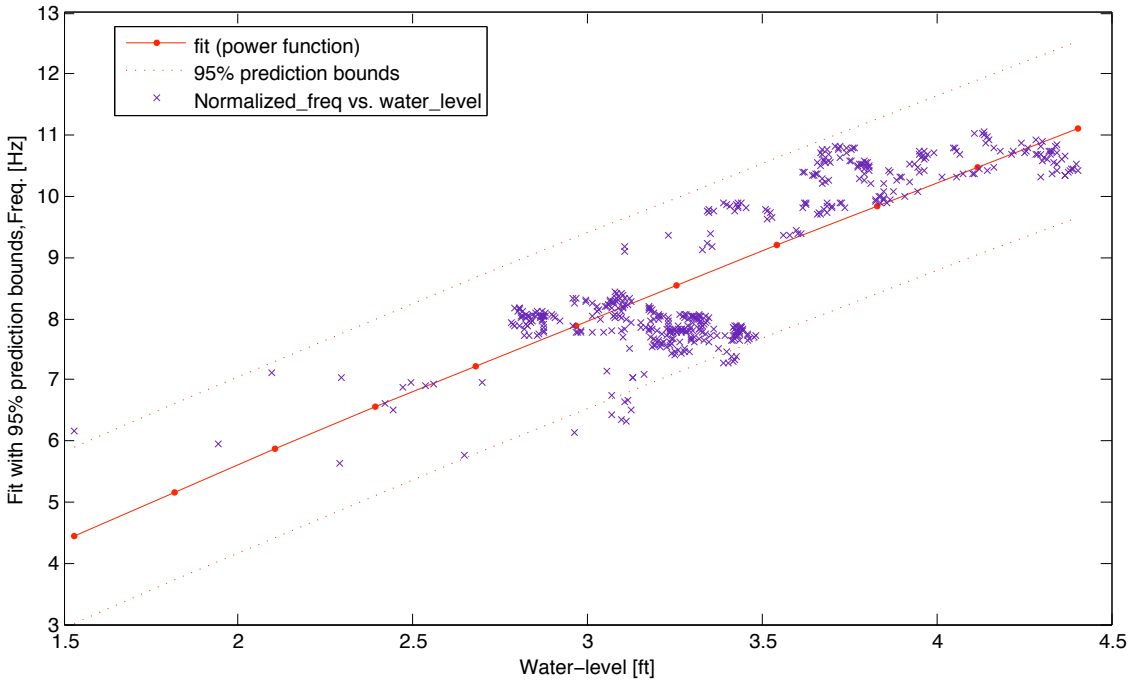

Figure 73: Non-linear regression and 95% prediction bounds result of a fit to the Normalized frequencies versus the water level.

7.7 Three Dimensional Regression Analysis

By fitting a linear plane to the available data of three variables (*i.e.*, temperature, ground water table and the rocking frequencies of the braced structure), the effect of environmental variability in identified frequencies can be characterized.

Utilizing the least-squares fit, which is the most common type of linear regression, the best-fit plane's coefficients are estimated; *i.e.*, the constant f_o (frequency) and the coefficients a and b (corresponding to temperature and water-level) for the following equation are estimated:

$$f = f_o + at + bw \tag{69}$$

where f, t and w are random variables corresponding to identified frequency, temperature and water level, respectively. The formulation for computing the coefficients are as follows:

$$a = \frac{\left(\sum w_i^2\right)\left(\sum t_i f_i\right) - \left(\sum t_i w_i\right)\left(\sum w_i f_i\right)}{\left(\sum t_i^2\right)\left(\sum w_i^2\right) - \left(\sum t_i w_i\right)^2} \tag{70}$$

$$b = \frac{\left(\sum t_i^2\right)\left(\sum w_i f_i\right) - \left(\sum t_i w_i\right)\left(\sum t_i f_i\right)}{\left(\sum t_i^2\right)\left(\sum w_i^2\right) - \left(\sum t_i w_i\right)^2} \tag{71}$$

$$f_o = \bar{f} - a\bar{t} - b\overline{w} \tag{72}$$

where $\bar{f}$, $\bar{t}$ and $\overline{w}$ are based on the 520 data points from the braced configuration, the plane parameters f_o, a and b are 8.3979 Hz, 0.0079 Hz/°F and 0.1433 Hz/ft, respectively. As a result, the plane that best fits to the collected data, for the braced SFSI test structure, can be written as:

$$f = 8.3979\ [\text{Hz}] + 0.0079\left[\text{Hz}/{}^{\circ}\text{F}\right] t + 0.1433\left[\text{Hz}/\text{ft}\right] w \tag{73}$$

The best-fit plane (as a result of a linear regression), and the data are plotted on a three dimensional axis in Figure 74. This simplified solution could assist in finding outliers representing abnormal (damaged) condition for the SFSI test structure.

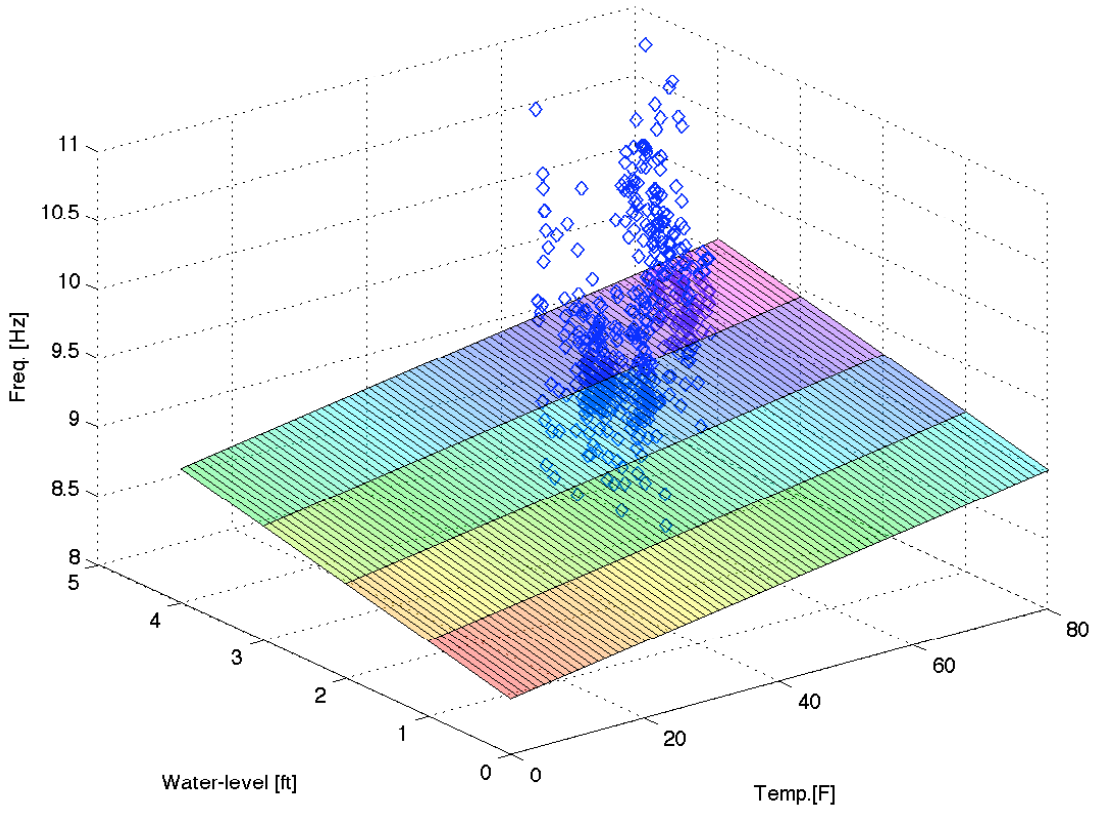

Figure 74: Three-dimensional demonstration of the temperature, water-level and identified frequencies of the SFSI test structure, and the best-fit plane to the collected data (estimated from multi-variat regression analysis).

In Figure 75, the dispersion of the collected data around the fit-plane is also shown. It is noticed the data is heavily dispersed around the linear plane.

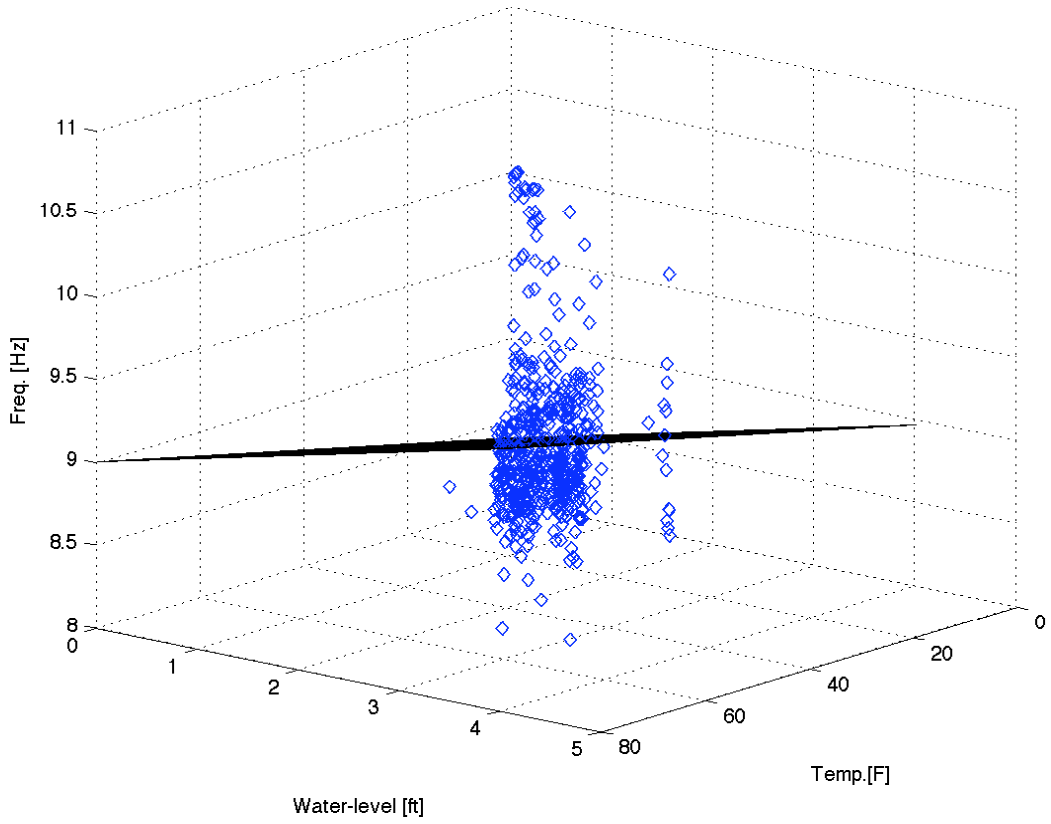

Figure 75: Three-dimensional demonstration of the temperature, water-level and identified frequencies of the SFSI test structure; the dispersion of the data around the best-fit plane has been illustrated.

Similarly, a three dimensional regression analysis is performed on the normalized (temperature-effect-free) data versus the water level and the measured temperature data points. The normalized data points — with mush less dispersion around the best-fit plane — are shown in Figure 76. That is, the dispersion of the normalized data with respect to

the temperature effect has been vanished and the points are almost laid down on the best-fit plane.

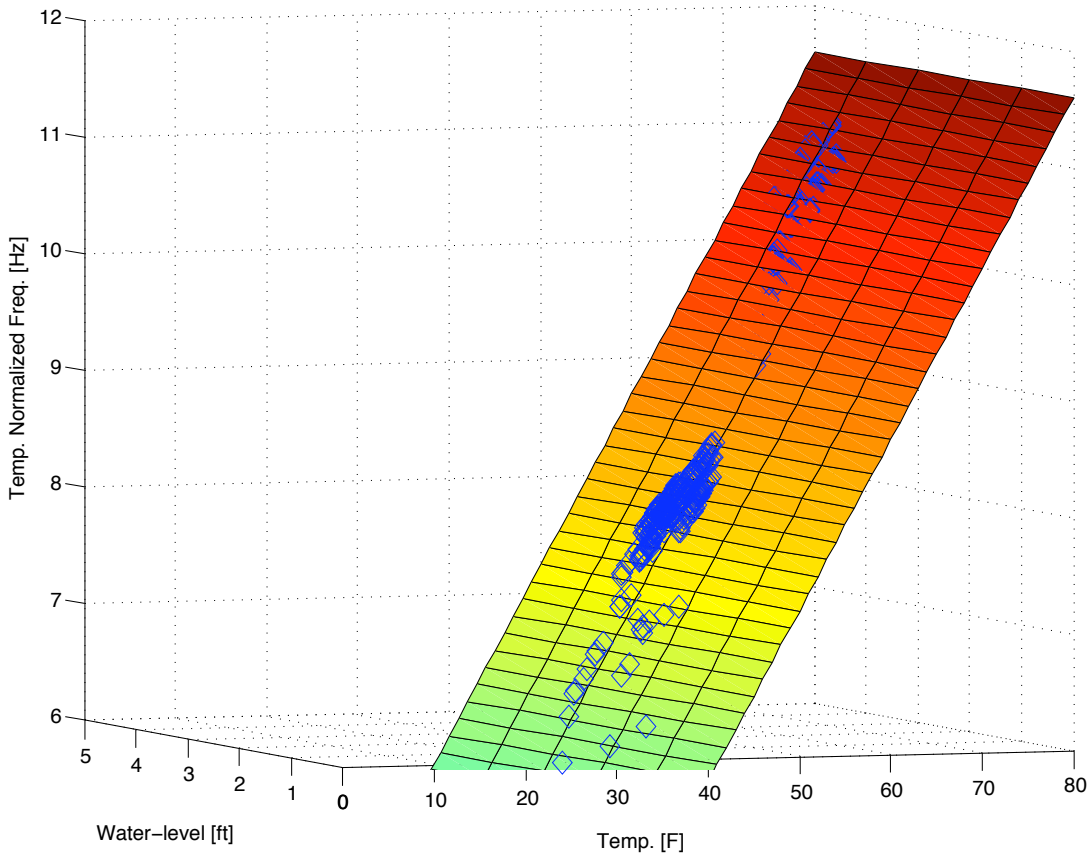

Figure 76: Three-dimensional demonstration of the temperature, water-level and normalized identified frequencies of the SFSI test structure, and the best-fit plane to the collected data (estimated from multi-variat regression analysis).

7.8 Summary

As elaborated, the novelty detection approach could be shown as a good classification technique when the training data does not contain information about the damaged condition. The notion of the developing statistical models as a promising approach to enhance the damage detection of the structural health monitor was also discussed.

In addition, the environmental variations suggested to be extracted out by introducing finite sub-spaces created over the environmental features and by discretization of each feature (*e.g.,* temperature) into finite intervals. Therefore, a new subsequent test data would require to be compared merely with the data of "normal condition" within its corresponding subspace with reduced variation.

Further, to cleans the data with respect to the environmental parameter(s), some regression analyses were carried out. In fact, the data was normalized with respect to the temperature effect, which has a daily variation. As a result, the normalized data set could assist in better understating of the effect of the other environmental parameter (*i.e.*, water level under the foundation) on the variability of the identified frequencies.

8 Conclusions

The environment — temperature, rainfall, humidity, etc. — affects dynamic properties of structures, which, in turn, impact the robustness of structural health monitoring techniques that use global dynamic response measurements. In this study, the controlled conditions of the NEES SFSI test structure at GVDSA were used and modeled to quantify these environmental effects on the soil-foundation-structure system. Repeated experimental modal analyses, coupled with monitoring of temperatures and ground water level, has resulted in the following conclusions:

- Significant correlation between the identified structural properties and measured environmental parameters (*i.e.,* temperature and ground water-level under the foundation) is present in this soil-foundation-structure system.
- Temperature effects on the measured modal frequencies of the structure are quite significant. Depending on the configuration of the structure, daily temperature-correlated variations are 3–10%.
- Saturation of the soil appears to have very complex effects on the dynamic properties of the SFSI system. While the saturation effects are partially masked by daily temperature-induced variability, the soil saturation is found to be on the order of a few percent. It depends on several factors, including:
    1. soil properties: type, stiffness, drained versus un-drained condition, etc.

2. foundation shape and type (*i.e.*, surface versus embedded).
3. relative dynamic properties of the fixed-base structure and the soil-structure system.

Further, a small-scale prototype model of the SFSI test structure was used to validate the observed variation in the full-scale SFSI Test Structure's identified fundamental frequencies. The increase of the water-level in the dry soil showed a trend similar to that observed in the SFSI test structure. The moisture in the soil seems to be affecting both the fundamental rocking frequency and damping of the SFSI system.

Different methodologies for modeling of soil-structure interaction systems were discussed, emphasizing that the intended use of each model needs to be specifically defined so that a proper predictive model can be developed. To model the soil saturation effect on the rocking frequency of a simple SDOF system representing the SFSI test structure, it was shown that the apparent fundamental rocking frequency of a SFSI system is a function of saturation level and soil properties and might increase or decrease depending on the characteristics of the structure relative to the soil. The simplified cone model applied in great detail in this research does not predict the observed decrease in the SFSI test structure's fundamental rocking frequency as the water table increases. The effects of other environmental parameters (*e.g.*, moisture in the soil, etc.) or soil behavior — such as cohesion or expansion — are speculated to be significant enough that they should be investigated further for this particular case. Suggested investigations might

include soil sampling and laboratory testing for cohesion and expansion, better soil moisture measurements, and localized in-situ soil property measurements underneath the structure. Future research attempting to model the observed behavior should perhaps look at a more complete physics-based approach to this particular soil.

Most vibration-based damage detection approaches can be described by a pattern recognition paradigm. A methodology for generalized detection of damage with environmentally-controlled variability has been proposed based on idea of *novelty detection*. Environmental variations can be extracted by introducing features (such as temperature) and then, by discretization of the newly introduced monitoring feature into finite intervals, new subspaces are created within which subsequent test data are compared with data of "normal condition". The notion of using novelty detection to develop robust statistical models for damage detection was discussed. This discussion is just a start; further research will be needed to apply this generalized technique to the SFSI Test Structure and to other full-scale structures.

Based on this research, it can be concluded that studying the environmental variability of identified vibration-based parameters and developing methodologies for cleansing data are critical to establishing more robust health monitoring in real civil structures.

References

Allemang, R.J., and D.L. Brown (1998). "A unified polynomial approach to modal identification." *Journal of Sound and Vibration,* **211**(3), 301–322.

Arminger, G., C.C. Clogg and M.E. Sobel (eds.) (1994). *Handbook of Statistical Modeling for the Social and Behavioral Sciences* (first edition), Springer, ISBN-10: 030644805X.

Asghari, A., E.A. Johnson and R.L. Nigbor (2006). "Environmental Effects on Identified Parameters on the NEES SFSI Test Structure."*4th World Conf. on Structural Control and Monitoring*, University of California, San Diego, CA, July 11–13. CD-ROM.

Asghari, A., E.A. Johnson and R.L. Nigbor (2008). "Characterization of Environmental Variability in Dynamic Properties of a Large-Scale Soil-Foundation-Structure System." *Inaugural International Conference of the Engineering Mechanics Institute (EM08)*, University of Minnesota, Minnesota, May 18–21. CD-ROM.

Beck, J.L., B.S. May and D.C. Polidori (1994a). "Determination of Stiffness Changes from Model Parameter Changes for Structural Health Monitoring." *Proceedings of the1st World Conference on Structural Control*, Pasadena, CA, August 3–5, 13–22.

Beck, J.L., M.W. Vanik and L.S. Katafygiotis (1994b). "Determination of Model Parameters from Ambient Vibration Data for Structural Health Monitoring." *Proceedings of the 1stWorld Conference on Structural Control*, Pasadena, CA, August 3–5, 3–12.

Beck, J.L., M.W. Vanik, D.C. Polidori and B.S. May (1998). "Structural Health Monitoring Using Ambient Vibrations." *Proceedings of the Structural Engineers World Congress*, Paper T118-3, San Francisco, July.

Bielak, J. (1971). Earthquake Response of Building-Foundation Systems. California Institute of Technology Technical Report: CaltechEERL:1971.EERL-71-04.

Bradford, S.C., J.F. Clinton and T.H. Heaton (2005). "Variations in the Natural Frequencies of Millikan Library Caused by Weather and Small Earthquake."

Metropolis & Beyond 2005:Proceedings of the 2005 Structures Congress and the 2005 Forensic Engineering Symposium, New York, NY. CD-ROM.

Bradford, S.C., T.H. Heaton and J.L. Beck (2004). "Structural Monitoring and Evaluation Tools at Caltech: Instrumentation and Real-Time Data Analysis." *Annual Asian-Pacific Network of Centers for Earthquake-Engineering Research (ANCER)*, July 29–30, Honolulu, Hawaii. CD-ROM.

Brown, D., G. Carbon and K. Ramsey (1977). "Survey of Excitation Techniques Applicable to the Testing of Automotive Structures." *Society of Automotive Engineers: International Automotive Engineering Congress and Exposition*. Detroit, USA. 28 February-4 March. l–15.

Cempel, C. (1985). "Determination of Vibration Symptom Limit Value in Diagnostics of Machinery." *Maintenance Management International* **(5)**, 297–304.

Clinton, J.F. (2004). "Modern Digital Seismology: Instrumentation, and Small Amplitude Studies in the Engineering World." Caltech Earthquake Engineering Research Laboratory, Technical Report EERL-2004-10, Pasadena, CA.

Clinton, J.F., S.C. Bradford, T.H. Heaton and J. Favela (2006). "The Observed Wandering of the Natural Frequencies in a Structure." *Bulletin of the Seismological Society of America*, **96**(1), 237–257.

Clogg, C.C. (1979). "Some Latent Structure Models for the Analysis of Likert-Type Data." *Social Sciences Research*, **8**, 287–301.

Clogg, C.C. (1981). "New Developments in Latent Structure Analysis." D.J. Jackson and E.F. Borgotta (eds.), *Factor analysis and measurement in sociological research*, Beverly Hills: Sage Publications, 215–246.

Cornwell, P.J., C.R. Farrar, S.W. Doebling and H. Sohn (1999). "Environmental Variability Of Modal Properties." *Experimental Techniques*, Nov/Dec, 45–48.

Dobry R., and G. Gazetas (1986). "Dynamic Response of Arbitrarily Shaped Foundations." *Journal of Geotechnical Engineering,* ASCE, **112**(2), 109–35.

Doebling, S.W., C.R. Farrar, M.B. Prime and D.W. Shevitz (1996). "Damage Identification and Health Monitoring of Structural and Mechanical Systems From Changes in Their Vibration Characteristics: A Literature Review." Los Alamos National Laboratory Report LA-13070-MS.

Dutta, S.C., and R. Roy (2002). "Critical Review on Idealization and Modeling for Interaction among Soil-Foundation-Structure System." *Computers and Structures*, **80**(20), 1579–1594.

Everitt, B.S. (1996). "An Introduction to Finite Mixture Distributions." *Statistical Methods in Medical Research*, **5**(2), 107–127.

Fan, W., M. Miller, S.J. Stolfo, L. Wenke, and P.K. Chan (2004). "Using Artificial Anomalies to Detect Unknown and Known Network Intrusions." *Knowledge and Information Systems*, **6**(5), 507–1527.

Farrar, C.R., and G.H. James III (1997). "System Identification from Ambient Vibration Measurements on a Bridge." *Journal of Sound and Vibration*, **205**(1), 1–18.

Farrar, C.R., T.A. Duffey, S.W. Doebling and D.A. Nix (1999). "A Statistical Pattern Recognition Paradigm for Vibration-Based Structural Health Monitoring." *2nd International Workshop on Structural Health Monitoring,* Stanford, CA, September 8–10.

Farrar, C.R., and H. Sohn (2000). "Pattern Recognition For Structural Health Monitoring." *Workshop on Mitigation Of Earthquake Disaster by Advanced Technologies*, Las Vegas, NV, USA. , November 30-December 1, LA-UR-00-5565.

Friswell, M.I., and J.E.T. Penny (1997). "Is Damage Location using Vibration Measurements Practical?" *International Workshop on Structural Damage Assessment using Advanced Signal Processing Procedures,* EUROMECH 365, Sheffield, UK, June/July.

Hagenaars, J.A., and A.L. McCutcheon (eds.) (2002). *Applied Latent Class Analysis* (first edition), Cambridge University Press, ISBN-10: 0521594510.

Hall, J.R., J.J. Kissenpfennig and P.C. Rizzo (1976). "Discussion on the Paper of Soil–Structure Interaction Analysis for Seismic Response." *Journal of Geotechnical Engineering Division,* ASCE, **102**(6), 650–665.

Hall, P., D. Marshall and R. Martin (2000). "Merging and Splitting Eigenspace Models." *IEEE Pattern Analysis and Machine Intelligence,* **22**(9), 1042–1049.

Halpern, M.R., and P. Christiano (1986)."Steady-State Harmonic Response of a RigidPlate Bearing on a Liquid-Saturated Poroelastic Half Space." *Earthquake Engineering and Structural Dynamics*, **14**(3),439–454.

Horvath, J.S. (1993). "Beam-Column-Analogy Model for Soil–Structure-Interaction Analysis." *Journal of Geotechnical Engineering*, **119**(2), 358–64.

James, G.H., T.G. Carne, J.P. Lauffer and A.R. Nord (1992). "Modal Testing using Natural Excitation." *Proceedings of the 10th International Modal Analysis Conference*, San Diego, CA, Feb 3–7, 1209–1216.

James, G.H., T.G. Carne and J.P. Lauffer (1993). "The Natural Excitation Technique for Modal Parameter Extraction from Operating Wind Turbines." Report No. SAND92-1666, UC-261, Sandia National Laboratories, Sandia, NM.

James, G.H., T.G. Carne and R.L. Mayes (1996). "Modal Parameter Extraction from Large Operating Structures using Ambient Excitation." *Proceedings of the 14th International Modal Analysis Conference*, Dearborn, MI, February 12–15.

Juang, J.N., and R.S. Pappa (1985). "An Eigensystem Realization Algorithm for Modal Parameter Identification and Model Reduction." *Journal of Guidance, Control and Dynamics*, **8**(5), 620–627.

Kassir, M.K., K.K. Bandyopadhyay and J. Xu (1989). "Vertical Vibration of a Circular Footing on a Saturated Half-space." *International Journal of Engineering and Science,* **27**(4), 353–61.

Kassir, M.K., J. Xu and K.K. Bandyopadyay (1996). "Rotary and Horizontal Vibrations of a Circular Surface Footing on a Saturated Elastic Half-space". *International Journal of Solids and Structures*, **33**(2), 265–81.

King, S.P., D.M. King, P. Anuzis, K. Astley, L. Tarassenko, P. Hayton and S. Utete (2002). "The Use of Novelty Detection Techniques for Monitoring High-Integrity Plant." *Proceedings of International Conference on Control Applications*, 18–20 September, **1**, 221–226.

Kullaa, J. (2002). "Elimination of Environmental Influences From Damage-sensitive Features in a Structural Health Monitoring System." (*Structural Health Monitoring 2002*, Proceedings of the First European Workshop on Structural Health Monitoring, Paris, 10-12 July, 2002), D.L. Balageas (ed.), DEStech Publications, 742–749.

Kullaa, J. (2003). "Is Temperature Measurement Essential in Structural Health Monitoring?" Structural Health Monitoring 2003(*Proceedings of the 4th International Workshop on Structural Health Monitoring*, Stanford University, September 15–17, 2003), DEStech, Lancaster, PA, 717–724.

Kullaa, J. (2004). "Structural Health Monitoring under Variable Environmental or Operational Conditions." *Structural Health Monitoring 2004* (Proceedings of the 2nd European Workshop on Structural Health Monitoring, Munich, July 7-9, 2004), DEStech, Lancaster, PA, 1262–1269.

Kullaa, J. (2008). "Eliminating Environmental or Operational Influence sin Structural Health Monitoring using the Missing Data Analysis." *Journal of Intelligent Material Systems and Structures*, in press. (DOI 10.1177/1045389X08096050)

Lam, P., J.L. Beck and T.H. Heaton (2004). "COMET: Caltech Online Monitoring and Evaluation Testbeds." http://comet.caltech.edu/

Liu, C., and J.T. DeWolf (2007). "Effect of Temperature on Modal Variability of a Curved Concrete Bridge under Ambient Loads." *Journal of Structural Engineering*, ASCE, **133**(12), 1742–51.

Mahalanobis, P.S. (1936)."On the Generalized Distance in Statistics." *Proceedings of the National Institute of Science of India,* **12**(1), 49–55.

Manson, G., G. Pierce and K. Worden (2001). "On the Long-term Stability of Normal Condition for Damage Detection in a Composite Panel." *Proceedings of 4th*

International Conference on Damage Assessment of Structures, Jun. 2001, Cardiff, UK. CD-ROM.

McCutcheon, A. L. (1987). *Latent Class Analysis* (Quantitative Applications in the Social Sciences), Sage Publications, Inc. ISBN-10: 0803927525.

Meek, J.W., and J.P. Wolf (1992). "Cone Models for Homogeneous Soil." *Journal of Geotechnical Engineering,* ASCE, **118**(1), 667–685.

Meek, J.W., and J.P. Wolf (1993a). "Why Cone Models Can Represent the Elastic Half-Space." *Journal of Earthquake Engineering and Structural Dynamics*, **22**(99), 759–771.

Meek, J.W., and J.P. Wolf (1993b). "Cone Models for Nearly Incompressible Soil." *Earthquake Engineering and Structural Dynamics*, **22**(8), 649–663.

Nairac, A., T. Corbett-Clark, R. Ripley, N. Townsend and L. Tarassenko (1997). "Choosing An Appropriate Model for Novelty Detection." *Proceedings of 5th IEE International Conference on Artificial Neural Networks*, Cambridge, 7–9 July, 227–232.

Nairac, A., N. Townsend, R. Carr, S. King, P. Cowley and L. Tarassenko (1999). "A System for the Analysis of Jet Engine Vibration Data." *Integrated Computer Aided Engineering*, **6**(2), 53–65.

Nayeri, R.D., S.F. Masri, R.G. Ghanem and R.L. Nigbor (2008). "A Novel Approach for the Structural Identification and Monitoring of a Full-Scale 17-Story Building based on Ambient Vibration Measurements." *Journal of Smart Materials and Structure,* **17**(2), in press. (DOI:10.1088/0964-1726/17/2/025006)

Nigbor, R., and A. Asghari (2003). "SFSI Test Structure at GVDA: Preliminary Design Report." University of Southern California, Los Angeles, CA. (unpublished)

Nigbor, R., A. Asghari, L. McMichael and K. Mish (2004a). "Development of a Prototype SFSI Simulation Tool." *Proceedings of 13 World Conference of Earthquake Engineering*, Vancouver BC, August 1–6. CD-ROM.

Nigbor, R., J. Steidl and T. Youd (2004b). "Permanently Instrumented Field Sites in NEES: A Resource for Future Geotechnical Research," *Geotechnical Engineering for Transportation Projects*, Los Angeles, CA, Jul. 2004, 1637–1644.

Odin, T., and G.D. Addison (2000). "Novelty Detection Using Neural Network Technology." *Proceedings of COMADEN conference*. Houston, TX, 3–8 Dec. 2000, 731–743.

Omenzetter, P., and J.M.W. Brownjohn (2006). "Application of Time Series Analysis for Bridge Monitoring." *Smart Materials and Structures*, **15**, 129–138.

Peeters, B., and G. De Roeck (2001). "One-Year Monitoring of the Z24-Bridge: Environmental Effects versus Damage Events." *Earthquake Engineering & Structural Dynamics*, **30**(2), 149–171.

Peeters, B., J. Maeck and G. De Roeck (2001). "Vibration-Based Damage Detection in Civil Engineering: Excitation sources and temperature effects," *Smart Materials and Structures*, **10**, 518–527.

Philippacopoulos, A.J. (1989). "Axisymmetric Vibration of Disk Resting on Saturated Layered Half Space." *Journal of Engineering Mechanics*, ASCE, **115**(10), 2301–22.

Porter, K.A., J.L. Beck, J.Y. Ching, J. Mitrani-Reiser, M. Miyamura, A. Kusaka, T. Kudo, K. Ikkatai and Y. Hyodo (2004). "Real-time Loss Estimation for Instrumented Buildings." Caltech Earthquake Engineering Research Laboratory, Technical Report EERL-2004-08, Pasadena, CA.

Powrie, W. (2004). *Soil Mechanics: Concepts and Applications*; 2nd edition, Spon Press London, UK.

Reynolds, P., and A. Pavic (2000). **"**Impulse Hammer versus Shaker Excitation for the Modal Testing of Building Floors Experimental Techniques." *Journal of Experimental Techniques*, **24**(3), 39–44.

Roberts, S.J. (2000). "Extreme Value Statistics for Novelty Detection in Biomedical Data Processing." *Journal of Science, Measurement and Technology*, **147**(6), 363–367.

Ruotolo, R., and C. Surace (1997). "A Statistical Approach to Damage Detection Through Vibration Monitoring." *Proceedings of 5th Pan American Congress of Applied Mechanics*, Puerto Rico, 2–4 Jan. 1997, 314–317.

SAP2000 Analysis Reference and Tutorials, Computers and Structures. http://www.csiberkeley.com/products_SAP.html.

Seed, H.B., and G. Lysmer (1975). "Soil–Structure Interaction Analysis for Seismic Response." *Journal of Geotechnical Engineering Division,* ASCE, **101**(5), 439–457.

Sohn, H., and K.H. Law (2000). "Bayesian Probabilistic Damage Detection of a Reinforced-Concrete Bridge Column." *Earthquake Engineering & Structural Dynamics*, **29**(8), 1131–1152.

Sohn, H., M. Dzwonczyk, E.G. Straser, A.S. Kiremidjian, K.H. Law and T. Meng (1999). "An Experimental Study of Temperature Effect on Modal Parameters of the Alamosa Canyon Bridge." *Earthquake Engineering & Structural Dynamics*, **28**(8), 879–897.

Sohn, H., and C.R. Farrar (2000). "Statistical Process Control and Projection Techniques for Damage Detection." *Proceedings of European COST F3 Conference on System Identification and Structural Health Monitoring*, Madrid, Spain, June 2000, 105–114.

Sohn, H., C.R. Farrar, N. F Hunter K. Worden (2001)."Structural Health Monitoring Using Statistical Pattern Recognition Techniques." *Journal of Dynamic Systems, Measurement, and Control*, **123**(4), 706–711.

Sohn, H., K. Worden and C.R. Farrar (2002). "Statistical Damage Classification under Changing Environmental and Operational Conditions." *Journal of Intelligent Material Systems and Structures*, **13**(9), 561–574.

Sohn, H., C.R. Farrar, F.M. Hemez, D.D. Shunk, D.W. Stinemates, B.R. Nadler and J.J. Czarnecki (2004). "A Review of Structural Health Monitoring Literature: 1996–2001." Los Alamos National Laboratory Report LA-13976-MS.

Sohn, H., D.W. Allen, K. Worden and C.R. Farrar (2005). "Structural Damage Classification Using Extreme Value Statistics." *Journal of Dynamic Systems, Measurement and Control,* **127**(1), 125–132.

Steidl, J. H., R.J. Archuleta, and L. F. Bonilla (2000). "Observations and Modeling of Ground Motion at the Garner Valley, California, Test Site." *Proceedings of the OECD-NEA Workshop on Engineering Characterization of Seismic Input*, NEA/CSNI/R(2000)2.

Steidl, J.H., and R.L. Nigbor (2004). "Network for Earthquake Engineering Simulation Experimental Arrays." *International Workshop for Site Selection, Installation and Operation of Geotechnical Strong-Motion Arrays*, Consortium of Organizations for Strong-Motion Observation System (COSMOS), GSMA, and Workshop1: http://www.cosmoseq.org/Projects/GSMA/GSMA1/Paper/2.2_Steidl_et_al.pdf.

Tax, D.M.J., and R.P.W. Duin (2000). "Data Description in Subspaces." *Proceedings of 15th International Conference on Pattern Recognition,* vol. 2, Barcelona, 672-675.

Tayabji, S.D., and E.O. Lukanen (eds.) (2000). *Nondestructive Testing of Pavements and Back Calculation of Module*, ASTM International, ISBN 0803128584, 9780803128583.

Todorovska, M.I., and Y. Al Rjoub (2006). "Effects of Rainfall on Soil-Structure System Frequency: Examples Based on Poroelasticity and a Comparison with Full-Scale Measurements." *Soil Dynamics and Earthquake Engineering*, **27**(6)**,** 708–717.

Uebersax, J.S., and W.M. Grove (1990). "Latent class analysis of diagnostic agreement." *Statistics in Medicine*, **9**(5), 559–572.

Vandiver, J.K. (1977). "Detection of Structural Failure on Fixed Platforms by Measurement of Dynamic Response." *Journal of Petroleum Technology*, **29**(3), 305–310.

Wolf, J.P. (1985). *Dynamic Soil-Structure Interaction*, International Series in Civil Engineering and Engineering Mechanics, Prentice-Hall.

Wolf, J. P. (1994). *Foundation Vibration Analysis Using Simple Physical Models*, PTR Prentice Hall. ISBN 0-13-010711-5.

Wolf, J.P., and J.W. Meek (2004). "Cones to Model Foundation Vibrations: Incompressible Soil and Axi-symmetric Embedment of Arbitrary Shape." *Earthquake Engineering and Structural Dynamics*, **24**(12), 185–193.

Wolfe, J. H. (1970). "Pattern Clustering by Multivariate Mixture Analysis." *Multivariate Behavioral Research*, **5**, 329–350.

Wood, M.G. (1992). "Damage Analysis of Bridge Structures using Vibrational Techniques". Ph.D. dissertation, University of Aston, Birmingham, U.K.

Worden, K., G. Manson and N.R. Fieller (2000). "Damage Detection Using Outlier Analysis." *Journal of Sound and Vibration,* **229**(3), 647–667.

Worden, K. (1997). "Structural Damage Detection Using a Novelty Measure." *Journal of Sound and Vibration*, **201**(1), 85–101.

Worden, K., H. Sohn and C.R. Farrar (2002). "Novelty Detection in a Changing Environment: Regression and Interpolation Approaches." *Journal of Sound and Vibration,* **258**(4), 741–761.

Worden, K., and G. Manson (2003). "Experimental Validation of a Structural Health Monitoring Methodology: Part 1. Novelty Detection on a Laboratory Structure." *Journal of Sound and Vibration,* **259**(2), 323–343.

Yang, J., and T. Sato (2000). "Influence of Water Saturation on Horizontal and Vertical Motion at a Poroussoil Interface Induced by Incident SV Wave." *Soil Dynamics and Earthquake Engineering*, **19**(5), 339–346.

Youd, T., J. Steidl and R. Nigbor (2004). "Lessons Learned and Need for Instrumented Liquefaction Sites." *Soil Dynamics and Earthquake Engineering*, **24**(9–10), 639–646.

Zhang, C., C. Xinfeng and W.A. Guanglun (1999). "Coupling model of FE-BE-IE-IBE for Non-linear Layered Soil–Structure Interactions." *Earthquake Engineering and Structural Dynamics*, **(28)**, 421–41.